BONE CANONICAL WNT/B-CATENIN SIGNALING IN MODELS OF REDUCED MICROGRAVITY

A Dissertation

by

BRANDON RICHARD MACIAS

Submitted to the Office of Graduate Studies of
Texas A&M University
in partial fulfillment of the requirements for the degree of

DOCTOR OF PHILOSOPHY

Approved by:

Chair of Committee,	Susan A. Bloomfield
Committee Members,	Harry A. Hogan
	Michael Massett
	John Ford
Head of Department,	Richard Kreider

December 2012

Major Subject: Kinesiology

ABSTRACT

Human exposure to reduced weightbearing results in bone loss. The rate of bone loss during microgravity exposure is similar to that of a post-menopausal women. In fact, the maintenance of bone mass is intimately dependent on exercise. Therefore, exercise associated mechanical loads to bone tissue are an important countermeasure to prevent disuse-induced bone loss. However, the types of exercise modalities required to prevent such bone loss are unclear. Moreover, how mechanical loading to bone translates into molecular osteogenic signals in bone cells is unknown. Radiation exposure is another potent inducer of bone loss, namely observed on Earth in the clinical setting following radiotherapy procedures. It is expected that long duration space missions outside the protection of Earth's magnetosphere will result in significant galactic cosmic radiation exposure. However, the magnitude of bone loss resulting from this galactic cosmic radiation exposure is unclear. Moreover, it is unknown if radiation exposure will exacerbate disuse-induced bone loss. Therefore, a series of experiments were designed to determine: 1) Will simulated galactic cosmic radiation exacerbate reduced weightbearing-induced bone loss? 2) Will pharmacological activation of the putative mechanosensing Wnt pathway enhance exercise-induced bone mass gain? To address these questions the experimental study series employed two animal models of reduced weightbearing, hindlimb unloading and partial weightbearing. These model test-beds enabled the evaluation of two novel countermeasures (simulated resistance exercise and glycogen synthase kinase-3 (GSK-3) therapeutic) and simulated exposure to

space radiation environments. To test the impact of simulated space radiation (^{28}Si) one study of the series was conducted at Brookhaven National Laboratory. To quantify the impact of the abovementioned countermeasures and space radiation on bone, mechanical testing, peripheral quantitative computed tomography, micro-computed tomography, histomorphometry, and immunohistochemistry served as primary outcome measures.

The primary findings are: 1) Low-dose high-LET radiation negativity impacts maintenance of bone mass by lowering bone formation and increasing bone resorption. This impaired bone formation response is in part due to sclerostin induced suppression of Wnt signaling. 2) Combining GSK-3 inhibition with high intensity exercise mitigates cancellous bone loss and restores cortical periosteal growth during disuse.

ACKNOWLEDGEMENTS

HaOne, Mom, Dad, and Nana, thank you for the enduring love and support. Thank you to Drs. Susan Bloomfield and Alan Hargens for the many years of support and helping to make so many opportunities a reality. To my committee members, thank you for your support and guidance. JM Swift's invaluable training provided an excellent foundation for work in the Bone Biology Laboratory. In addition, great appreciation to all the students who helped make these labor intensive animal studies a reality.

It should be noted that the article titled, "Simulated resistance training, but not alendronate, increases cortical bone formation and suppresses sclerostin during disuse," that appears as Appendix A presents work of a collaborative effort by JM Swift, MI, Nilsson, HA Hogan, SD Bouse, and SA Bloomfield (Macias BR, Swift JM, Nilsson MI, Hogan HA, Bouse SD, Bloomfield SA. Simulated resistance training, but not alendronate, increases cortical bone formation and suppresses sclerostin during disuse. J Appl Physiol 112:918-925, 2012). Without their major contributions, this labor intensive study would not have been possible. Beyond, dynamic histomorphometry analysis, statistical analysis, interpretation, and writing this published work, BR Macias major contribution to this work was employment of the sclerostin immunohistochemistry assay.

Thank you to the outstanding funding institutions for supporting graduate student research and education:

Texas A&M Space Life Science Graduate Student Training Program funded by the National Space Biomedical Research Institute (NASA NCC 9-58)

National Science Foundation (NSF) Graduate Research Fellowship Program

Nordic Research Opportunity made possible by the NSF, Swedish Research Council, and the Laboratory of Professor Per Aspenberg.

Texas A&M University Office of Graduate Studies

Texas A&M Association of Former Students

Huffines Institute for Sports Medicine and Human Performance

American College of Sports Medicine's NASA Space Physiology Grant

TABLE OF CONTENTS

LIST OF TABLES

LIST OF FIGURES

CHAPTER I

INTRODUCTION

Human exposure to reduced weightbearing results in bone loss. In fact, the maintenance of bone mass is intimately dependent on mechanical loading. Reduced weightbearing, for example during 6-month International Space Station (ISS) spaceflight missions (with moderate use of exercise equipment) results in 1-2% bone loss per month. The National Aeronautic and Space Administration (NASA) recognized the risk of microgravity-induced bone loss early in the space program's history, prior to the existence of the ISS (69). Therefore, exercise countermeasures, human ground-based analogs, and ground-based animal models were developed to test countermeasures to mitigate bone loss during spaceflight. In the 1970's a team of scientist at NASA-Ames research center developed a ground-based animal model to simulate the "microgravity" effects of reduced load bearing to bone and muscle. This model is now often referred to as the "Hindlimb Unloading," (HU) model.

Exercise countermeasures have been employed early in the Space Program's history, starting with the Gemini era. Skylab missions were equipped with a cycle ergometer, isokinetic rope-pull resistance exercise systems, and treadmill. Presently onboard the ISS, exercise countermeasures include treadmills, cycle ergometer, and high-force resistance exercise equipment. Both studies on the ground and in-flight indicate that high intensity resistance exercise is required to generate an anabolic response in bone. In summary, bone is a dynamic tissue responsive to reduced and

increased levels of load. Bone tissue is of critical importance for the maintenance of ambulatory function. Moreover, the skeleton functions as a mineral reservoir for basic physiological cellular function and physiological fluid homeostasis. Beyond broken bones or altered gait, the loss of bone tissue and/or imbalance in bone turnover can negatively affect other physiological systems, for example, muscle cell contractility, kidney function, or neurological function.

Human exploration of the moon, Mars, or even distant planetary bodies, such as, asteroids will expose astronauts to galactic cosmic radiation (GCR). The estimated high-linear energy transfer radiation dose for a Mars mission is approximately 0.4 to 0.5 Gy (19). GCR includes but is not limited to high-energy heavy ions, characterized by high charge and energy (19). Data on the biological effect of high-energy heavy ions is limited; furthermore, a possible synergistic interaction between radiation and microgavity-induced physiological deconditioning (including but not limited to deconditioning of bone matrix, bone cells, and bone progenitor cells) is unknown. The effects of radiation on biological systems are complex and to date there are no human data that document the risk to GCR exposure (31). Ground based research models of GCR in bone with high dose X-ray irradiation (15-30 Gy) have shown deleterious effects on bone. While these studies provide invaluable data, at present there are few data reporting the effect ionizing radiation on bone.

The development of exercise and pharmaceutical countermeasures to mitigate disuse- and radiation-induced bone loss is of critical importance for the realization of long duration human exploration class missions. The two experiments presented herein

were designed to test exercise and/or pharmaceutical countermeasures for bone loss using animal ground-based models of microgravity. A second objective was to employ a new murine model of reduced weightbearing, to determine if radiation exposure would exacerbate bone loss during simulated Lunar gravity. Given that the bone matrix embedded osteocyte is the putative mechaoregulator cell in bone, these studies sought to determine how cortical sclerostin-osteocyte levels respond to unloading and radiation exposure. These experiments are the first to investigate the combined effects of 1) Partial weightbearing and radiation exposure, and 2) Simulated resistance exercise and pharmacological activation of Wnt signaling during disuse.

CHAPTER II

LITERATURE REVIEW

Bone Remodeling and Modeling

Osteoblasts are the basic bone forming cell and osteoclasts are the basic bone resorbing cell (70). During bone remodeling osteoblasts can become embedded in the organic bone matrix. Once embedded these osteoblasts often terminally differentiate into mature osteocytes. Osteoblasts derive from the mesenchymal cell lineage, while osteoclasts derive form the hematopoietic cell lineage. Osteoclasts and osteoblasts form the basic multicellular unit (BMU) that actively remodels the skeleton throughout life. Osteoclasts function on bone surfaces to resorb bone, facilitating repair of weak bone sites and/or liberating minerals, such as calcium. These osteoclasts working on bone surfaces are often followed by a "team" of osteoblasts laying down osteoid (new bone matrix). An imbalance in bone turnover, for example, an excess of osteoclast activity, can result in bone loss. Alternatively, more vigorous osteoblast activity than resorbing osteoclasts can result in net bone gain. Osteoclasts present the protein Receptor Activator of Nuclear Factor κ B (RANK) to the cellular surface. Whereas, nearby osteoblasts present the membrane protein RANK-Ligand (RANK-L). Lower levels of RANK-L reduce osteoclastogenesis and induce osteoclast apoptosis. In addition, osteoblasts can secrete osteoprotegerin (OPG) that functions as a decoy receptor to bind to the RANK-L and interfere with RANK signaling. Thus, the OPG/RANK-L axis functions to couple osteoblast and osteoclast activity; in addition, the OPG:RANK-L

ratio functions as one important laboratory measures of bone turnover status. The uncoupled action of osteoblasts from osteoclasts is termed bone modeling. Modeling allows the deposition of new bone matrix without prior osteoclast bone resorption. Bone modeling occurs during skeletal growth and development. Bone modeling occurs less frequently in the adult skeleton. Mechanical loading of bone is one such stimulus capable of initiating bone modeling. Bone modeling occurs more frequently on cortical bone surfaces than cancellous bone surfaces.

Osteocyte Control of Bone Remodeling

Recent evidence suggests that osteocyte-secreted proteins regulate osteoblast proliferation, activity, and bone matrix synthesis. Osteocytes are the most abundant cell in bone tissue; however, less is known about osteocyte function (10:1, osteocyte: osteoblast) as compared to osteoclasts and osteoblasts. Recent osteocyte cell culture studies show that osteocytes secrete factors in response to mechanical and shear forces (10-12). Sclerostin is one such osteocyte-secreted factor that inhibits Wnt signaling, osteoblastogenesis, and thus results in reduced bone formation capacity. More recently, it has been demonstrated that osteocytes also secrete RANK-L, a key regulator of osteoclast maturation and activity (60,99). Taken together, these recent osteocyte biology developments suggest that osteocytes are the key responders to mechanical loading and can regulate both bone formation and bone resorption activity.

Bisphosphonates

Bisphosphonates, such as alendronate, are now a Food and Drug Administration (FDA: Application No. NDA-020560) approved class of pharmaceuticals designed for

the treatment and prevention of post-menopausal osteoporosis in women, treatment of osteoporosis in men, treatment of glucocorticoid-induced osteoporosis in men and women, and treatment of Pagets' disease. Bisphosphonates potently inhibit bone resorption and reduce facture incidence (15,48). Currently, alendronate (oral dose of 70 mg of alendronate taken weekly starting 3 weeks prior to flight) is being administered to some astronauts in an ongoing experiment on the ISS to test its efficacy as a countermeasure for microgravity-induced bone loss. Several studies document the efficacy of alendronate to mitigate disuse-induced bone loss (3-4). The highly charged phosphate backbone within the bisphosphonate molecule provides a high affinity interaction with calcium hydroxyapetite bone surfaces. Therefore, during bone remodeling bisphosphonate coated bone surfaces reduce the incidence of osteoclast attachment to bone. These bisphosphonates become incorporated into the bone matrix. Moreover, osteoclast-digested bisphosphonates inhibit the mevalonate pathway, causing osteoclast detachment from the bone surface and in some cases apoptosis (68,89).

Wnt Signaling in Bone Tissue

Bone mass and architecture adapt to mechanical load; for example, when mechanical load is below the physiologic threshold (e.g., microgravity), bone is resorbed. Data published over the last ten years implicate the Wnt pathway in control of load-induced bone formation; however, the basic molecular mechanisms governing the osteogenic response to mechanical load are unknown. Loss-of-function mutation of the low-density lipoprotein receptor-related protein 5 (Lrp5) gene impairs response to mechanical load, decreases bone mass, and osteoblast proliferation (24). In contrast, a

gain-of-function mutation of Lrp5 that disrupts the binding site of sclerostin is associated with a high bone mass phenotype. The Wnt pathway coordinates communication between mechanosensing osteocytes (via secreted sclerostin) and bone-forming osteoblasts (Figure 1).

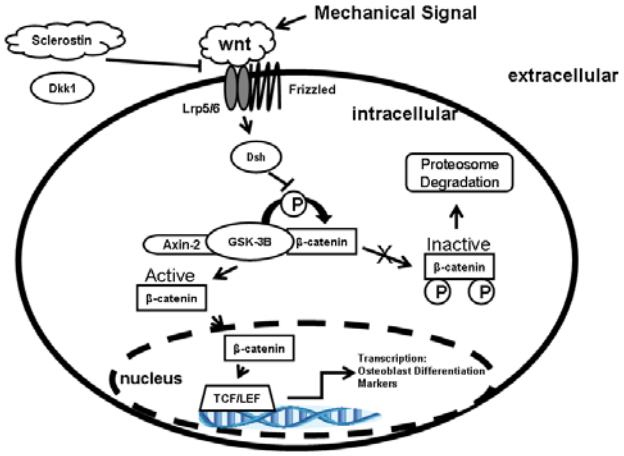

Figure 1. Mechanotransduction via Wnt/β-catenin (canonical) pathway in an osteoblast. Mechanical loading promotes formation of the Wnt-LRP5/6-Frizzled transmembrane complex. Disheveled (Dsh) inhibits a cytoplasmic complex composed of GSK-3β and Axin-2. Intracellular β-catenin levels rise and β-catenin translocates to the nucleus where it associates with T-cell factor (TCF)/lymphoid enhancer-binding factor (LEF) transcription factors to regulate gene expression.

Interestingly, mechanical loading *in vivo* down-regulates sclerostin (71) and up-regulates osteogenic gene expression. When mice lacking sclerostin are subjected to simulated microgravity, the Wnt pathway is unaffected and bone loss does not occur (47). However, it is unknown if *in vivo* mechanical loading can overcome the potent stimulus of reduced weight bearing; furthermore, it is unknown if the Wnt pathway is active at graded levels of reduced weight bearing.

Interleukin-6 (IL-6) in Wnt Signaling

Data in the last ten years clearly demonstrates that Wnt signaling regulates osteoblast differentiation and bone accrual in adult vertebrates (human and rodent). Recently, cytokines such as tumor necrosis factor (TNF-α) and extracellular antagonists such as RANK-L, sclerostin and Dickkopf-1 (Dkk-1) have been shown to impair bone formation. This impairment may result in bone loss. It appears that these proteins disrupt mechanotransduction in bone by inhibiting Wnt-Ligand and LRP4/5/6 complex formation. Sclerostin and Dkk-1 are known potent inhibitors of Wnt signaling; *in vitro* TNF-α has been shown to potentiate Dkk-1 inhibition of Wnt signaling (61). However, it is unclear how Dkk-1, TNF-α, and IL-6 interact to regulate bone formation and bone resorption (39). IL-6 is considered a potent osteoclastogenic cytokine (62). Primary cultures of bone cells from HU animals exhibit slowed osteoblast differentiation and higher IL-6 production compared to cage controls (25). Moreover, IL-6 has been show to increase RANK-L secretion in a paracine/autocrine manner (56). It appears that IL-6 expression in osteoblast is regulated by oxidized phospholipids (88). Interestingly, there is some evidence that reactive oxygen species are elevated in patients with osteoporosis (90) and that antioxdants provide some protection against disuse-induced bone resorption (77). Therefore, the interaction of Dkk-1, TNF-α, and IL-6 may be an important signaling complex that regulates bone formation and bone resorption (Figure 2).

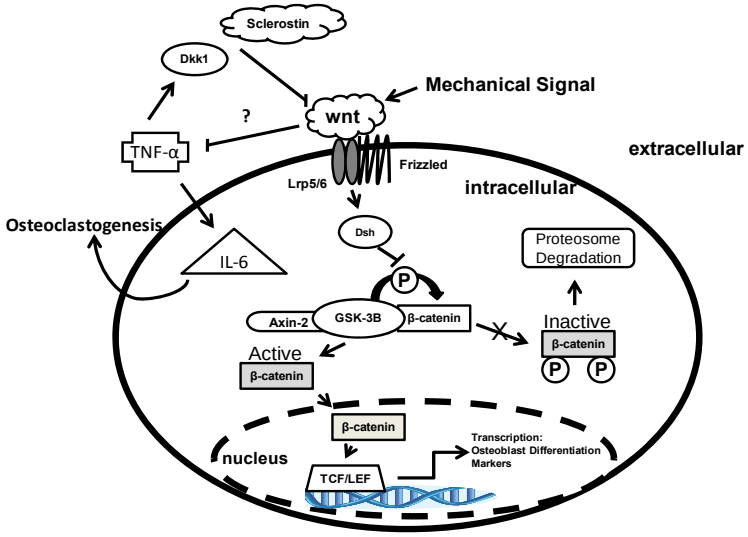

Figure 2. Dkk-1 and TNF-α inhibition of mechanotransduction via the Wnt/β-catenin pathway in an osteoblast. Mechanical loading promotes formation of the Wnt-LRP5/6-Frizzled transmembrane complex and thus downstream intracellular signaling and gene expression. Wnt signaling diverts the mesenchymal stem cells down the pathway of osteoblast differentiation. Sclerostin and Dkk-1 are potent extracellular antagonists of Wnt signaling. Dkk-1 binds to the Wnt receptor complex on the surface of the osteoblast lineage cell and blocks Wnt signaling, arresting osteoblast proliferation and differentiation. Blockade of Dkk-1 or TNF-α permits progression of osteoblast differentiation.

SOST and Sclerostin Expression in Wnt Signaling

SOST gene expression is responsive to disuse. Unloading for 3 days in mice results in a significantly higher SOST gene expression in tibial bone homogenates (cortical, cancellous, and marrow) compared to normal cage controls (71). Conversely, externally applied mechanical loading of rodent bone produces an anabolic response and can lower SOST expression. For example, SOST gene expression is downregulated following repeated bouts of daily 3-minunte loading cycles using the ulnar-loading model (53). Similarly, external mechanical loading of 11-wk old female C57/B6 mouse

tibias (peak strain of -1300 uE, 2Hz for 30sec) produces a 3-fold lower SOST expression (101).

SOST and sclerostin expression in response to mechanical loading may be bone-site specific. SOST expression levels are similar in cortical and cancellous bone at metaphyseal, epiphyseal, and diaphyseal sites (75). In addition, sciatic neurectomy-induced bone loss is accompanied by significantly higher numbers of sclerostin-positive osteocytes in both the primary and secondary spongiosa of metaphyseal bone (59). Interestingly, however, external axial loading of tibiae in neurectomized limbs (at 1800 uE) significantly lowers the proportion of sclerostin-positive osteocytes in the metaphyseal cortical bone but not midshaft cortical bone compared to ambulatory control mice (59). Those cortical bone regions exhibiting the largest increases in newly formed bone area also exhibit the greatest decreases in sclerostin-positive osteocytes of proximal tibias (59). Therefore, there may be important site-specific differences in how SOST and sclerostin expression respond to altered mechanical loading.

Pharmacological Intervention via Wnt/β-catenin (canonical) Signaling

Glycogen synthase kinase-3-beta (GSK-3β) is a key modulator of the Wnt signaling pathway. Therefore, GSK-3β is an attractive target of drug development to resolve metabolic and neurological diseases. Inhibition of GSK-3β can normalize blood glucose levels in an animal model (17) and suppress neuronal apoptosis (6). GSK-3β inhibitors have recently been used to activate Wnt signaling in bone cells and increase bone mass in various rodent models (38,54). GSK-3β inhibition prevents ovariectomy-induced femoral bone loss (38). Similarly, femoral cancellous and cortical BMD are

higher in normal healthy animals treated with a GSK-3β inhibitor (54). However, it is unknown whether inhibition of GSK-3β can mitigate bone loss during disuse or how GSK-3β inhibition interacts with increased mechanical loading.

Wnt Signaling Activators

More recently, a new class of pharmaceuticals is being tested and developed to target Wnt signaling in bone tissue. When activated, Wnt signaling initiates a profound increase in osteoblastogenesis, resulting bone mass gain. New antibody pharmaceuticals currently under development are designed to target Dkk-1 and Sclerostin (1,2,45,63). In addition, (Glycogen synthase kinase-3) GSK-3 inhibitors are being developed to target Wnt signaling. (2'Z,3'E)-6-Bromoindirubin-3'-oxime, also known as BIO, is a potent and selective inhibitor of the intracellular protein GSK-3 (Figure 3). GSK-3 inhibitors function by inhibiting GSK-3 dependent phosphorylation of beta-catenin. The lack of phosphorylation side chains on the beta-catenin protein prevents trafficking of beta-catenin to the proteosome for degradation. Thus, GSK-3 inhibition raises intracellular beta-catenin levels which can then cross the nuclear membrane to activate an osteogenic gene expression profile.

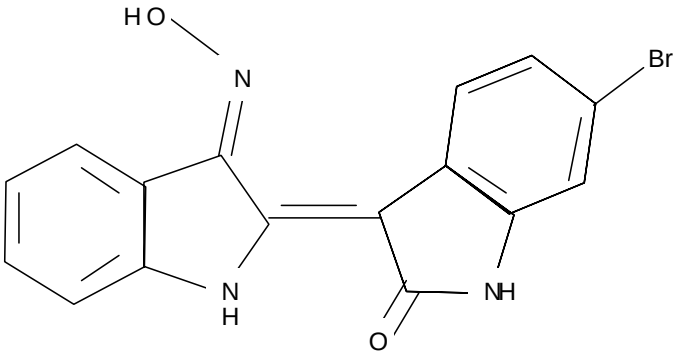

Figure 3. Molecular structure of (2'Z,3'E)-6-Bromoindirubin-3'-oxime, BIO, a potent and selective, ATP-competitive glycogen synthase kinase-3 (GSK-3) inhibitor (95).

Space Radiation Environment

The space radiation environment is primarily composed of galactic cosmic radiation (GCR), solar particle events, and secondary radiation products. Ongoing advancements in solar storm monitoring, materials, and high velocity space vehicles will reduce the radiation risk to astronauts (51). However, despite expected future engineering advancements, crew members will accrue some low dose GCR exposure during exploration class missions. The GCR spectrum is low fluence and primarily composed of heavy charged particles (C through Fe) and protons. A 1000-day human exploration mission to Mars is expected to result in a total absorbed dose of about 0.42 Gy (19). A round trip 88-day mission to the moon would involve a total dose equivalent to the bone marrow of 0.074 Gy (26). Radiation risk models estimate a 4.2% (95% CI: 1.3-13.6) fatal risk for missions to Mars and for similar exploration class missions to

other distant objects. This estimated risk level violates the current 3% career limit for excess cancer mortality recommended by the [National Council on Radiation Protection] for space activities for both sexes and all ages (26). However, the radiation risk estimate for radiation-induced bone loss is unknown.

Radiation Induced Bone Loss and Fractures

Radiation exposure to bone tissue increases the risk of skeletal fracture; for example, pelvic fracture rate is two-fold higher after radiation therapy for anal cancer (5,7,65,67). In addition, radiation therapy early in life results in reduced bone density later in life (65). Therefore, dividing a large gamma or proton radiation dose into small fractions is a common therapeutic strategy to deliver a sufficient radiation dose (for example, 10-50 Gy) to pathological tissue while sparing neighboring healthy normal tissue (102). Similar fractionation strategies have been employed in ground based studies to test the effects of high-LET and low-fluence GCR that astronauts might experience on distant missions. Utilizing fractionated dose regimes may help better simulate the low dose rate exposures to GCR during sojourns in space.

Exercise Countermeasures for Humans during Spaceflight

Current exercise hardware and exercise prescriptions performed during ISS missions (~6 months) do not completely prevent musculoskeletal deconditioning, but may mitigate some of the musculoskeletal loss (42,73,76,78-79,81,87). Recent data show that when exercise on the advanced resistive exercise device (aRED) is combined with adequate nutrition, astronauts exhibit no net bone loss after 6 month ISS missions at most bone sites (76). However, it is unclear how these DEXA derived measures of bone

mass translate into mitigation of bone strength loss following 6-month ISS missions. These human exercise evaluations during microgravity provide further evidence that high impact resistive exercise prescriptions are necessary to prevent bone loss during long duration space missions.

Exercise Countermeasures in Ground-Based Rodent Models

The rodent hindlimb unloading (HU) model is a well-established ground-based model for investigating disuse effects on bone (58,72,91,93). Our recent publication details how high intensity muscle contractions at 75-to-100% peak isometric torque (P_0), produced during simulated resistance training (SRT) (Figure 4) which is undertaken during a period of HU, produce significant gains in proximal tibia cancellous and mid-diaphyseal tibia cortical bone (50,83). These gains were associated with a significantly greater bone formation rate (BFR) as compared to control animals (50,83). Therefore, high intensity exercise provides some protection against disuse-induced bone loss in rodent ground-based simulations of microgravity. In fact, SRT produces bone mass gains during HU for several key bone measures.

Mechanical loading, SRT, during disuse dampens sclerostin secretion from osteocytes, resulting in Wnt signaling activation and bone gain (50). When the hindlimbs of rats are subjected to HU, sclerostin-positive osteocytes are significantly increased (50). However, when HU rats are subjected to SRT the number of sclerostin positive osteocytes are similar to weightbearing controls. The reduction of the number of sclerostin positive osteocytes by mechanical loading may explain the recovery of the normal bone mineral accretion during disuse (50). Therefore, these data suggest that

osteocytes embedded in bone matrix monitor the mechanical environment and respond by altering sclerostin protein levels.

During bone deposition some osteoblasts become embedded in bone matrix, when this occurs these cells are called osteocytes. Visual inspection of newly embedded osteocytes on the periosteal rim show very low sclerostin staining (50). This observation is consistent with previous reports (59). In fact, gene expression profile of newly embedded osteocytes is different from more mature osteocytes (70). Taken together, these data suggest that newly embedded osteocytes are genetically programmed to limit sclerostin production or local signaling inhibits sclerostin expression.

Sclerostin is a potent inhibitor of Wnt signaling in osteoblasts. HU effectively increases sclerostin levels and added SRT lowers the number of sclerostin-positive osteocytes (50). SRT imposed every third day during HU and prevents higher numbers of sclerostin-positive osteocytes (50). These data suggest high intensity exercise every third day provides a sufficient mechanical stimulus to reduce sclerostin levels and activate Wnt signaling.

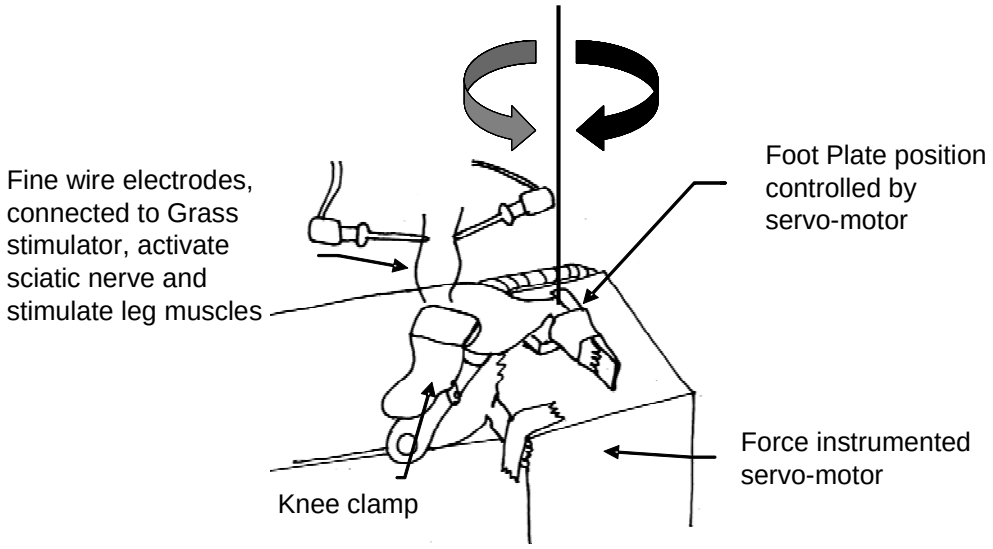

Figure 4. Simulated Resistance Training (SRT). Isometric plus eccentric exercise using percutaneous of sciatic nerve to produce active plantarflexor muscle contractions at 75% of peak isometric torque. The Force instrumented servo-motor and footplate enable isometric and eccentric muscle contractions and simultaneous force measurements.

The ground-based tail suspension rodent hindlimb unloading model effectively reproduces the suppressed bone formation and increased bone resorption observed during spaceflight missions (57-58). However, the HU model requires the rodent be suspended at a 30° angle to appropriately load the tail and forelimbs, and to simulate a head-ward fluid shift (29). A novel harnessed mouse model has been developed for ground-based studies for the precise titration of ground reaction forces to all four limbs in order to study partial weightbearing effects (94). Three weeks of partial weightbearing at ~38% total body weight results in approximately a 26% reduction in cancellous BV/TV and 20% reductions in diaphyseal cortical thickness relative to full weightbearing controls (21,94).

CHAPTER III

SIMULATING THE LUNAR ENVIRONMENT: PARTIAL WEIGHTBEARING AND HIGH-LET RADIATION INDUCES BONE LOSS AND INCREASED SCLEROSTIN-POSITIVE OSTEOCYTES

Introduction

Human exposure to reduced weightbearing and radiation independently result in bone loss, however it was unclear if these two factors interact to exacerbate bone loss. Maintenance of bone mass is intimately dependent on mechanical loading. Reduced weightbearing, for example during 6-month International Space Station (ISS) spaceflight missions, results in 1-2% bone loss per month relative to preflight baseline values at the femoral neck and lumbar spine (40-41,92). In addition, radiation exposure early in life lowers bone mineral density later in life (65). Long duration human spaceflight missions outside the protection of Earth's magnetosphere will result in low-dose radiation exposure (19). Therefore, the lack of weightbearing during spaceflight and space-radiation exposure present serious skeletal tissue degenerative health risks for astronauts on long duration exploration class missions. Moreover, it remains unclear how reduced weightbearing and added radiation exposure may impact bone mass on long duration space missions.

The magnitude of BMD loss and adaptations in bone geometry during a 6-month ISS mission produces declines in estimated bone strength equivalent to the median lifetime loss of that observed for Caucasian women (35). Of particular concern are high-

risk fracture sites such as the femoral neck and lumbar vertebrae. These skeletal sites are composed of a thin cortical shell and reduction in mass of the shell and cancellous core can increase the risk of fracture. Approximately 3 years, 6-times the typical ISS mission period, may be required to recover both mass and estimated strength to some of these skeletal sites (74).

The space radiation environment is primarily composed of galactic cosmic radiation (GCR), radiation emitted from solar particle events, and secondary radiation products (31). Ongoing advancements in radiation biology and engineering research will help reduce the radiation risk to astronauts. The GCR profile is of low-dose rate and primarily composed of heavy charged particles (C through Fe) and protons (hydrogen), and helium (31). A 1000-day human exploration mission to Mars is expected to result in total absorbed dose of about 0.42 Gy (19). A round trip 88-day mission to the moon would involve a total dose equivalent to the bone marrow of 74 mSv (26). Therefore, more data on radiation-induced bone loss are required to reduce the large uncertainties in estimates of radiation quality and to improve radiation risk estimates for exploration class missions.

Simulated GCR exposure of rodents provides the only experimental method to study the tissue level effects of low-dose high-linear energy transfer (LET) radiation. LET is the average local energy deposition per unit length of distance traveled in a material. GCR is primarily composed of high-LET radiation, radiation that is highly energetic and extremely penetrating. Radiation exposure to mice can independently induce potent cancellous bone loss and bone resorption (36,97). In fact, gamma

radiation doses as low as 1 Gy of can cause significant murine cancellous bone mass loss within 1-wk following radiation exposure (36). However, it remains less clear if low-dose high-LET radiation, a radiation species not typically encountered on Earth, cause similar levels of bone loss.

The ground-based tail suspension rodent hindlimb unloading (HU) model effectively reproduces the suppressed bone formation and increased bone resorption observed during spaceflight missions (57-58). The HU model requires the rodent be suspended at a 30° angle to appropriately load the tail and forelimbs and simulate the head-ward fluid shift (29). A new harness suspension mouse model has been developed for ground-based studies for the precise titration of ground reaction forces to all four limbs (94). Partial weightbearing at ~38% shows approximately a 26% reduction in cancellous BV/TV and 20% reductions in diaphyseal cortical thickness relative to full weightbearing controls (21,94).

The aim of this experiment was to simulate the partial weightbeaing conditions and radiation environment on the Lunar surface. The experimental design employed both X-ray reference radiation and ^{28}Si radiation to determine the radiation quality effect of high LET species on bone tissue. In addition, we employed a fractionated dose group to simulate the low-dose received over the course of an extended deep space mission. We hypothesized that simulated galactic cosmic radiation would exacerbate bone loss observed after reduced 1/6th partial weightbearing and fractionation of the highest dose group would mitigate detrimental effects observed with one acute dose.

Materials and Methods

Animals

This study was approved by Texas A&M University's Institutional Animal Use and Care Committee (IACUC) and Brookhaven National Laboratory (BNL) IACUC. Radiation doses used in this study were chosen to ensure sufficient probability that each cell would be exposed to one ^{28}Si particle and thus the X-ray energy equivalent was used.

X-Ray Experiment

Four-month old female BALB/cBYJ mice (Stock# 001026, Jackson Laboratories, Bar Harbor, Maine) were rank ordered by body weight and block assigned to one of 6 groups: (1) normal ambulatory cage control or 1 gravity group (1G SHAM, n=10), (2) 1G plus exposure to a fractionated 0.33 Gy X-ray dose (1G 3F x 0.33 Gy, n=10), (3) 1G plus exposure to a single 1 Gy dose (1G 1 Gy, n=10), (4) $1/6^{th}$ weight bearing (G/6) group to simulate Lunar gravity (G/6 SHAM, n=12, (5) G/6 plus exposure to a fractionated 0.33 Gy X-ray dose (G/6 3F x 0.33 Gy, n=13), (6) G/6 plus exposure to a single 1Gy dose (G/6 1 Gy, n=14). The single acute 1 Gy dose was given on Day 0; the fractionated 0.33 Gy X-ray dose was given on Days 0, 7, and 14. Sham exposed mice were treated in the same manner as those exposed mice but without radiation exposure. The dose-rate for these X-rays exposures was 0.191 Gy/min (Norelco MG300 X-ray industrial radiograph). Animals were irradiated prior to suspension on Day 0. At the A&M radiation laboratory mice were placed in a plastic box at the center of the beam. No anesthesia was used on Day 0 exposures. Animals in the fractionated dose

group (3F x 0.33 Gy) were anesthetized on Day 7 and 14 (ketamine100mg/kg + xylazine 10mg/kg) before leaving the vivarium to limit any ambulatory activity during the transportation and irradiation periods. Suspended mice were anesthetized but remained in suspension. All animals were given a subcutaneous injection of saline (0.25ml) to prevent dehydration.

^{28}Si Experiment

Four-month old female BALB/cBYJ mice (Jackson Laboratories, Bar Harbor, Maine) were ranked ordered by body weight and block assigned to one of 8 groups: (1) normal ambulatory cage control or 1 gravity group (1G SHAM, n=8), (2) 1G plus exposure to a single 0.17 Gy dose (1G 0.17 Gy, n=8) (3) 1G plus exposure to a fractionated 0.17 Gy ^{28}Si dose (1G 3F x 0.17 Gy, n=7), (4) 1G plus exposure to a single 0.5 Gy dose (1G 0.5 Gy, n=8), (5) 1/6th weight bearing group to simulate Lunar gravity (G/6 SHAM, n=11), (6) G/6 plus exposure to a single 0.17 Gy dose (G/6 0.17 Gy, n=9), (7) G/6 plus exposure to a fractionated 0.17 Gy ^{28}Si dose (G/6 3F x 0.17 Gy, n=11), (8) G/6 plus exposure to a single 0.5 Gy dose (G/6 0.5 Gy, n=10). The fractionated 0.17 Gy ^{28}Si dose was given on Days 0, 2, and 7. The single acute 0.5 Gy ^{28}Si dose was given on Day 0. The dose-rate for these radiation exposures was 0.25 Gy/min. The sham mice were treated similarly as the irradiate mice and positioned in the beam line but without radiation exposure. Due to logistical constraints at the NASA Space Radiation Laboratory (NSRL) the fractionated dose schedule differed from the X-ray experiment (Days 0, 7, and 14 versus Days 0, 2, and 7). All mice were placed in special 50ml conical tube foam rack system for sham and irradiation exposures. Animals in the

fractionated dose group (3F x 0.17 Gy) were anesthetized on Day 2 and 7 (ketamine100mg/kg + xylazine 10mg/kg) before placement into the tube/rack system to prevent ambulatory activity during irradiation.

For both experiments, the mice were acclimated for one week with standard conditions of temperature (23 ± 2°C) and light-controlled environment (12-hr light/dark cycle) and single-housed for two weeks prior to the experiment in cages with removable polypropylene perforated floors. Food (standard rodent chow, Harlan Teklad 8604) and water were available *ad libitum*. All animals were monitored for health and body weight was recorded daily.

For both experiments, animals were anesthetized with a ketamine:xylazine cocktail before euthanasia on day 21. To ensure the animals limbs did not bear weight to limbs prior to termination, all G/6 animals were anesthetized before removal from the suspension apparatus. Immediately after euthanasia cocktail injections, blood was collected via cardiac puncture, clotted and spun down to isolate serum. Following blood collection, animals were euthanized by decapitation and both femora and tibiae were harvested, stripped of soft tissue, and stored in either 70% ethanol at 4°C for micro computed tomography (μCT), histomorphometric analyses, wrapped in PBS-soaked gauze immediately and stored at −30°C for mechanical testing or snap frozen in liquid nitrogen and stored at -80°C for later determination of lipid peroxidation products.

Suspension Devices

Custom built mouse polycarbonate suspension cages (13" x 13" x 13") with removable polypropylene perforated floors were used in this experiment. The

suspension system was composed of a stainless steel rod, plastic pulley, i-hook, and spring. This suspension system was modeled after that designed and tested previously to provide easy access to food and water but prevent animals from resting against the cage walls (94).

A specialized weighing apparatus was built to allow accurate measurement of total body mass over the course of the experimental protocol and allow for $1/6^{th}$ weightbearing titrations as described previously (94). This custom precision engineered weighing apparatus was built around an electronic scale (Ohaus Corp., Pine Brook, NJ) for daily weighing of all mice while suspended in its suspension harness. Small adjustments to the i-hook screw and spring suspension system were made to maintain $1/6^{th}$ weightbearing over the course of the study. A more detailed overview of this suspension and weighing system has been previously described (94).

Micro-computed Tomography (μCT)

Right distal femurs were scanned *ex vivo* with microcomputed tomography (μCT SkyScan 1172; SkyScan, Kontich, Belgium) to quantify 2D and 3D micro architecture. A 60kV X-ray source was used over an angular range of 180° with 0.70° rotational steps. [Note: These uCT scans and reconstructions were performed in a colleague's laboratory (MR Allen, Indiana University School of Medicine, Indianapolis). Data reduction, statistical analysis, and interpretation of the results were performed by BR Macias.] Six micrometer resolution projection images generated, reconstructed and analyzed (NRecon and CTAn; SkyScan). For cancellous bone measurements, a 1mm segment within the distal metaphysis secondary spongiosa was identified and manually

traced. To distinguish between bone from soft tissue a threshold was applied (range, 100 to 255), and specimen analyzed in 3D for bone volume/ trabecular volume (BV/TV), trabecular number (Tb.N), and trabecular thickness (Tb.Th). One slice, 3 mm proximal to the most distal end of the metaphyseal segment was analyzed to determine cortical bone area (Ct.Ar), polar moment of inertia (*J*), and Ct.Th. All nomenclature used follows those guidelines established for micro-computed tomographic evaluation of bone (13).

Cortical Dynamic Histomorphometry Analysis

Intraperitoneal injections of calcein (Sigma Chemical, St. Louis, 15 mg/kg body weight) was administered for fluorochrome labeling 7 and 2 days prior to euthanasia. Undemineralized distal left tibiae were serial dehydrated and embedded in methylmethacrylate (Sigma-Aldrich M5, 590-9, St. Louis, MO). Serial cross sections (150 to 200 μm) of cortical bone were sectioned (Isomet diamond wafer low-speed saw: Buehler, Lake Bluff, IL) proximal to the tibiofibular junction (TFJ), rinsed of dust debris and mounted on glass slides. The histomorphometric analyses were performed by using the OsteoMeasure Analysis System, Version 1.3 (OsteoMetrics, Atlanta, GA). Measures of labeled surfaces and interlabel widths were obtained at 200x magnification of two sections per animal. If double label did not appear on the first two sections an additional two sections we obtained to search for double label. After an exhaustive search and no double label observed a value of 0.3 um/day was used as the estimated physiological lower limit of MAR (22,66). Periosteal and endocortical mineral apposition rates (MAR, μm/d) were calculated by dividing the average interlabel width by the time

between labels (5 days), and mineralizing surface (MS) for both periosteal and endocortical bone surfaces (BS) using the formula %MS/BS = {(single-labeled surface/2) + double-labeled surface]/surface perimeter} X 100. Bone formation rate (BFR) was calculated as (MAR x MS/BS).

Sclerostin Immunohistochemistry

The distal half of left femora were fixed in 4% phosphate-buffered formalin for 48 hours at 4ºC, then decalcified in a sodium citrate-formic acid solution for 14 days, and stored in 70% EtOH. Five millimeter midshaft femoral cross sections were cut and placed in cassettes for paraffin embedding. Following decalcification, they were embedded in paraffin and transverse cortical sections at the midshaft were cut 8 μm thick and mounted on slides. Tissues were processed for sclerostin IHC as described previously (50). Tissues were then placed on a wet-incubation tray and each sample was loaded with the sclerostin primary antibody (1:500 dilution, R&D Systems, Minneapolis, MN) and incubated at 4°C overnight. The quantification of total (N.Ot) and sclerostin-positive osteocytes (SOST+ Ot) was performed over the entire cortical bone cross-section using the OsteoMeasure Analysis System, Version 1.3 (OsteoMetrics, Atlanta, GA). The percentage of sclerostin-positive osteocytes was calculated as (SOST+ Ot/Total Ot) X 100.

Serum TRAP 5b

To quantify systemic osteoclast number, serum concentrations of TRAP 5b were measured. TRAP5b levels were determined by with a TRAP 5b ELISA kit (IDS, Fountain Hills, AZ) according to the manufacturer's instructions. Assay results were

analyzed using a DTX 880 microplate reader (Beckman Coulter; Brea, CA). The intra- and inter-assay coefficients of variation were < ± 6.5% and 8%, respectively for this ELISA kit.

Lipid Peroxidation

Tibias were snap-frozen and stored at -80°C. Whole tibias were pulverized into a fine powder with a mortar and pestle, kept cold with liquid nitrogen. The pulverized bone sample was resuspended in 20 mM of ice-cold PBS. The manufacturer's standard ELISA recommended protocol was followed for the quantification of the decomposed lipid peroxidation products malondialdehyde (MDA) and 4-hydroxyalkenals (HAE) (Oxford Biomedical Research, Inc., Oxford, MI).

Mechanical Testing

Femoral necks for mechanical testing were brought to room temperature and wrapped in PBS soaked gauze before testing to failure on an Instron 3345 as previously described (82). [Note: These mechanical tests were performed in a colleague's laboratory (HA Hogan, Mechanical Engineering, Texas A&M University). BR Macias was assisted by students in Dr. Hogan's laboratory to perform these mechanical tests. In addition, data reduction, statistical analysis, and interpretation of the results were performed by BR Macias.] In short, the proximal half of the femur was placed upright in a custom metal plate support. A quasi-static load was applied in displacement control at 1.27 mm/min. The applied load was measured with a 100 Newton (N) load cell. All data collected during tests were digitized and analyzed by Bluehill software (version 2.14.582, Instron Bluehill).

Statistical Analysis

All data are presented as mean ± standard deviation (SD) and evaluated using the statistical package SPSS (v.15; Chicago, III). Body mass data are presented as mean ± standard error (SE) for graphical clarity. Data were analyzed using a 2-way ANOVA to test the main effects of partial weightbearing and radiation, with interactions. A fisher's least significant difference post hoc analyses were performed for pairwise comparisons. For all data, statistical significance was accepted at $p<0.05$.

Results

Body weight is reduced during partial weightbearing as compared to cage controls but added radiation exposure does not cause further losses (Figure 5 and 6).

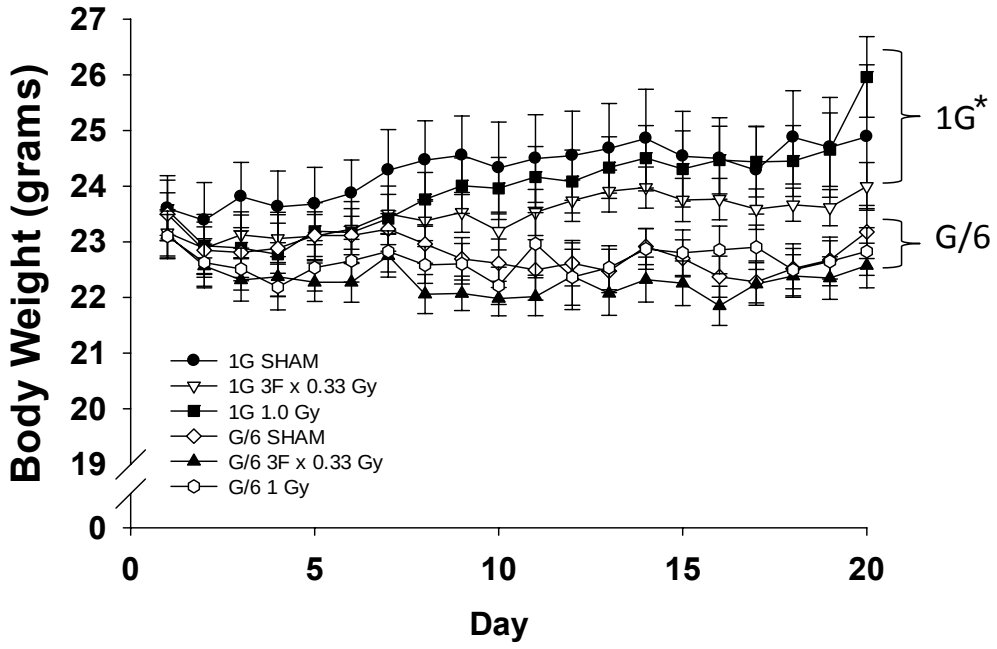

Figure 5. Effects of G/6 weightbearing and X-ray radiation exposure on body mass. Data are presented as mean ± standard error (SE) for graphical clarity. *The 1G group is significantly different on day 21 from G/6, $P<0.05$.

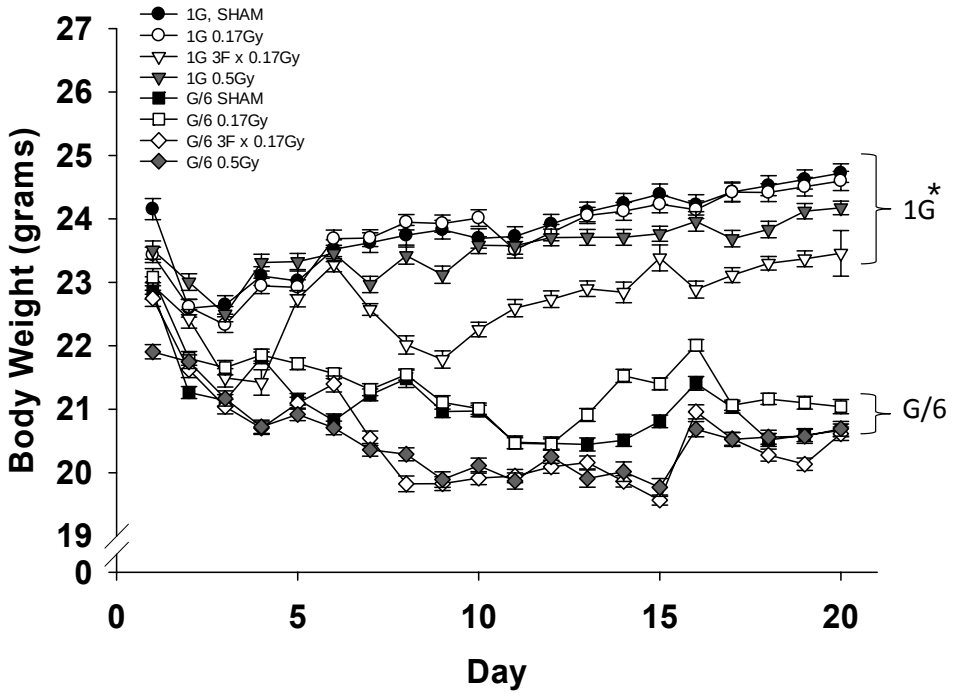

Figure 6. Effects of G/6 weightbearing and ^{28}Si radiation exposure on body mass.
Data are presented as mean ± standard error (SE) for graphical clarity. *The 1G group is significantly different on day 21 from G/6, $P<0.05$.

Partial Weightbearing and Radiation Exposure Result in Cancellous Bone Loss

Partial weightbearing (G/6) for 21-days results in lower percent BV/TV at the distal femur compared to the full weightbearing cage controls (1G) (Figure 7A and 7D). Fractionating the 1.0 Gy X-ray dose mitigated decrements in cancellous microarchitecture both at 1G and G/6 (Figure 7A-C). Surprisingly however, fractionating ^{28}Si did not show the same protective effect as fractionated X-rays (Figure 7D-F). During full weightbearing, three fractions of 0.17 Gy ^{28}Si produced a 18% lower BV/TV and one acute 0.5 Gy ^{28}Si dose produced a 14% lower BV/TV, compared to SHAM exposed (Figure 7D).

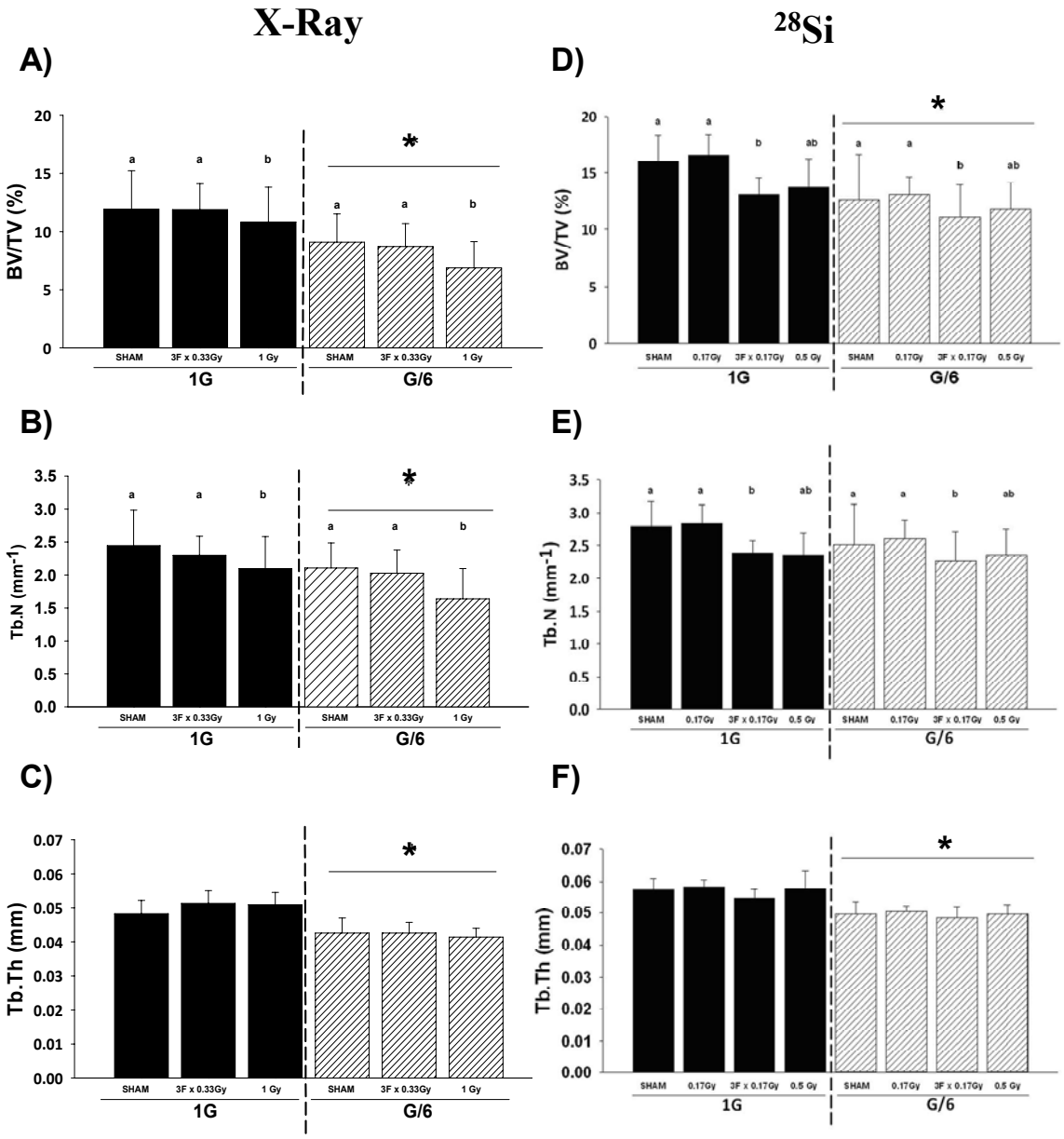

Figure 7. Cancellous microarchitecture during partial weightbearing and X-ray or ^{28}Si exposure. X-ray: A) BV/TV, Bone Volume B) Tb.N, Trabecular Number C) Tb.Th, Trabecular Thickness. Cancellous microarchitecture during partial weightbearing and ^{28}Si exposure: D) BV/TV, Bone Volume. E) Tb.N, Trabecular Number F) Tb.Th, Trabecular Thickness. *significant main effect for load condition (1G versus G/6, $p<0.05$). Those radiation groups within the respective 1G or G/6 load condition not sharing the same letter are significantly different, $p<0.05$.

Similarly, during partial weightbearing, three fractions of 0.17 Gy ^{28}Si produced a 12.3% lower percent BV/TV and one acute 0.5 Gy ^{28}Si dose showed a 8.8% lower BV/TV compared to SHAM exposed (Figure 7D). The highest X-ray dose, 1 Gy, when combined with partial weightbearing, resulted in 33% lower Tb.N compared to full weightbearing SHAM controls (Figure 7B). The magnitude of loss in percent BV/TV was greater when X-ray exposure was combined with partial weightbearing. In addition, fractionating an X-ray dose during partial weighbearing reduced BV/TV by 4% compared to partial weightbearing SHAM exposed animals, not observed in the full weightbearing groups, suggesting that fractionating low LET during partial weightbearing may show a small but different effect compared to that observed during full weightbearing. Partial weightbearing reduced Tb.Th by ~12-13% in both the ^{28}Si or X-ray experiments. X-ray and ^{28}Si exposure during full- or partial-weightbearing conditions did not impact Tb.Th.

Partial Weightbearing and Radiation Exposure Impact Cortical Bone Geometry

X-ray exposure did not cause significant decrements in Ct.Ar, J, or Ct.Th (Figure 8A-C). Partial weightbearing suppressed the cortical bone growth at the mid shaft femur (Figure 8D). The fractionated ^{28}Si radiation dose resulted in a lower Ct.Ar. compared to a full single radiation dose during full weightbearing (Figure 8D). Similarly, polar CMSI (J), was lower with G/6 compared to full weightbearing (Figure 8E). When ^{28}Si radiation exposure was combined with partial weightbearing, the decrements in Ct.Ar and J are similar to the G/6 SHAM group but lower than the 1G groups.

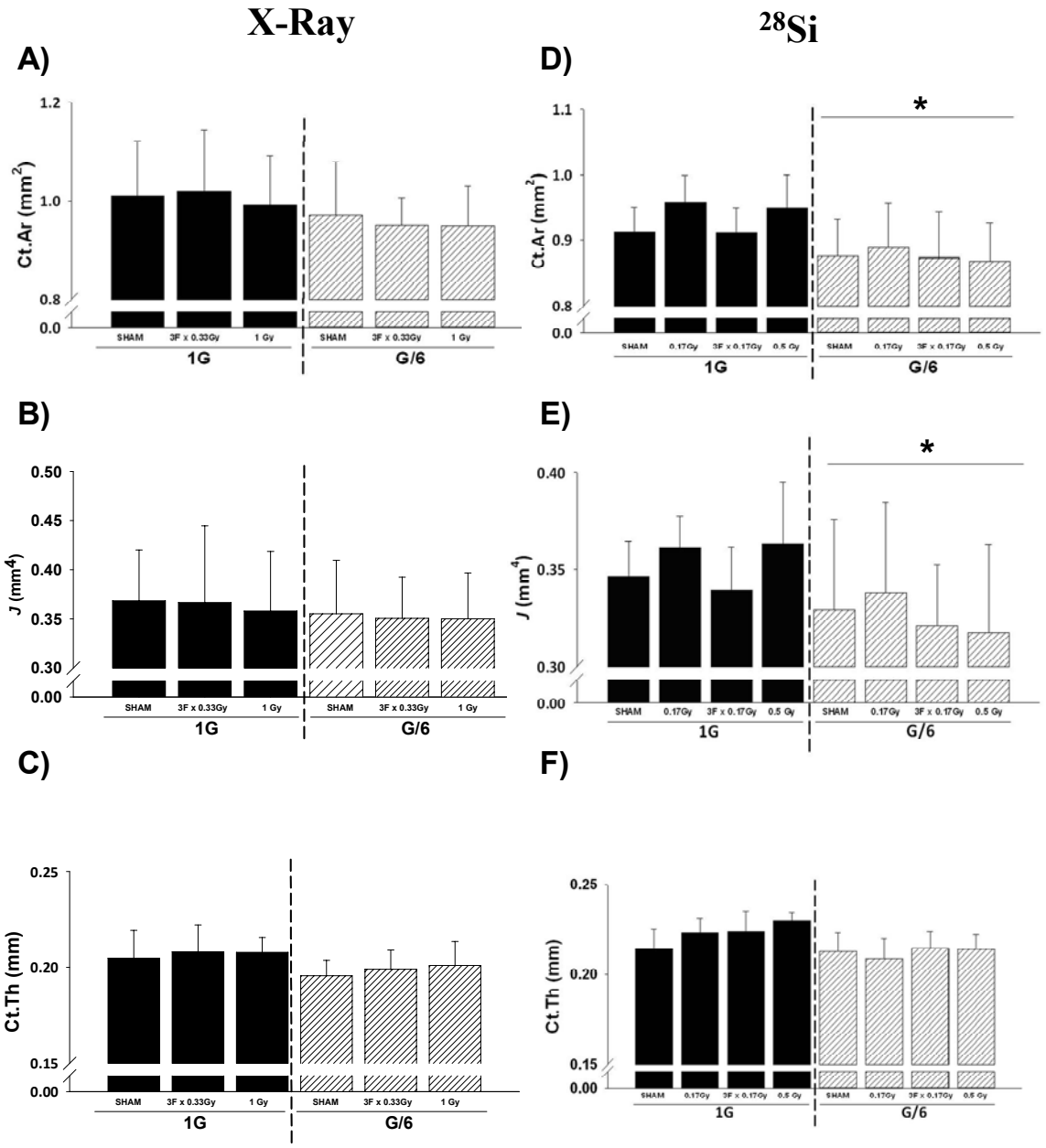

Figure 8. Partial Weightbearing, X-ray radiation, and ^{28}Si radiation effects on midshaft femoral cortical geometry. X-ray radiation: A) Cortical bone area, Ct.Ar. B) Polar moment of inertia, J C) Cortical thickness, Ct Th; ^{28}Si radiation: A) Cortical bone area, Ct.Ar. B) Polar moment of inertia, J C) Cortical thickness, Ct Th. *significant main effect for load condition (1G versus G/6, $p<0.05$).

Partial Weightbearing and Radiation Exposure Reduce Femoral Neck Strength

All groups exposed to partial weightbearing show lower femoral neck strength (Figure 9A and 9D). Partial weightearing combined with a fractionated 0.5 Gy dose of ^{28}Si exacerbates disuse-related reductions in femoral neck strength compared to 1G SHAM or the 1G fractionated dose (p=0.003). Partial weightbearing, radiation, or the combination of those factors did not significantly lower femoral neck stiffness (Figure 9B and 9E).

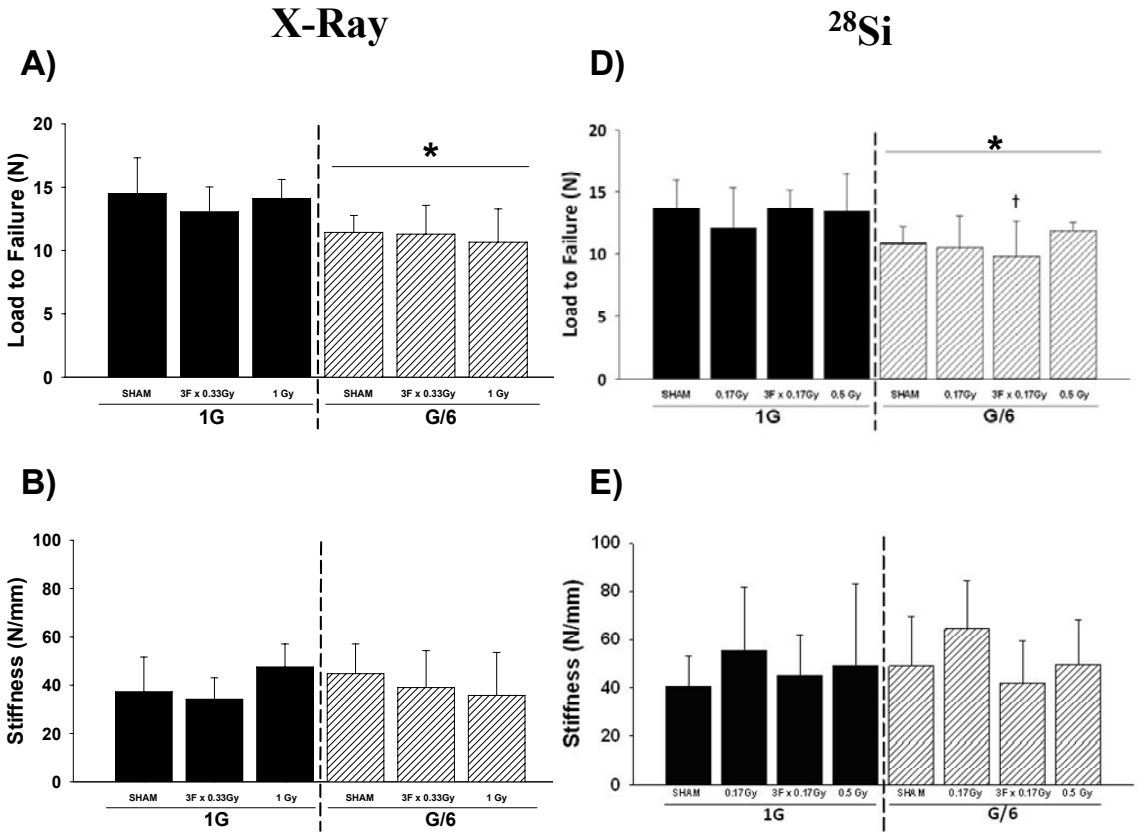

Figure 9. Partial Weightbearing and radiation effects on femoral neck mechanical properties. A) Partial weightbearing and ^{28}Si radiation exposure lower load to failure of the femoral neck. B) Partial weightbearing and X-ray radiation exposure lower load to failure of the femoral neck. C) Partial weightbearing and ^{28}Si radiation effects on femoral neck stiffness. D) Partial weightbearing and X-ray radiation effects on femoral neck stiffness. *significant main effect for load condition (1G versus G/6, $p<0.05$). † Significantly different from 1G 3F x 0.17 Gy group (p=0.003).

Partial Weightbearing Elevates Marker of Osteoclast Number

Partial weightbearing elevates serum TRAP5b levels, a marker of osteoclast number (Figure 10). There was no independent effect of ^{28}Si radiation.

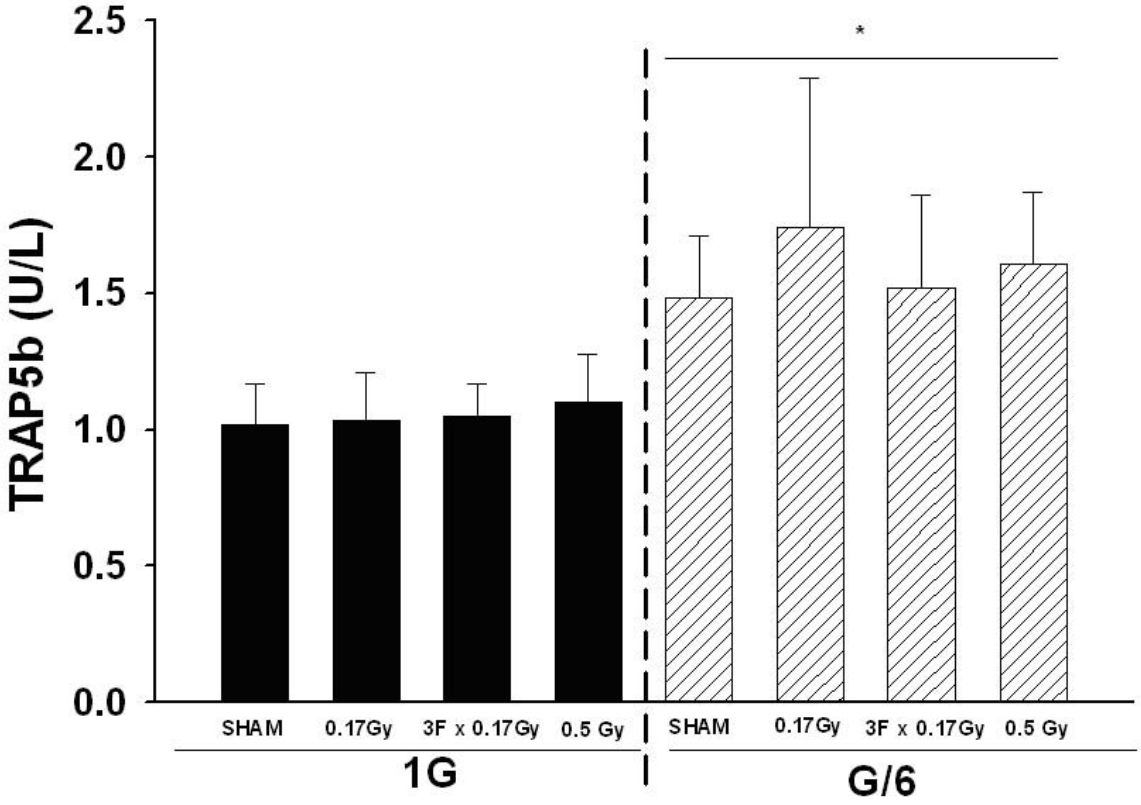

Figure 10. Partial Weightbearing for 21-days and ^{28}Si radiation exposure elevates serum TRAP 5b levels compared to 1G cage controls animals. The values are given as mean ± SD. *significant main effect for load condition (1G versus G/6, $p<0.05$).

Partial Weightbearing Combined with ^{28}Si Radiation Exposure Exacerbates the Proportion of Cortical Sclerostin-Positive Osteocytes

The proportion of sclerostin positive osteocytes in cortical bone was higher during G/6 then 1G (Figure 11A and 11B). Unexpectedly, added ^{28}Si radiation exposure during partial weightbearing significantly raised the proportion of sclerostin-positive osteocytes at the mid shaft femur (Figure 11A). X-ray radiation exposure combined with partial weightbearing does not appear to cause the same effect (Figure 11B). However

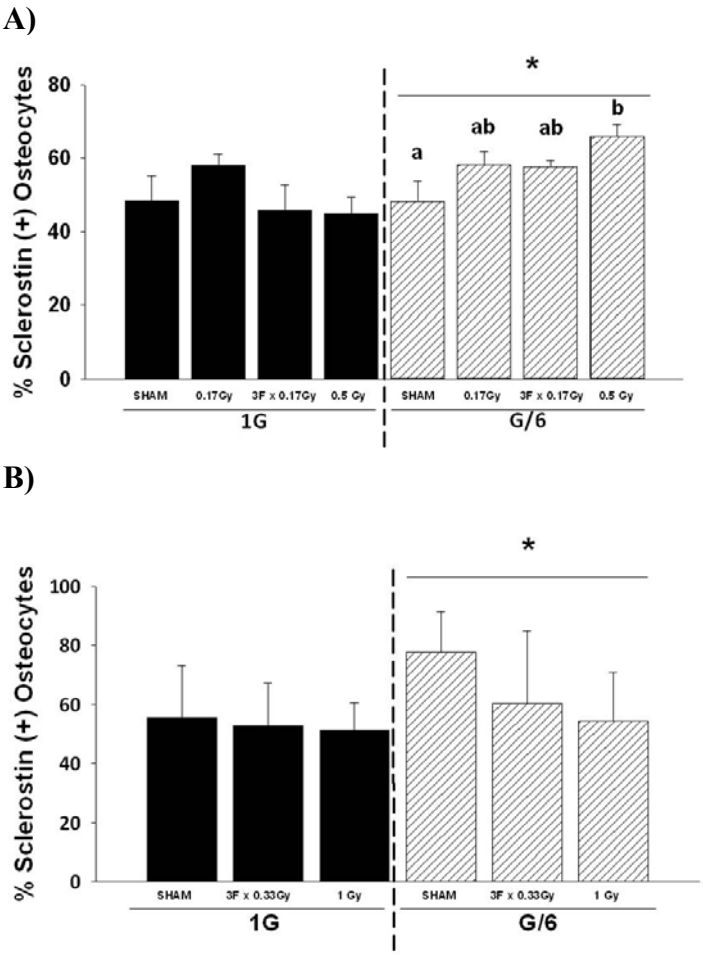

Figure 11. Proportion of sclerostin positive osteocytes during partial weightbearing and radiation exposure. A) Partial weightbearing and ^{28}Si radiation exposure demonstrates a higher proportion of sclerostin positive osteocytes. B) Partial weightbearing groups demonstrate a higher proportion of sclerostin positive osteocytes. *significant main effect for load condition (1G versus G/6, $p<0.05$). Within the G/6 load condition those groups not sharing the same letter are significantly different, $p<0.05$.

due to limited availability of tissue samples in the combined X-ray and partial weightbearing groups (n=6) we can not conclude if low-dose low LET causes the same elevation of cortical sclerostin positive osteocytes as observed in the ^{28}Si radiation experiment. Nevertheless, in the X-ray experiment we find significantly higher proportion of sclerostin positive osteocytes compared to the full weightbearing controls.

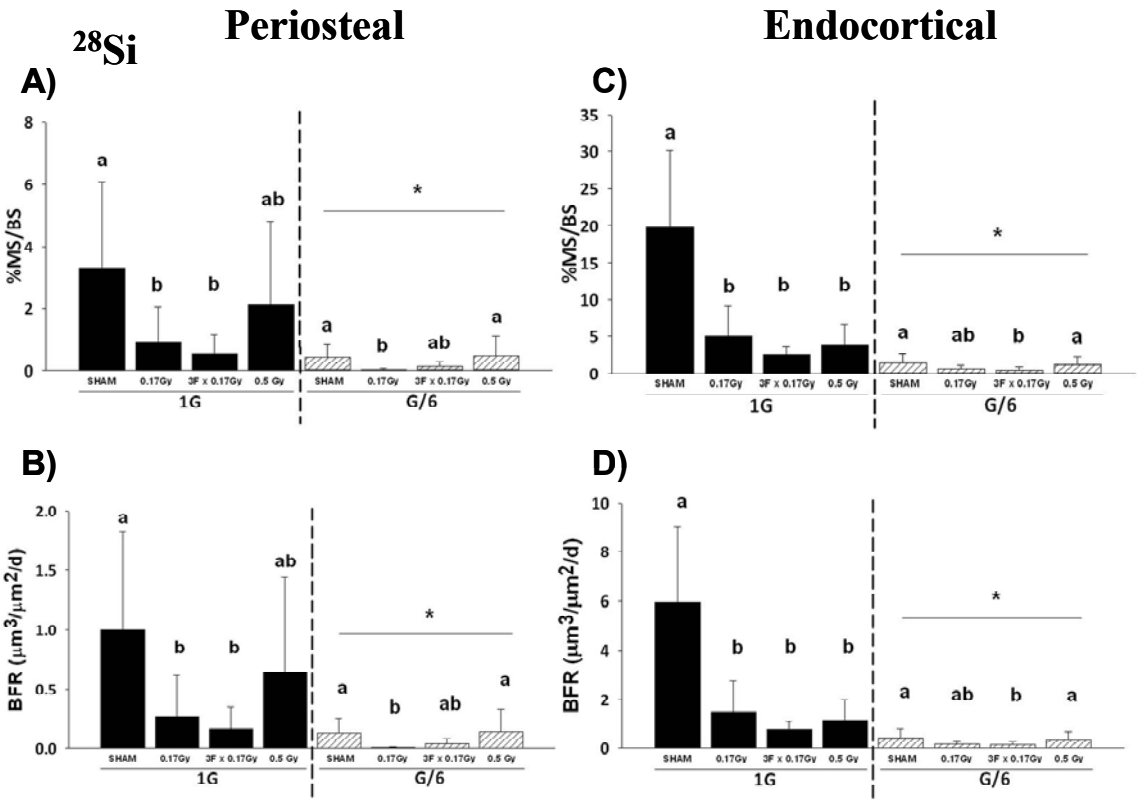

Figure 12. Partial Weightbearing and ^{28}Si radiation effects on tibial cortical dynamic histomorphometry Effects of reduced gravitational loading on periosteal and endocortical bone surface dynamic histomorphometric analyses measured at the tibia mid-diaphysis. A: Periosteal mineralizing surface (MS/BS). B: Periosteal bone formation rate (BFR). C: Endocortical mineralizing surface (MS/BS). D: Endocortical bone formation rate (BFR).The values are given as mean ± SD. *significant main effect for load condition (1G versus G/6, $p<0.05$). Those radiation groups within the respective 1G or G/6 load condition not sharing the same letter are significantly different, $p<0.05$.

Weightbearing at Less Than 1G Suppresses Bone Formation

Partial weighbearing potently suppresses mineralization on both periosteal and endosteal surfaces (Figures 12 and 13). Interestingly, a fractionated ^{28}Si exposure during full weightbearing conditions showed further reductions in MS/BS as compared to SHAM exposed mice (Figure 12C). The fractionated dose group shows a similar suppression of bone formation as compared to the single full dose during partial weightbearing.

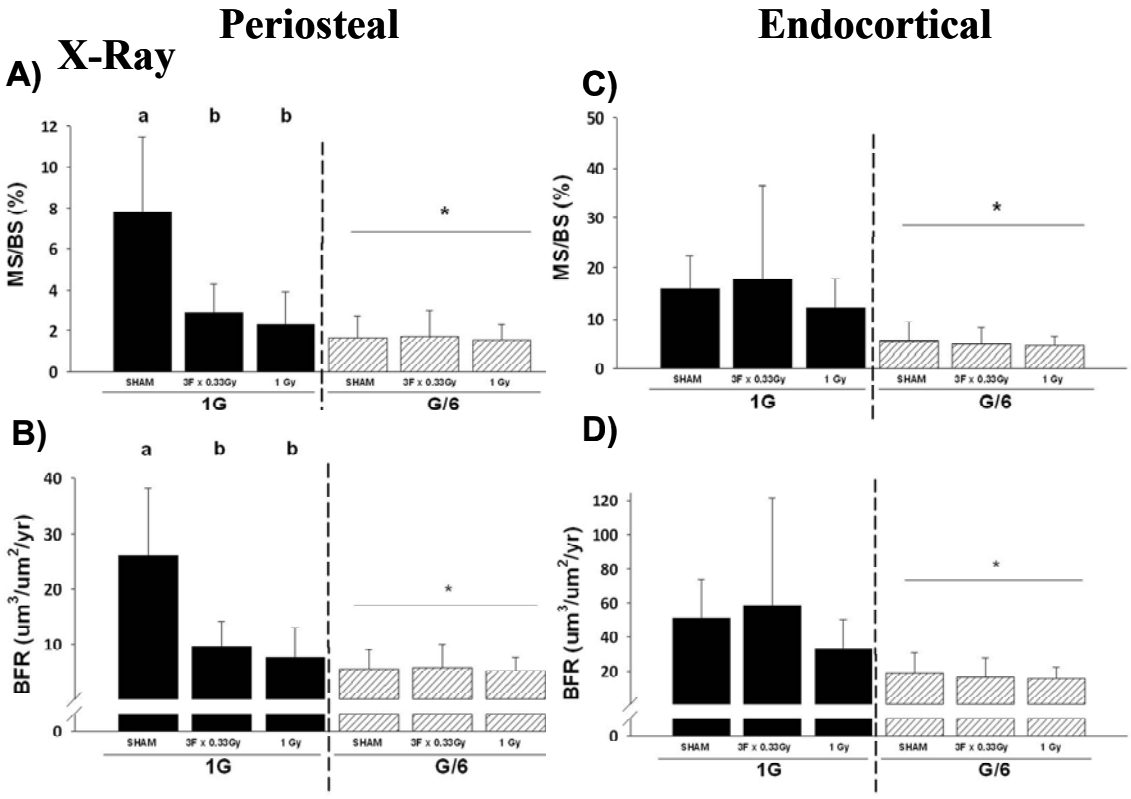

Figure 13. Partial Weightbearing and X-ray radiation effects on tibial cortical dynamic histomorphometry. Effects of reduced gravitational loading on periosteal and endocortical bone surface dynamic histomorphometric analyses measured at the tibia mid-diaphysis. A: Periosteal mineralizing surface (MS/BS). B: Periosteal bone formation rate (BFR). C: Endocortical mineralizing surface (MS/BS). D: Endocortical bone formation rate (BFR). *significant main effect for load condition (1G versus G/6, $p<0.05$). Those radiation groups within the respective 1G or G/6 load condition not sharing the same letter are significantly different, $p<0.05$.

Lipid Peroxidation

A single 0.5 Gy dose of ^{28}Si during full weightbearing caused a significant doubling of MDA+4HNE in whole tibia homogenates compared to 0 Gy SHAM exposed (Figure 14).

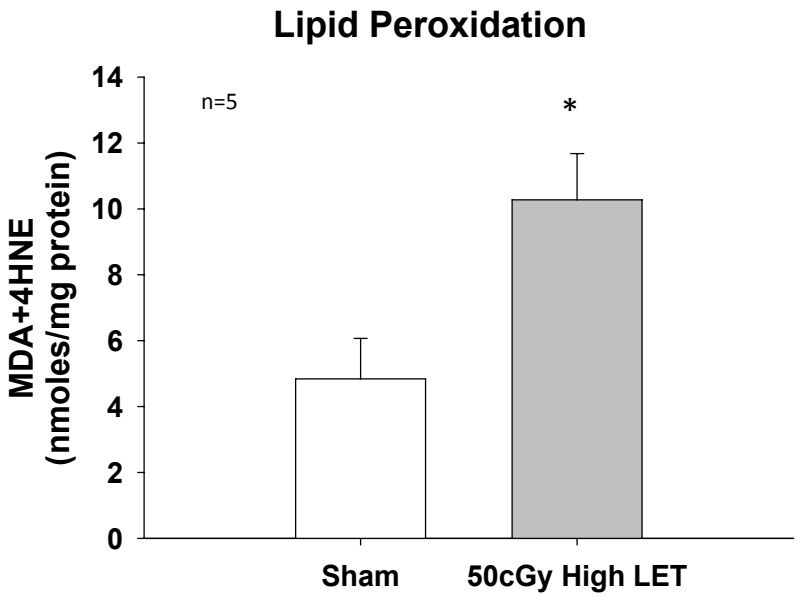

Figure 14. The highest acute ^{28}Si radiation dose during 1G raises lipid peroxidation levels in tibias after 21-days. *unpaired t-test, significantly different from SHAM exposed, p=0.031.

Discussion

In support of our hypothesis, low-dose high LET radiation exposure exacerbates cancellous bone loss (BV/TV) seen with partial weightbearing. Fractionating low-dose high LET radiation (^{28}Si) does not prevent cancellous bone loss. However, fractionating low-dose low LET radiation (X-rays) does protect against cancellous bone loss during

full weightbearing conditions. Thus, the present data suggest that the effect of fractionation is dependent on LET for cancellous bone tissue.

Dividing a large gamma or proton radiation dose into small fractions is a common therapeutic strategy to deliver a sufficient radiation dose, for example 5-10 Gy to pathological tissue but spare neighboring healthy normal tissue (102). Therefore, utilizing fractionated doses regimes similar to those used in the present study may better simulate the low-dose rate exposures observed in space.

As expected, midshaft cortical areas of the partial weightbearing groups were smaller than in weightbearing cage controls. At the lower 0.5 Gy ^{28}Si dose tested in the present study there were not significant negative effects on femoral neck mechanical properties. Exposure to radiation doses 2-Gy and above may potently suppress cortical bone growth, potentially masking differences between low- and high LET effects. In addition, these studies further highlight the temporal and tissue dependent effects of radiation exposure.

Three low-dose high LET radiation exposures cause similar cancellous bone loss as compared to a single dose. At higher radiation doses cancellous bone loss after 110-days of 2 Gy high LET (^{56}Fe) radiation or low-LET (gamma) radiation were similar (28). Similar to our findings, doses as low as 0.5 Gy ^{56}Fe radiation demonstrate significant impacts on cancellous bone loss (100).

X-ray radiation impairs osteoblast proliferation and enhances osteoclast maturation (46). The present data show more circulating osteoclasts as evidenced by the higher serum TRAP5b levels in G/6 groups with or without radiation. Radiation induced

elevation of TRA5b is up by 50% as early as 1-day following 2-Gy X-ray radiation, and TRAP5b has been shown to remain elevated 3-days following irradiation by 14% (96). Moreover, higher lipid peroxidation of whole tibia homogenates 21-days after radiation exposure suggests persistent radiation induced oxidative damage in bone tissue. It has been reported previously that oxidative stress can lead to higher bone resorption (37). Limited numbers of snap frozen tissues limited lipid peroxidation measurement to sham and 50 cGy ^{28}Si full weightbearing groups. The present data suggest that lipid peroxidation of bone tissue may play a role in radiation induced bone loss.

Both partial weightbearing and radiation exposure impair bone formation rate, primarily as a result of a lower MS/BS. This lower MS/BS may indicate impairment of pre-osteoblast proliferation capacity or fewer osteoblasts directed to bone surfaces. We find a lower cortical bone formation rate with partial weightbearing exposure than with radiation exposure during full weightbearing. This disuse-associated suppression of cortical bone formation is consistent with previous investigations (37).

Radiation, especially high-LET radiation, generates a substantial amount of reactive oxygen species, namely hydroxyl radicals (27). Reports suggest that Wnt signaling is antagonized by oxidative stress (52). Nitric oxide is one key molecule implicated in signal transduction of mechanical signals in bone tissue to osteoblasts and osteocytes (14). Thus, elevated levels of reactive oxygen species beyond endogenous cellular antioxidants capacity could quench this mechanically induced nitric oxide signal. This reduction in nitric oxide levels could result in lower than normal mechanical loading signals to osteoblasts and osteocytes leading to an increase in

sclerostin production. Alternatively, radiation-induced suppression of osteoblast proliferation may indirectly result in higher sclerostin-positive osteocytes. Recent data suggest that the mechanical loading-mediated downregulation of sclerostin expression in osteocytes is located near regions of new bone formation (59). Therefore, radiation-induced suppression of osteoblastogenesis could lower the number of mature osteoblasts on bone surface and prevent local signal processing between osteocytes nearby bone cells, resulting in more sclerostin-positive osteocytes.

BALB/cBYJ are highly responsive to the mechanical load environment (33). Thus, use of the BALB/c mice strain may have limited our ability to detect small enhancement of bone loss due to radiation effects when combined with reduced weightbearing. However, utilization of BALB mice for these series of experiment enables direct comparisons with previous data from partial weightbearing literature (46,94).

Data on bone quality during or after Lunar missions do not exist. Moreover, no data exist testing the skeletal consequences of combining low-dose high-LET radiation and partial weightbearing. NCRP's report 98 highlights the need for more data on the effects of low-dose high-LET radiation.

In support of our hypothesis, low-dose high LET radiation exposure during partial weightbearing conditions exacerbates cancellous bone loss (BV/TV). In addition, fractionating our higher ^{28}Si dose does not prevent cancellous bone loss. Radiation-induced oxidative stress may explain some of the resultant cancellous bone loss. The number of sclerostin positive osteocytes is higher when exposed to partial weightbearing

and added low-dose high LET radiation compared to SHAM controls. It remains to be determined if bone mass can recover following low-dose high LET exposure. Exercise regimens that reproduce high impact force profiles observed during full weightbearing are an essential component of the bone loss mitigation strategy for both crew members and clinical population.

CHAPTER IV

COMBINED SIMULATED RESISTANCE TRAINING AND GSK3 INHIBITION INCREASES BONE MASS DURING DISUSE

Introduction

Approximately 1.5 million osteoporotic-related fractures occur annually in the United States (9) and these fractures are one of the most common causes of disability (20). As a result, the direct care expenditures for osteoporotic fractures are estimated to be as high as $17.9 billion (86).

Weight bearing exercise early in life contributes to high peak bone mass; however, bone loss ensues if the exercise program terminates (34). Mechanical loading of bone, as during high impact exercise activities, induces site-specific changes in bone architecture and increased bone mass (30,43). Moreover, regular physical activity improves mobility and muscle function; it may also indirectly reduce the risk of falls thereby reducing fracture incidence. In fact, exercise during extreme periods of disuse in humans such as bed rest maintains aerobic capacity (44), promotes bone formation (80), and maintains lumbar spine structure and function (49).

Reduced weightbearing conditions during spaceflight result in 1-2% bone loss per month of preflight baseline values at the femoral neck and lumbar spine (40). The rodent hindlimb unloading (HU) model is a well-established ground-based model for investigating disuse effects on bone (58). Recently, high intensity muscle contractions at 75-to-100% peak isometric torque (P_0), produced during simulated resistance training

(SRT) undertaken during a period of HU show significant gains in mid-diaphyseal tibia cortical bone mineral density (BMD) (50,83). These gains were associated with a 2.6- to 5-fold greater periosteal bone formation rate as compared to control animals (50,83). Therefore, high intensity exercise provides some protection against disuse-induced bone loss in rodent ground based simulations of microgravity.

Data over the last ten years strongly suggests that the Wnt pathway is a major regulator of bone formation; however, the basic molecular mechanisms governing the osteogenic response to mechanical load are unknown. Loss-of-function mutation of the low-density lipoprotein receptor-related protein 5 (Lrp5) gene impairs the response to mechanical load and decreases osteoblast proliferation and bone mass (24). Mechanical loading promotes formation of the Wnt-LRP4/5/6-Frizzled transmembrane complex. Formation of the receptor complex permits disheveled (Dsh) to inhibit the cytoplasmic formation of GSK-3β, APC and Axin-2 and allowing intracellular β-catenin levels to rise. Once β-catenin levels are sufficiently high, β-catenin translocates to the nucleus where it associates with T-cell factor (TCF)/lymphoid enhancer-binding factor (LEF) transcription factors to activate the osteogenic gene expression program (18). Moreover, the Wnt pathway functions to coordinate communication between mechanosensing osteocytes (via secreted sclerostin) and bone-forming osteoblasts by the binding of sclerostin to other Lrp receptors, for example Lrp4 and Lrp6 (16,47,98).

GSK-3β is a key modulator of the Wnt signaling pathway and has been a target of drug development to resolve metabolic and neurological diseases. Inhibition of GSK-3β can normalize blood glucose levels in an animal model (17) and suppress neuronal

apoptosis (6). Given the efficacy of GSK-3β inhibitors to affect downstream Wnt signaling, they have recently been used to experimentally activate Wnt signaling in bone cells and increase bone mass in rodent models (38,54). GSK-3β inhibition prevents ovariectomized-induced femoral bone loss in rodents (38). In another report, femoral cancellous and cortical BMD were higher when treated with a GSK-3β inhibitor as compared to vehicle-treated controls (54). However, it is unclear whether inhibition of GSK-3β can mitigate bone loss during disuse or how GSK-3β inhibition interacts with increased mechanical loading.

Current exercise hardware and exercise prescriptions performed during ISS missions (~6 months) does not completely prevent musculoskeletal deconditioning but may mitigate some of the musculoskeletal loss (73,76,78,81,87). Recent data show that when exercise on the advanced resistive exercise device (aRED) is combined with adequate nutrition astronauts show no net bone loss after 6 month ISS missions at most bone sites (76). These human exercise evaluations during microgravity provide further evidence that high impact resistive exercise prescriptions are necessary to prevent bone loss during long duration space missions.

Pharmaceuticals targeting the Wnt signaling pathway are currently being developed to treat osteoporosis and aid fracture healing (NCT01144377). It is unclear how pharmaceutical perturbations of Wnt signaling during disuse or with exercise affect bone loss. Therefore, the purpose of this study was to investigate the interaction of GSK-3 inhibition and resistance exercise imposed during simulated microgravity. We hypothesized that simulated resistance training combined with a GSK-3 inhibitor

treatment during hindlimb unloading would most effectively mitigate disuse-induced decrements in cancellous and cortical bone geometry.

Materials and Methods

Animals and Experimental Design

Forty male, Sprague-Dawley rats (6-mo-old) were obtained from Harlan (Houston, TX) at 6 months of age and allowed to acclimate for 14 days prior to initiation of the study. All animals were singly housed after arriving at our animal facility in a temperature-controlled (23 ± 2ºC) room with a 12-hour light-dark cycle in an American Association for Accreditation of Laboratory Animal Care-accredited animal care facility and were provided standard rodent chow (Harlan Teklad 8604) and water ad-libitum. Animal care and all experimental procedures described in this investigation were approved by the Texas A&M University Laboratory Animal Care Committee.

Six experimental groups were studied: (1) cage control (CC+Vh, n=10), (2) CC animals administered a GSK-3 inhibitor 0.2mg/kg (2'Z,3'E)-6-Bromoindirubin-3'-oxime (BIO) via subcutaneous injection once per week (CC+BIO, n=10), (3) hindlimb unloaded (HU+Vh, n=10), (4) HU animals administered 0.2mg/kg BIO via subcutaneous injection 1 time/week (HU+BIO, n=10), (5) HU subjected to simulated resistance training (HU+SRT/Vh, n=10), and (6) HU rats subjected to both BIO and SRT (HU+SRT/BIO, n=10). All animals completed the 28-day protocol and maintained normal activity and appeared healthy. Animals in all groups except CC underwent 28 days of HU. HU+SRT and HU+SRT/BIO animals underwent 9 sessions of simulated

resistive exercise conducted once every three days during the 28 day protocol. The CC animals were allowed normal ambulatory cage activity.

Calcein injections (25 mg/kg body mass) were given subcutaneously 9 and 2 days prior to euthanasia to label mineralizing bone for histomorphometric analysis. HU animals were anesthetized before removal from tail suspension at the end of the study to prevent any weight bearing by the hindlimbs. At the end of the experiment, on day 28, all animals were anesthetized with 50 mg/kg BW of ketamine (Fort Dodge Animal Health; Fort Dodge, IA) and 0.5 mg/kg BW of medetomidine (Pfizer; New York, NY) and euthanized by decapitation. Approximately 5 to 6 ml of blood was collected by cardiac puncture and allowed to clot for 20 minutes before centrifugation. Serum was collected and stored at -80°C until analysis. Proximal left tibiae were fixed in formalin, then stored in 70% ethanol at 4°C for histomorphometry analyses; proximal femurs were thoroughly cleaned of soft tissue, wrapped in gauze soaked with phosphate-buffered saline (PBS), and stored at -20°C for *ex vivo* pQCT scanning and mechanical testing.

Hindlimb Unloading

Hindlimb unloading was achieved by tail suspension as previously described (82). The height of the animal's hindquarters was adjusted to prevent any contact of the hindlimbs with the cage floor, resulting in approximately a 30° head-down tilt. The forelimbs of the animal maintained contact with the cage bottom, allowing the rat full access to the entire cage. All animals were monitored daily for health, including assessment of tail integrity, and body weights were measured weekly.

Simulated Resistance Training (SRT) Paradigm

Simulated resistance training was completed as previously described (100). Briefly, left plantarflexor muscles from animals in the HU+SRT/Vh and HU+SRT/BIO groups were trained once every 3 days during 28-day HU using a custom-made rodent isokinetic dynamometer. Animals were anesthetized with isoflurane gas (~2.5%; Minrad Inc., Bethlehem, PA) mixed with oxygen before removal from tail suspension to prevent any weight bearing by the hind limbs. Each rat was then placed in right lateral recumbency on a platform, the left foot was secured onto the foot pedal, and the left knee was clamped so that the lower leg was perpendicular to the foot and the femur and tibia were at right angles to each other. This was referred to as the resting, 0° position. For isometric contractions, the foot pedal was held fixed in this position; to generate eccentric contractions of the plantarflexor muscles, the foot pedal moved the foot into 40° of dorsiflexion. For all contractions, the footplate was rotated in synchrony with muscle stimulation by a Cambridge Technology lever system (Model 6900) interfaced with a 80486 66-MHz PC using custom software written in TestPoint (v.4.0; Capital Equipment Corp., Billerica, MA). Torque generated around the footplate pivot (at the rat's ankle joint) was measured by the lever system's servomotor. Plantarflexor muscle stimulation was performed with fine wire electrodes consisting of insulated chromium nickel wire (Stablohm 800B, H-ML Size 003, California Fine Wire Co.), inserted intramuscularly straddling the sciatic nerve in the proximal thigh region. The stimulation wires were then attached to the output poles of a Grass Instruments stimulus isolation unit (Model SIU5; Astro-Med, Inc; W. Warwick, RI) interfaced with a

stimulator (S88; Astro-Med, Inc; W. Warwick, RI) which delivered current to the sciatic nerve and induced muscle contraction.

Voltage optimization to achieve peak isometric torque and stimulation frequency optimization of the eccentric torque were performed at the beginning of each session, as described previously (83). The eccentric phase of the muscle contraction was titrated to equal ~75% of each animal's daily peak isometric torque (P_o). The HU+SRT/Vh and HU+SRT/BIO animals completed a combined isometric+eccentric simulated resistance training (SRT) exercise paradigm, consisting of 4 sets of 5 repetitions, once every 3 days during HU (n=9 total exercise sessions). The training paradigm consisted of a 1000 ms isometric contraction (75% P_o), immediately followed by a 1000 ms eccentric contraction (75% P_o).

(2'Z,3'E)-6-Bromoindirubin-3'-oxime Treatment

Animals in the CC+BIO, HU+BIO, and HU+SRT/BIO groups were administered 0.2mg/kg (2'Z,3'E)-6-Bromoindirubin-3'-oxime (BIO) (R&D Systems, Inc.; Minneapolis, MN) via subcutaneous injection once per week for the duration of the 28-day study. BIO is a potent and selective glycogen synthase kinase-3 (GSK-3) inhibitor (55). The BIO dose of 0.2mg/kg/week was previously shown to attenuate reductions in cancellous bone loss (%BV/TV) at the proximal tibia of rats during six weeks of methylprednisolone treatment (95). Rats in the CC+Vh, HU+Vh, and HU+SRT/Vh groups were administered an equal concentration and volume of vehicle (dimethyl sulfoxide) by subcutaneous injection each week.

Peripheral Quantitative Computed Tomography (pQCT)

On days -1 and 28 of the study, pQCT scans were performed *in vivo* at the proximal tibia metaphysis (PTM) and tibia mid-diaphysis with a Stratec XCT Research-M device (Norland Corp., Fort Atkinson, WI), using a voxel size of 100 μm and a scanning beam thickness of 500 μm. Two slices centered at 50% of the tibial total length (determined from a scout view on the CT scanner) were collected. Calibration of this machine was performed on each day of scanning with a hydroxyapatite standard cone phantom. A standardized analysis for diaphyseal bone (contour mode 1, peel mode 2, outer threshold of 0.650 g/cm^3, inner threshold of 0 g/cm^3) was applied to each section.

Values of cortical bone mineral content (BMC), cortical bone area, and the polar cross-sectional moment of inertia (CSMI) were averaged across the 2 slices at the tibial mid-diaphysis to yield a mean value. Polar CSMI was based on geometry only and not weighted by density. Machine precision for cortical vBMD (based on manufacturer's data) is ±9 mg/cm^3 for cortical bone. Reproducibility in our laboratory was determined from five repeat scans using a *in vivo* multiple-slice scanning method; resulting coefficients of variation for cortical tibia BMD was ±0.59%.

Values of total volumetric bone mineral density (vBMD), total bone mineral content (BMC), total bone area, and cancellous vBMD were averaged across the 3 slices at the proximal tibia to yield a mean value. Machine precision (based on manufacturer's data) is ±3 mg/cm^3 for cancellous vBMD. Coefficients of variation were ± 0.6, 1.6, 1.9,

and 2.13% for *in vivo* proximal tibia total vBMD, total BMC, total area, and cancellous vBMD respectively, as determined from repeat scans on each of 6 adult male rats.

Ex Vivo pQCT

Following euthanasia, excised femurs were scanned *ex vivo* at the femoral neck (FN) using a voxel size of 70 μm to characterize mineral properties and cross-sectional geometry. The proximal half of the femur was placed in a mold designed to hold the femoral neck in alignment with the scanning axis of the CT scanner (8,32). A scout view scan was performed, and three adjacent scan slices (500 μm) were made of the femoral neck starting just below the femoral head, with values averaged for 2 or 3 slices.

Dynamic Histomorphometry Analysis

Undemineralized distal left tibiae were subjected to serial dehydration and embedded in methylmethacrylate (Sigma-Aldrich M5, 590-9, St. Louis, MO). Serial cross sections (150 to 200 um) of midshaft cortical bone were cut starting 2.5mm proximal to the tibiofibular junction (TFJ) with an Isomet diamond wafer low-speed saw (Buehler, Lake Bluff, IL). The histomorphometric analyses were performed by using the OsteoMeasure Analysis System, Version 1.3 (OsteoMetrics, Atlanta, GA). Measures of labeled surfaces and interlabel widths were obtained at 200x magnification of up to two slides per animal. Periosteal and endocortical mineral apposition rates (MAR, um/d) were calculated by dividing the average interlabel width by the time between labels (7 days), and mineralizing surface (MS) for both periosteal and endocortical bone surfaces (BS) using the formula %MS/BS = {[(single-labeled surface/2) + double-labeled

surface]/surface perimeter} X 100. Bone formation rate (BFR) was calculated as (MAR x MS/BS).

Micro-computed Tomography (μCT)

Microcomputed tomography (*μ*CT SkyScan 1172; SkyScan, Kontich, Belgium) was used to quantify 2D and 3D microarchitecture. [Note: These uCT scans and reconstructions were performed in a colleague's laboratory (MR Allen, Indiana University School of Medicine, Indianapolis). Data reduction, statistical analysis, and interpretation of the results were performed by BR Macias.] The *ex-vivo* right and left proximal tibia were scanned using an X-ray source set at 60kV over an angular range of 180 degrees with rotational steps of 0.70 degrees. Projection images were attained at 6-μm resolution and then reconstructed and analyzed using manufacturer-provided software (NRecon and CTAn; SkyScan). For trabecular bone analyses, a 1 mm long segment of the distal metaphysis secondary spongiosa was defined and the trabecular region within the segment was manually traced. A threshold was applied to separate bone from soft tissue (range, 100 to 255), and then the specimen was analyzed in 3 dimensions for bone volume/ trabecular volume (BV/TV), trabecular number (Tb.N), and trabecular thickness (Tb.Th). All nomenclature follows currently accepted guidelines for micro-computed tomographic evaluation of bone (13).

Femoral Neck Mechanical Testing

Specimens were brought to room temperature and all tests were performed on hydrated specimens using a material testing machine (Instron 3345, Norwood, MA) with a 1000-N load cell. [Note: These mechanical tests were performed in a colleague's

laboratory (HA Hogan, Mechanical Engineering, Texas A&M University). BR Macias was assisted by students in Dr. Hogan's laboratory to perform these mechanical tests. In addition, data reduction, statistical analysis, and interpretation of the results were performed by BR Macias.] Load and displacement data were collected at 10Hz during tests and analyzed using Bluehill software (version 2.14.582, Instron Bluehill) and a custom-written Matlab (version 7.12.0, The MathWorks, Inc.) program. Mechanical properties of the femoral neck were evaluated using an axial loading configuration. Each proximal femur was placed upright with the diaphysis portion of the bone firmly inserted into a properly sized and fitted hole in a ½-inch thick aluminum plate fixture. A 10-mm cylindrical platen with a flat head was used to apply a load to the femoral head, parallel to the axis of the shaft of the femur. Quasi-static loading was applied in displacement control (2.54 mm/min) until fracture occurred. Load-displacement curves were analyzed to determine the structural variables of ultimate force (F) and stiffness (S), the latter of which was defined to be the slope of the elastic linear portion of the loading curve.

Serum Interleukin 6 (IL-6)

Serum IL-6 on cardiac blood samples collected at sacrifice was determined using the Rat IL-6 immunoassay Quantikine® ELISA (R&D Systems, Inc.; Minneapolis, MN) according to the manufacturer's instructions. All samples were run in duplicate and fit onto one plate to run this assay. Assay results were analyzed using a DTX 880 microplate reader (Beckman Coulter, Brea, CA, USA). The interassay coefficient of variation was found to be 8%.

Statistical Analyses

All data were expressed as means ± SD and evaluated using the statistical package SPSS (v.15; Chicago, Ill). Data were first analyzed using a two-factor ANOVA (exercise and drug) to compare group differences between HU groups (HU+Vh, HU+BIO, HU+SRT/Vh, and HU+SRT/BIO). A Tukey's post-hoc test was used for pair-wise comparisons. Subsequently, a one-factor ANOVA was used to compare HU groups' values vs. that of the comparator cage control (CC) group (Tukey's post-hoc test for pairwise comparisons). A one-factor ANOVA was employed to determine significant longitudinal pQCT variable changes within each treatment group (*in vivo* pQCT data only). An un-paired t-test tested differences between the HU+SRT and HU+SRT/BIO groups to determine the effect of added BIO treatment. For all data, statistical significance was accepted at $p<0.05$.

Results

Simulated Resistance Exercise Combined with Inhibition of GSK-3 Prevents Disuse Induced Cancellous Volumetric BMD Losses

Cancellous proximal tibia total BMC was significantly lower by 11% after 28-days of HU ($p<0.05$) (Table 1). BIO treatment halved this HU-induced 11% loss of total BMC at the proximal tibia metaphysis (HU+Vh versus HU+BIO, $p=0.03$). SRT significantly increased total BMC and total bone area at the proximal tibia metaphysis during HU ($p<0.001$ and $p=0.002$, respectively). The gain in total BMC after 28-days was similar between the HU+SRT/Vh and HU+SRT/BIO groups. Similarly, SRT significantly increased total bone area (area inside periosteal edge) at the proximal tibia

metaphysis by ~2% compared to the suppressed growth in the non-exercise control groups ($p<0.001$). Moreover, BIO treatment combined with SRT enhanced gains in cancellous vBMD after 28-days HU, producing a significant 8.8% increase as compared to the 2.7% (non-significant) increase with SRT alone (HU+SRT/Vh).

Table 1. Proximal Tibia Morphometry

	CC+Vh	CC+BIO	HU+Vh	HU+BIO	HU+SRT/Vh	HU+SRT/BIO
Total BMC (mg)						
Day 0	10.70 ± 0.50	10.88 ± 0.78	11.21 ± 0.92	10.44 ± 0.86	11.17 ± 0.58	10.82 ± 0.86
Day 28	11.20 ± 0.47*	11.29 ± 0.62*	9.96 ± 0.51*[a]	9.87 ± 0.85*[b]	11.98 ± 0.54*[c]	11.52 ± 0.94*[c]
%-Change	*4.69%*	*3.98%*	*-10.81%*	*-5.37%*	*7.39%*	*6.57%*
Total vBMD (mg/cm^3)						
Day 0	608.84 ± 33.64	612.35 ± 29.66	612.41 ± 30.44	599.64 ± 24.09	614.59 ± 34.94	602.72 ± 21.12
Day 28	635.93 ± 36.96*	624.40 ± 32.59*[†]	573.94 ± 41.46*[a]	569.31 ± 25.71*[a]	646.33 ±38.57*[b]	629.30 ± 20.34*[b]
%-Change	*4.46%*	*1.96%*	*-6.36%*	*-5.06%*	*5.24%*	*4.44%*
Total Bone Area (mm^2)						
Day 0	17.67 ± 1.63	17.79 ± 1.14	18.39 ± 2.19	17.45 ± 1.67	18.25 ± 1.42	18.00 ± 1.76
Day 28	17.71 ± 1.53	18.13 ± 0.86	17.47 ± 1.70[a]	17.38 ± 1.73[a]	18.61 ± 1.21[b]	18.33 ± 1.42[b]
%-Change	*0.31%*	*2.03%*	*-4.56%*	*-0.30%*	*2.19%*	*2.07%*
Cancellous vBMD (mg/cm^3)						
Day 0	201.42 ± 32.63	217.98 ± 34.72	215.18 ± 45.92	199.37 ± 25.30	210.05 ± 24.85	201.57 ± 28.21
Day 28	187.94 ± 34.87	204.16 ± 30.44	198.55 ± 35.05*[a]	187.91 ± 28.32[a]	214.32 ± 28.60[b]	218.74 ± 31.29*[b]
%-Change	*-6.44%*	*-5.90%*	*-6.71%*	*-5.28%*	*2.74%*	*8.80%*

BIO treatment attenuates disuse associated decreases in total BMC ($p=0.03$). [†]Significantly less than CC+Vh, $p=0.014$. [*]$p<0.05$ vs. pre value. Those HU groups not sharing the same letter for each variable are significantly different from each other ($p<0.05$).

The lower cancellous vBMD after 28-days in both cage control groups may suggest some age-related losses; however, the change was non-significant. However, when HU was imposed for 28 days, cancellous vBMD was significantly lower by 6.7%.

Simulated Resistance Exercise or Combined GSK-3 Inhibitor Administration Improves Cancellous Microarchitecture

Both SRT treatment alone or SRT treatment combined with weekly BIO treatment caused significant gains in proximal tibia cancellous BV/TV ($p<0.05$) (Figure 15). However, these *ex vivo* end-point μCT measures were unable to detect a difference between the HU+SRT/Vh and HU+SRT/BIO groups. Both T.Th and T.N show a similar

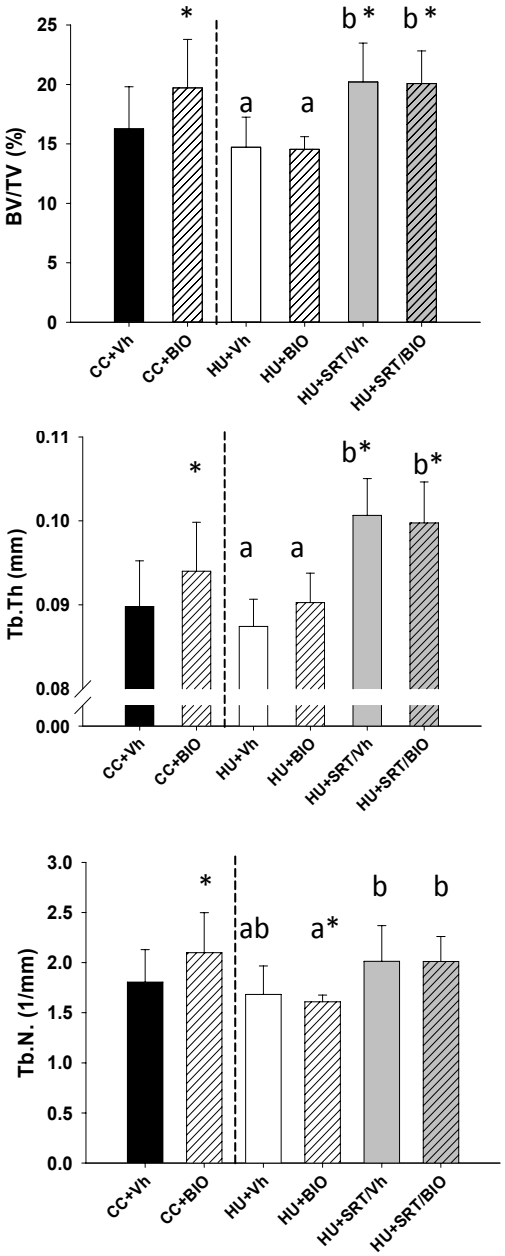

Figure 15. Effects of hindlimb unloading (HU) with or without GSK-3 (BIO) treatment and/or simulated resistance training (SRT) on cancellous bone microarchitecture. *A*: Bone Volume (%BV/TV). *B*: Trabecular Thickness (Tb.Th.). *C*: Trabecular Number (Tb.N.). Vertical dashed line indicates separation of CC from the experimental groups for preliminary 2-way ANOVA. Those HU groups not sharing the same letter for each variable are significantly different from each other ($p<0.05$). *Significantly different versus CC ($p<0.05$).

response to the 3-times weekly SRT or the combined weekly BIO administration. In rats given BIO treatment only during 28-days HU (HU+BIO), similar decrements in BV/TV, T.Th, and Tb.N as seen in the HU+Vh control group are observed. Interestingly, BIO administration to full weightbearing animals show higher BV/TV, T.Th and Th.N compared to the CC+Vh control group ($P<0.05$).

Simulated Resistance Exercise Combined with GSK-3 Inhibitor Administration not only Mitigates Suppressed Cortical Growth but also Stimulates Gain during Disuse

The magnitude of change in cortical BMC of the HU+SRT/BIO was significantly greater than the magnitude of change observed in the other HU groups (Table 2). When SRT and BIO treatments are combined, the magnitude of change for cortical BMC was greater (6.5%) at the midshaft tibia as compared to the ~4% increase observed in the other HU groups, but non-significant ($p=0.06$). Similarly, the 2.6% increase in cortical area in the HU+SRT/BIO was significantly greater than the 0.7% increase observed in the HU+SRT/Vh group ($p<0.05$). These gains in cortical midshaft tibia BMC and area likely contributed to the significant increase in cortical thickness observed when SRT was combined with BIO treatment during disuse ($p<0.05$). These gains in cortical midshaft BMC, area, and thickness resulted in the 7% gain in polar CSMI ($p=0.06$).

Table 2. Cortical Midshaft Tibia Bone Morphometry

	CC+Vh	CC+BIO	HU+Vh	HU+BIO	HU+SRT/Vh	HU+SRT/BIO
Cortical BMC (mg)						
Day 0	8.42 ± 0.57	8.54 ± 0.77	8.94 ± 0.76	8.56 ± 0.58	8.98 ± 0.82	8.41 ± 0.65
Day 28	8.75 ± 0.74*	8.95 ± 0.67*	9.28 ± 0.74*	8.89 ± 0.62*	9.33 ± 0.79*	8.95 ± 0.64*‡
%-Change	*3.87%*	*5.80%*	*3.83%*	*3.90%*	*3.93%*	*6.48%*
Cortical Area (mm^2)						
Day 0	8.78 ± 0.91	8.94 ± 89	9.03 ± 0.81	8.93 ± 0.73	8.97 ± 0.87	8.61 ± 0.86
Day 28	8.843 ± 0.88	9.01 ± 0.67	9.04 ± 0.83	9.09 ± 0.75	9.03 ± 0.79	8.81 ± 0.68†
%-Change	*0.84%*	*1.09%*	*0.43%*	*1.82%*	*0.73%*	*2.65%*
Cortical Thickness (mm)						
Day 0	0.74 ± 0.03	0.74 ± 0.04	0.77 ± 0.03	0.74 ± 0.03	0.79 ± 0.04	0.75 ± 0.03
Day 28	0.76 ± 0.03	0.77 ± 0.04*	0.79 ± 0.03*	0.75 ± 0.04	0.80 ± 0.04	0.78 ± 0.03*†
%-Change	*2.14%*	*4.16%*	*2.97%*	*1.26%*	*1.70%*	*4.66%*
CSMI (mm^4)						
Day 0	12.00 ± 2.39	12.35 ± 2.26	12.92 ± 2.39	12.43 ± 1.96	12.76 ± 2.55	11.51 ± 2.29
Day 28	12.18 ± 2.32	12.54 ± 1.70	13.17 ± 2.52	12.99 ± 2.16#	13.05 ± 2.32	12.21 ± 1.83+
%-Change	*2.09%*	*2.54%*	*1.22%*	*4.64%*	*2.82%*	*7.12%*

Cortical bone mineral content (BMC), cortical area, cortical thinkness, and polar cross-sectional moment of inertia (CSMI). Values are group mean ± standard deviation of the mean. *$p<0.05$ vs. pre value. †The magnitude of change in the HU+SRT/BIO group is significantly greater than that in the HU+SRT/Vh, $p<0.05$. ‡The magnitude of change in the HU+SRT/BIO group was greater than the HU+SRT/Vh but non-significant ($p=0.055$). +The magnitude of change in the HU+SRT/BIO group was greater than the HU+SRT/Vh but non-significant ($p=0.06$). #The magnitude of change in the HU+BIO group was greater than the HU+Vh but non-significant ($p=0.07$).

Simulated Resistance Exercise or Combined GSK-3 Inhibitor Administration Increases Bone Formation on Cortical Surfaces

Cortical midshaft tibia MS/BS, MAR, and BFR were suppressed after 28-days HU as compared to the full weightbearing controls (Figure 16). Rats experiencing SRT during HU exhibited a significantly higher MS/BS on both the periosteal and endocortical surfaces ($p<0.05$). SRT produced significantly higher MAR and BFR on the periosteal surface ($p<0.05$) and a non-significant increase in MAR and BFR on the endocortical surface. In addition, by day 28 MAR of the SRT groups was not significantly different from levels in full weight bearing cage controls. Periosteal BFR in HU/SRT rats remained lower than in full weight bearing controls; however, when SRT was combined with a GSK-3 inhibitor BFR was not significantly different from full weight bearing controls.

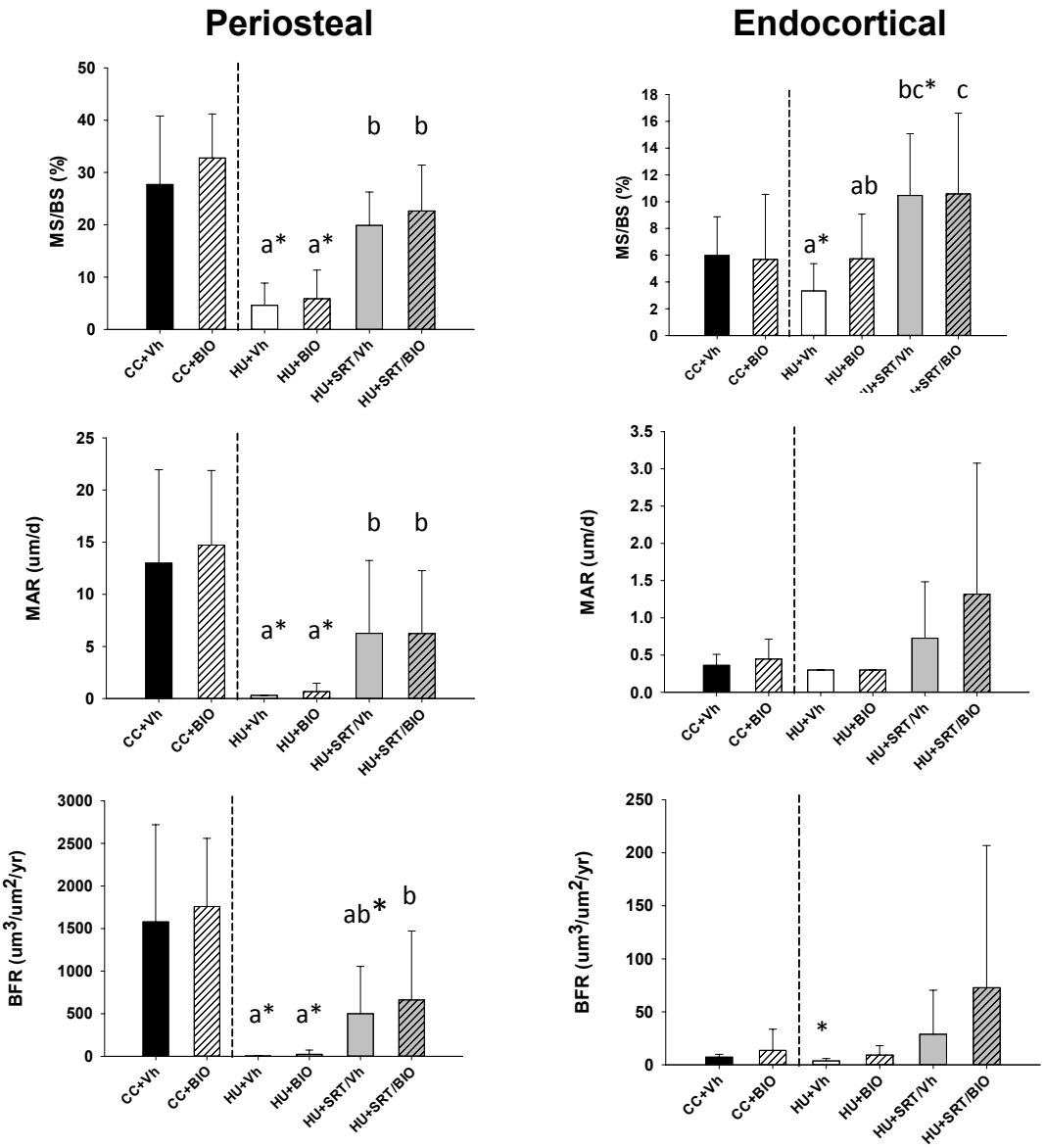

Figure 16. Effects of hindlimb unloading (HU) with or without GSK-3 (BIO) and/or simulated resistance training (SRT) on periosteal and endocortical surface dynamic histomorphometric analyses measured at the tibia diaphysis. A: Mineralizing Surface (%MS/BS). B: Mineral Apposition Rate (MAR). C: Bone Formation Rate (BFR). Vertical dashed line indicates separation of cage control (CC) from the experimental groups for preliminary ANOVA. Those HU groups not sharing the same letter for respective surface measures are significantly different from each other ($p<0.05$). *Significantly different vs. CC ($p<0.05$). Error bars not visible above bars have small SD values.

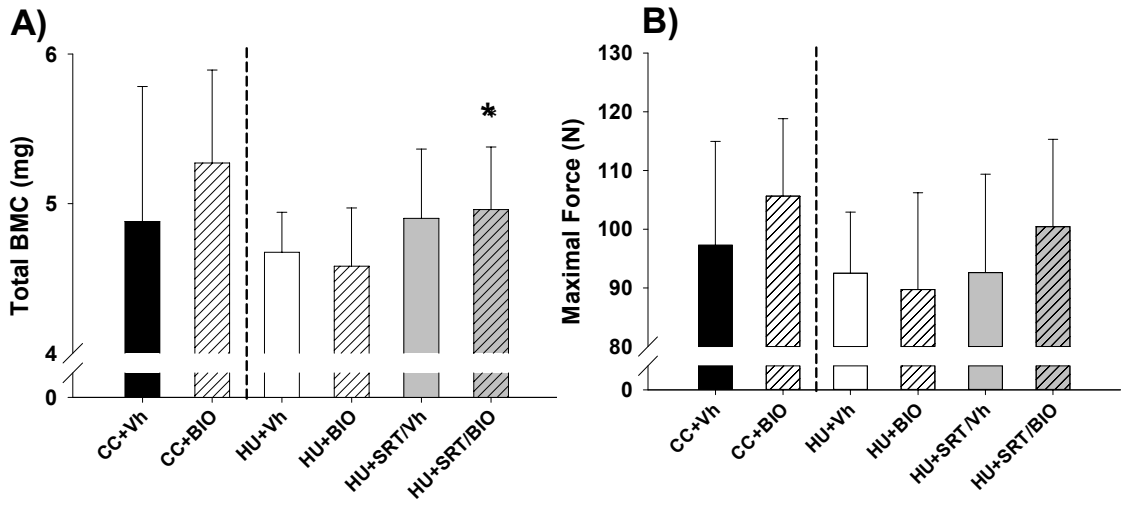

Figure 17. Femoral neck bone mineral content and strength. A: Combined SRT and GSK3 inhibition produced higher total bone mineral content at the femoral neck compared to the non-treated control, HU+Vh group (*unpaired t-test, p=0.08). B: Combined SRT and GSK3 inhibition (HU+SRT/BIO) resulted in higher femoral neck maximal force compared to HU+BIO (paired t-test, p=0.09).

Simulated Resistance Exercise Combined with GSK-3 Inhibitor Administration during Disuse Restores Femoral Neck Bone Mineral Content

SRT during HU produced non-significant increases in total BMC at the femoral neck; the higher value in the HU+SRT/BIO group compared to HU+Vh group produced a p-value equal to 0.08 (Figure 17A). Femoral neck strength was not affected by SRT+BIO (Figure 17B).

Disuse for 28-days Shows Higher Serum IL-6 Levels

Circulating IL-6 as measured in cardiac serum was significantly higher after 28-days of HU as compared to the full weight bearing controls (HU+Vh), $p<0.05$ (Figure 18). BIO treatment mitigated this increase resulting in serum IL-6 levels not significantly higher than in cage control rats.

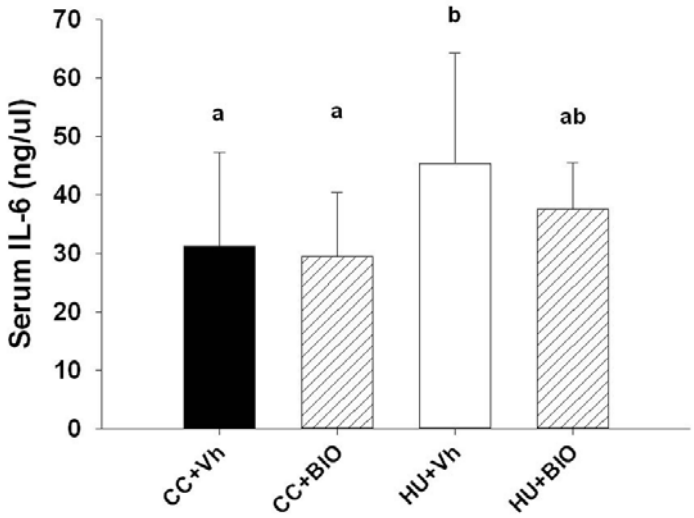

Figure 18. Serum IL-6 after 28-days of disuse (HU+Vh) is significantly higher compared to those levels in full weight bearing controls. Those groups not sharing the same letter are significantly different from each other ($p<0.05$).

Discussion

In support of our hypothesis, simulated resistance training (SRT) combined with pharmacological activation of the Wnt signaling pathway resulted in greater cortical and cancellous bone mass gains than SRT alone during disuse. Higher bone formation rate observed in the SRT legs explains the observed cortical morphological adaptations. These are the first data to test the combination of mechanical loading and pharmacological activation of Wnt signaling during disuse. The present data do not, however, demonstrate a consistent a synergistic effect of combined SRT and GSK-3 inhibition. However, the combined treatment did result in larger gains in several measures of cortical and cancellous bone compared to the SRT control (HU+SRT/Vh). For example, in the HU+SRT/BIO group we observe an increased cancellous vBMD, midshaft tibia cortical BMC, cortical area, cortical thickness, CSMI, and periosteal BFR

compared to HU+SRT/Vh group. Disuse potently stimulates bone resorption and suppresses bone formation. SRT has previously been shown to restore bone formation but may not affect elevated resorption observed during disuse. However, SRT combined with bisphosphonate therapy has been shown to simultaneously increase bone formation and decrease a serum marker of bone resorption (84). Combining mechanical loading and GSK-3 inhibition provides a small additional increment in bone formation capacity; however, net bone mass gains may be limited by the disuse-induced elevation of bone resorption.

Treatment with GSK3 inhibitors significantly increases cortical and cancellous bone mass during full weightbearing status. A orally bio-available GSK-3 inhibitor given once daily (20mg/kg) produces a 172% increase in bone mineral content, with most of this increase in bone mass was localized to the cancellous bone compartment (54). This increase in bone mass was matched by a 5-fold increase in cancellous bone formation rate and a significant but less robust elevation in periosteal osteoblast activity (54). BIO administration (the same drug and dose as used in the present study) attenuated glucocorticoid-induced cancellous bone loss and normalized cancellous bone formation rate (95). GSK-3 inhibition when combined the SRT treatment in our study resulted in greater periosteal expansion, as evidenced by the higher total bone area and total BMC at the proximal and midshaft tibia in the present study. This bone gain may have been a result of the higher BFR on the periosteal surface. Notably, there was a higher endocortical mineralizing surface (%MS/BS) in SRT treated animals than in other HU groups. Although there were not significant gains in endocortical BFR with added

GSK-3B inhibition during exercise, any increase in BFR on this surface is of special physiological significance, since few exercise or drug interventions increase endocortical bone formation rate. Treatment with GSK-3 inhibitors during normal full weight bearing status, without added exercise interventions, does not affect bone formation rate on the endocortical surface (54). Interestingly, the present data show combining simulated resistance exercise with drugs that activate Wnt signaling may stimulate additional increments in both periosteal and endocortical bone formation rate compared to high intensity exercise modalities alone.

GSK-3 is a key intracellular protein within the putative mechanosensing Wnt pathway. Pharmacological inhibition of GSK-3 combined with SRT may allow sufficient accumulation of β-catenin levels and activate gene expression patterns to increase osteoblastogenesis and osteoblast activity. The mechanical loading to bone tissue provided by SRT likely induced progenitors to differentiate towards the osteoblast cell fate (84). In previously published work, Swift and co-workers demonstrated that SRT causes a shift in marrow cell populations away from adipocytes and towards a greater number of osteoblasts (84). Inhibiting GSK-3 may have amplified this committed subpopulation of progenitors with osteogenic potential, as GSK-3β inhibitor cell culture studies suggest (23). The fluorochrome label data in the present study suggest that SRT significantly increased the number of osteoblasts on cortical bone surface (%MS/BS). While HU+SRT/BIO limb bone did not exhibit significantly higher MAR and BFR compared to the HU+SRT group, the mean value was higher. Using a higher BIO dose or more potent drug may produce significant effects of combined

pharmacological and exercise therapies to better restore osteoblast activity during disuse on the endocortical surface.

It is clear that NASA management is open to exploring pharmacological management of flight-induced bone loss. However, employing a pharmacological approach is challenging in the context of long duration spaceflight. For example, pharmacokinetics can be altered during spaceflight and use of pharmaceuticals approved for treatment of disease, may be problematic for use in normal healthy astronauts. In addition, NASA must choose only the most critical pharmaceutical therapies in order to minimize spacecraft mass and volume. Alendronate is a type of bisphosphonate that potently suppress accelerated osteoclast-mediated bone resorption. Currently, alendronate, an anti-resorptive bisphosphonate, is being administered to some astronauts aboard the ISS to investigate the efficacy of this bone loss countermeasure strategy (41).

Elevated IL-6 levels are associated with increased bone resorption. Bone cells isolated from animals exposed to disuse showed a significantly higher production of IL-6 compared to full weight bearing control samples (25). The present finding of higher serum IL-6 after 28 days of HU is consistent with those reports of higher IL-6 in bone tissue cultures studies (25). In bone metabolism, the inflammatory cytokine TNF-α is one of the most potent osteoclastogenic cytokines. It stimulates synthesis of IL-6 in osteoblasts, and IL-6 functions to induce osteoclast formation and stimulate bone resorption (85). However, the mechanism behind TNF-α induced IL-6 synthesis in osteoblasts is unclear. Recently, data from cell culture experiments suggest that Wnt3a reduces TNF-α stimulated IL-6 release and expression via the Wnt pathway in

osteoblasts (61), suggesting a mechanistic role for Wnt signaling in the regulation of osteoclastogenesis. However, little is known about TNF-α mediated Wnt signaling *in vivo* or with mechanical loading. In the present study, thrice weekly high intensity exercise to the left leg was sufficient to prevent local bone loss but was unable to reduce systemic serum levels of IL-6. Taken together, these data suggest that suppressed Wnt signaling in just one unloaded limb may be sufficient to increase IL-6 release from bone cells and cause systemic levels of IL-6 to remain above normal. Alternatively, disuse may increase IL-6 production in other tissues (e.g., muscle) overshadowing any mitigation of disuse-induced IL-6 release from bone cells by SRT.

It remains to be determined if high resistance aRED exercises performed during 6-month ISS missions effectively mitigates microgravity-induced bone resorption. DEXA-derived measures of bone mass during ISS missions show that exercise performed on aRED, concurrent with improved nutrition intake, does mitigate much of the usually observed bone loss (76). Currently, NASA is testing the efficacy of an anti-resorptive bisphosphonate (alendronate) in preventing microgravity-induced bone loss. However, it is not clear how alendronate administration combined with exercise will impact on bone maintenance during space flight. The rate and amount of bone loss that occurs over the course of 6-month ISS missions is highly variable, similar to that observed in the general earth-bound population. Animal studies do demonstrate that alendronate can hinder exercised-induced gains in cancellous and cortical BFR (50,84). Future investigations may show if this high variability in bone loss also applies to a high variability in the response to exercise or drug interventions.

A limitation of the present study is that the GSK3 inhibitor we used does not discriminate between the inhibition of the alpha and beta forms, both of which are involved in modulating β-catenin levels (64). However, since these isoforms can compensate for each others' reduced activity and maintain β-catenin levels, use of BIO in the present study, an inhibitor of both alpha and beta forms, almost certainly affected β-catenin levels. Future studies using more selective inhibitors of GSK-3 alpha or beta may allow determination of the relative impact of those specific isoforms on osteoblastogenesis and maintenance of bone mass during disuse.

In conclusion, we find that combining GSK-3 inhibition with high intensity exercise mitigates cancellous bone loss and restores cortical periosteal growth during disuse. Future studies are warranted to better understand how combined pharmacological activation of Wnt signaling (with more specific Wnt signaling drugs) and mechanical loading of bone can prevent bone loss.

CHAPTER V

CONCLUSIONS

The data presented here-in demonstrate that thrice weekly simulated resistance exercise can restore disuse-suppressed cortical bone formation and normalize the number sclerostin positive osteocytes. Secondly, the data show that simulated GCR (with low dose high LET radiation exposure) causes significant decrements in cancellous and cortical bone mass. In addition, this simulated GCR appears to exacerbate partial weightbearing-induced cancellous bone loss. Interestingly, fractionating low dose high-LET radiation does not protect against cancellous bone loss as was observed with fractionation of low dose low-LET radiation. Cortical bone in rats exposed to partial weightbearing conditions exhibits higher levels of sclerostin-positive osteocytes compared to full weightbearing controls. Unexpectedly, however, reduced weightbearing with added radiation exposure results in a greater number of sclerostin-positive osteocytes than with either treatment alone. In addition, simulated resistance exercise combined with GSK-3 inhibition shows added gains in cortical and cancellous bone mass compared to a single exercise or drug treatment alone. Taken together, these data suggest that regular high intensity resistance exercise may be an effective strategy to mitigate bone loss observed during long duration spaceflight or Lunar missions. Moreover, the data provide more evidence that Wnt signaling is highly responsive to mechanical loading conditions in cortical and cancellous bone.

REFERENCES

1. Agholme F, Isaksson H, Kuhstoss S, Aspenberg P. The effects of Dickkopf-1 antibody on metaphyseal bone and implant fixation under different loading conditions. Bone 48:988-996, 2011.

2. Agholme F, Li X, Isaksson H, Ke HZ, Aspenberg P. Sclerostin antibody treatment enhances metaphyseal bone healing in rats. J Bone Miner Res 25:2412-2418, 2010.

3. Apseloff G, Girten B, Walker M, Shepard DR, Krecic ME, Stern LS, Gerber N. Aminohydroxybutane bisphosphonate and clenbuterol prevent bone changes and retard muscle atrophy respectively in tail-suspended rats. J Pharmacol Exp Ther 264(3):1071-1078, 1993.

4. Apseloff G, Girten B, Weisbrode SE, Walker M, Stern LS, Krecic ME, Gerber N. Effects of aminohydroxybutane bisphosphonate on bone growth when administered after hind-limb bone loss in tail-suspended rats. J Pharmacol Exp Ther 267(1):515-521, 1993.

5. Baxter NN, Habermann EB, Tepper JE, Durham SB, Virnig BA. Risk of pelvic fractures in older women following pelvic irradiation. JAMA 294:2587–2593, 2005.

6. Bhat R, Xue Y, Berg S, Hellberg S, Ormo M, Nilsson Y, Radesater AC, Jerning E, PO Markgren, Borgegard T, Jerning E, Markgen P, Borgegard T, Nylof M, Gimenez-Cassina A, Hernandez F, Lucas JJ, Diaz-Nido J, Avila J. Structural insights and biological effects of glycogen synthase kinase 3-specific inhibitor AR-A014418. J Biol Chem 278:45937-45945, 2003.

7. Bliss P, Parsons CA, Blake PR. Incidence and possible aetiological factors in the development of pelvic insufficiency fractures following radical radiotherapy. Br J Radiol 69:548–554, 1996.

8. Bloomfield SA, Allen MR, Hogan HA, Delp MD. Site- and compartment-specific changes in bone with hindlimb unloading in mature adult rats. Bone 31:149-157, 2002.

9. Bone Health and Osteoporosis: A Report of the Surgeon General, U.S. Department of Health and Human Services, Office of the Surgeon General, Rockville, MD, 2004.

10. Bonewald LF. Generation and function of osteocyte dendritic processes. J Musculoskelet Neuronal Interact. 5(4):321-324, 2005.

11. Bonewald LF and Johnson ML. Osteocytes, mechanosensing, and wnt signaling. Bone 42:606-615, 2008.

12. Bonewald LF. The amazing osteocyte. J Bone Miner Res 26(2):229-238, 2011.

13. Bouxsein ML, Boyd SK, Christiansen BA, Guldberg RE, Jepsen KJ, Muller R. Guidelines for assessment of bone microstructure in rodents using micro-computed tomography. J Bone Miner Res 25:1468-1486, 2010.

14. Burger EH and J Klein-Nulend. Mechanotransduction in bone-role of the lacunocanalicular network. FASEB Journal 13(9001):S101-S112, 1999.

15. Center JR, Bliuc D, Nguyen ND, Nguyen TV, Eisman JA. Osteoporosis medication and reduced mortality risk in elderly women and men. J Clin Endocrinol Metab 96:1006-1014, 2011.

16. Choi HY, Dieckmann M, Herz J, Niemeier A. Lrp4, a novel receptor for dickkopf 1 and sclerostin, is expressed by osteoblasts and regulates bone growth and turnover in vivo. PLoS ONE 4:e7930, 2009.

17. Cline GW, Johnson K, Regittnig W, Perret P, Tozzo E, Xiao L, Damico C, Shulman GI. Effects of a novel glycogen synthase kinase-3 inhibitor on insulin-stimulated glucose metabolism in Zucker diabetic fatty (fa/fa) rats. Diabetes 51: 2903-2910, 2002.

18. Cohen P and Goedert M. GSK3 inhibitors: development and therapeutic potential. Nat Rev Drug Discov 3:479-487, 2004.

19. Cucinotta FA and Durante M. Cancer risk from exposure to galactic cosmic rays: implications for space exploration by human beings. Lancet Oncol 7:431-435, 2006.

20. Cummings SR, Melton III LJ. Epidemiology and outcomes of osteoporotic fractures. Lancet 359:1761–1767, 2002.

21. Ellman R, Spatz J, Cloutier A, Bouxsein ML. Musculoskeletal adaptations to partial weightbearing in mice. Orthopedic Research Society Meeting Abstract, 2011.

22. Foldes J, Shih M, Parfitt M. Frequency distributions of tetracycline-based measurements: Implications for the interpretation of bone formation indices in

the absence of double-labeled surfaces. J Bone Miner Res 5(10):1063-1067, 1990.

23. Gambardella A, Nagaraju CK, O'Shea PJ, Mohanty ST, Kottam L, Pilling J, Sullivan M, Djerbi M, Koopmann W, Croucher PI, Bellantuono I. Glycogen synthase kinase-3alpha/beta inhibition promotes in vivo amplification of endogenous mesenchymal progenitors with osteogenic and adipogenic potential and their differentiation to the osteogenic lineage. J Bone Miner Res 26:811-821, 2011.

24. Gong Y, Slee RB, Fukai N, Rawadi G, Roman-Roman S, Reginato AM, Wang H, Cundy T, Glorieux FH, Lev D, Zacharin M, Oexle K, Marcelino J, Suwairi W, Heeger S, Sabatakos G, Apte S, Adkins WN, Allgrove J, Arslan-Kirchner M, Batch JA, Beighton P, Black GCM, Boles RG, Boon LM, Borrone C, Brunner HG, Carle GF, Dallapiccola B, Paepe AD, Floege B, Halfhide ML, Hall B, Hennekam RC, Hirose T, Jans A, Jüppner H, Kim CA, Keppler-Noreuil K, Kohlschuetter A, LaCombe D, Lambert M, Lemyre E, Letteboer T, Peltonen L, Ramesar RS, Romanengo M, Somer H, Steichen-Gersdorf E, Steinmann B, Sullivan B, Superti-Furga A, Swoboda W, van den Boogaard M, Van Hul W, Vikkula M, Votruba M, Zabel B, Garcia T, Baron R, Olsen BR, Warman ML, and The Osteoporosis-Pseudoglioma Syndrome Collaborative Group. LDL receptor-related protein 5 (LRP5) affects bone accrual and eye development. Cell 107:513-523, 2001.

25. Grano M, Mori G, Minielli V, Barou O, Colucci S, Giannelli G, Alexandre C, Zallone AZ, Vico L. Rat hindlimb unloading by tail suspension reduces osteoblast differentiation, induces IL-6 secretion, and increases bone resorption in ex vivo cultures. Calcif Tissue Int 70:176-185, 2002.

26. Guidance on radiation received in space activities: Report No.098, National Council on Radiation Protection and Measurements, Bethesda, MD, 1989.

27. Hall EJ and Giaccia AJ. (2000) Radiobiology for the Radiologist. Lippincott Williams and Wilkins, Philadelphia, PA, pp 16-29.

28. Hamilton SA, Pecaut MJ, Gridley DS, Travis ND, Bandstra ER, Willey JS, Nelson GA, Bateman TA. A murine model for bone loss from therapeutic and space-relevant sources of radiation. J Appl Physiol 101(3):789-793, 2005.

29. Hargens AR, Steskal J, Johansson C, Tipton CM. Tissue fluid shift, forelimb loading, and tail tension in tail-suspended rats. The Physiologist 27(6):S37-S38, 1984.

30. Huddleston AL, Rockwell D, Kulund DN, Harrison RB. Bone mass in lifetime tennis athletes. JAMA 244(10):1107-1109, 1980.

31. Information needed to make radiation protection recommendations for space missions beyond low-earth orbit: Report No. 153, National Council on Radiation Protection and Measurements, Bethesda, MD, 2007.

32. Jokihaara J, Jarvinen TLN, Jolma P, Koobi P, Kalliovalkama J, Tuukkanen J, Saha H, Sievanen H, Kannus P, Porsti I. Renal insufficiency-induced bone loss is associated with an increase in bone size and preservation of strength in rat proximal femur. Bone 39:353-360, 2006

33. Judex S, Garman R, Squire M, Busa B, Donahue LR, Rubin C. Genetically linked site-specificity of disuse osteoporosis. J Bone Miner Res 19:607-613, 2004.

34. Judex S, Rubin J, Rubin CT. (1996) Mechanisms of exercise effects on bone quantity and quality. In: Bilezikian JP, Raisz LG, and Martin TJ (eds.) Principles of bone biology. Academic Press, San Diego, CA, pp 1819.

35. Keyak JH, Koyama AK, LeBlanc A, Lu Y, Lang TF. Reduction in proximal femoral strength due to long-duration spaceflight. Bone 44:449-453, 2009.

36. Kondo H, Searby ND, Mojarrab R, Phillips J, Alwood J, Yumoto K, Almeida EA, Limoli CL, Globus RK. Total-body irradiation of postpubertal mice with 137Cs acutely compromises the microarchitecture of cancellous bone and increases osteoclasts. Radiat Res 171:283–289, 2009.

37. Kondo H, Yumoto K, Alwood JS, Mojarrab R, Wang A, Almeida EAC, Searby ND, Limoli CL, Globus RK. Oxidative stress and gamma radiation-induced cancellous bone loss with musculoskeletal disuse. J Appl Physiol 108(1):152-161, 2010.

38. Kulkarni NH, Onyia JE, Zeng Q, Tian X, Liu M, Halladay DL, Frolik CA, Engler T, Wei T, Kriauciunas A, Martin TJ, Sato M, Bryant HU, Ma YL. Orally bioavailable GSK-3alpha/beta dual inhibitor increases markers of cellular differentiation in vitro and bone mass in vivo. J Bone Miner Res 21:910-920, 2006.

39. Kwan TS, Padrines M, Théoleyre S, Heymann D, Fortun Y. IL-6, RANKL, TNF-alpha/IL-1: interrelations in bone resorption pathophysiology. Cytokine Growth Factor Rev 15:49-60, 2004.

40. Lang T, LeBlanc A, Evans H, Lu Y, Genant H, Yu A. Cortical and trabecular bone mineral loss from the spine and hip in long-duration spaceflight. J Bone Miner Res 19:1006-1012, 2004.

41. LeBlanc A, Schneider V, Shackelford L, West S, Oganov V, Bakulin A, Voronin L. Bone mineral and lean tissue loss after long duration space flight. J Musculoskelet Neuronal Interact 1:157-160, 2000.

42. LeBlanc AD, Spector ER, Evans HJ, Sibonga JD. Skeletal responses to space flight and the bed rest analog: a review. J Musculoskelet Neuronal Interact 7:33-47, 2007.

43. Lee EJ, Long KA, Risser WL, Poindexter HB, Gibbons WE, Goldzieher J. Variations in bone status of contralateral and regional sites in young athletic women. Med Sci Sports Exerc 27:1354-1361, 1995.

44. Lee SM, Schneider SM, Boda WL, Watenpaugh DE, Macias BR, Meyer RS, Hargens AR. LBNP exercise protects aerobic capacity and sprint speed of female twins during 30 days of bed rest. J Appl Physiol 106(3):919-928, 2009.

45. Li X, Warmington KS, Niu QT, Asuncion FJ, Barrero M, Grisanti M, Dwyer D, Stouch B, Thway TM Stolina M, Ominsky MS, Kostenuik PJ, Simonet WS, Paszty C, Ke HZ. Inhibition of sclerostin by monoclonal antibody increases bone formation, bone mass, and bone strength in aged male rats. J Bone Miner Res 25: 2647-2656, 2010.

46. Lima F, Swift JM, Greene ES, Allen MR, Macias BR, Bloomfield SA. Partial Weightbearing does not Prevent Bone loss Compared to Non-Weightbearing Model. IBMS Sun Valley Workshop Abstract, 2010.

47. Lin C, Jiang X, Dai Z, Guo X, Weng T, Wang J, Li Y, Feng G, Gao X, He L. Sclerostin mediates bone response to mechanical unloading through antagonizing wnt/b-catenin signaling. J Bone Miner Res 24:1651-1661, 2009.

48. Lyles KW, Colon-Emeric CS, Magaziner JS, Adachi JD, Pieper CF, Mautalen C, Hyldstrup L, Recknor C, Nordsletten L, Moore KA, Lavecchia C, Zhang J, Mesenbrink P, Hodgson PK, Abrams K, Orloff JJ, Horowitz Z, Eriksen EF, Boonen S, for the HORIZON Recurrent Fracture Trial. Zoledronic Acid in Reducing Clinical Fracture and Mortality after Hip Fracture. N Engl J Med 357:nihpa40967, 2007.

49. Macias BR, Cao P, Watenpaugh DE, Hargens AR. LBNP treadmill exercise maintains spine function and muscle strength in identical twins during 28-day simulated microgravity. J Appl Physiol 102(6):2274-2278, 2007.

50. Macias BR, Swift JM, Nilsson MI, Hogan HA, Bouse SD, Bloomfield SA. Simulated resistance training, but not alendronate, increases cortical bone formation and suppresses sclerostin during disuse. J Appl Physiol 112:918-925, 2012.

51. Managing Space Radiation Risk in the New Era of Space Exploration: Ongoing advancements in solar storm monitoring, materials, and high velocity space vehicles: Committee on the Evaluation of Radiation Shielding for Space Exploration, National Research Council, 2008

52. Manolagas SC and Almeida M. Gone with the Wnts: B-Catenin, T-cell factor, forkhead box O, and oxidative stress in age-dependent diseases of bone, lipid, and glucose metabolism. Mol Endocrinology 21(11):2605-2614, 2007.

53. Mantila Roosa SM, Liu Y, Turner CH. Gene expression patterns in bone following mechanical loading. J Bone Miner Res 26:100-112, 2011.

54. Marsell R, Sisask G, Nilsson Y, Sundgren-Andersson AK, Andersson U, Larsson S, Nilsson O, Ljunggren O, Jonsson KB. GSK-3 inhibition by an orally active small molecule increases bone mass in rats. Bone 50:619-627, 2011.

55. Meijer L, Skaltsounis AL, Magiatis P, Polychronopoulos P, Knockaert M, Leost M, Ryan XP, Vonica CA, Brivanlou A, Dajani R, Crovace C, Tarricone C, Musacchio A, Roe SM, Pearl L, Greengard P. GSK-3-Selective Inhibitors Derived from Tyrian Purple Indirubins. Chem Bio 10:1255-1266, 2003.

56. Menaa C, Reddy SV, Kurihara N, Maeda H, Anderson D, Cundy T, Cornish J, Singer FR, Bruder JM, Roodman GD. Enhanced Rank ligand expression and responsivity of bone marrow cells in Paget's disease of bone. J Clin Invest 105:1833-1838, 2000.

57. Morey-Holton ER and Globus RK. Hindlimb unloading of growing rats: a model for predicting skeletal changes during space flight. Bone 22:83S-88S, 1998.

58. Morey-Holton E, Globus RK, Kaplansky A, Durnova G. The hindlimb unloading rat model: literature overview, technique update and comparison with space flight data. Adv Space Biol Med 10:7-40, 2005.

59. Moustafa A, Sugiyama T, Prasad J, Zaman G, Gross TS, Lanyon LE, Price JS. Mechanical loading-related changes in osteocyte sclerostin expression in mice are more closely associated with the subsequent osteogenic response than the peak strains engendered. Osteoporos Int. 23:1225-1234, 2012.

60. Nakashima T, Hayashi M, Fukunaga T, Kurata K, Oh-Hora M, Feng JQ, Bonewald LF, Kodama T, Wutz A, Wagner EF, Penninger JM, Takayanagi H. Evidence for osteocyte regulation of bone homeostasis through RANKL expression. Nat Med 17:1231-1234, 2011.

61. Natsume H, Tokuda H, Adachi S, Matsushima-Nishiwaki R, Kato K, Minamitani C, Otsuka T, Kozawa O. Wnt3a regulates tumor necrosis factor-α-stimulated interleukin-6 release in osteoblasts. Mol Cell Endo 331:66-72, 2011.

62. Ohsaki Y, Takahashi S, Scarcez T, Demulder A, Nishihara T, Williams R, Roodman GD. Evidence for an autocrine/paracrine role for interleukin-6 in bone resorption by giant cell tumors of bone. Endocrinology 131:2229-2234, 1992.

63. Ominsky MS, Vlasseros F, Jolette J, Smith SY, Stouch B, Doellgast G, Gong J, Gao Y, Cao J, Graham K, Tipton B, Cai J, Deshpande R, Zhou L, Hale MD, Lightwood DJ, Henry AJ, Popplewell AG, Moore AR, Robinson MK, Lacey DL, Simonet WS, Paszty C. Two doses of sclerostin antibody in cynomolgus monkeys increases bone formation, bone mineral density, and bone strength. J Bone Miner Res 25:948-959, 2010.

64. Ougolkov AV and Billadeau DD. (2008) Wnt Signaling. In: Elizabeth Vincan (ed.) Inhibition of Glycogen Synthase Kinase-3, Humana Press, Totowa, NJ, pp 67.

65. Overgaard M. Spontaneous radiation-induced rib fractures in breast cancer patients treated with postmastectomy irradiation. A clinical radiobiological analysis of the influence of fraction size and dose-response relationships on late bone damage. Acta Oncol 27:117-122, 1988.

66. Parfitt AM, Drezner MK, Glorieux FH, Kanis JA, Malluche H, Meunier PJ, Ott SM, Recker RR. Bone histomorphometry: standardization of nomenclature, symbols, and units. Report of the ASBMR Histomorphometry Nomenclature Committee. J Bone Miner Res 2:595-610, 1987.

67. Pierce SM, Recht A, Lingos TI, Abner A, Vicini F, Silver B, Herzog A, Harris JR. Longterm radiation complications following conservative surgery (CS) and radiation therapy (RT) in patients with early stage breast cancer. Int J Radiat Oncol Biol Phys 23:915–923, 1992.

68. Plotkin LI, Manolagas SC, Bellido T. Dissociation of the pro-apoptotic effects of bisphosphonates on osteoclasts from their anti-apoptotic effects on osteoblasts/osteocytes with novel analogs. Bone 39(3):443-452, 2006.

69. Rambaut PC, Leach CS, Whedon GD. A study of metabolic balance in crewmembers of Skylab IV. Acta Astronaut 6:1313-1322, 1979.

70. Robling AG, Castillo AB, Turner CH. Biomechanical and Molecular Regulation of Bone Remodeling. Annu Rev Biomed Eng 8:455-498, 2006.

71. Robling AG, Niziolek PJ, Baldridge LA, Condon KW, Allen MR, Alam I, Mantila SM, Gluhak-Heinrich J, Bellido TM, Harris SE, Turner CH. Mechanical stimulation of bone in vivo reduces osteocyte expression of SOST/sclerostin. J Biol Chem 283(9):5866-5875, 2008.

72. Sakata T, Sakai A, Tsurukami H, Okimoto N, Okazaki Y, Ikeda S, Norimura T, Nakamura T. Trabecular bone turnover and bone marrow cell development in tail-suspended mice. J Bone Miner Res 14:1596-1604, 1999.

73. Sibonga JD, Cavanagh PR, Lang TF, LeBlanc AD, Schneider VS, Shackelford LC, Smith SM, Vico L. Adaptation of the skeletal system during long-duration spaceflight. Clinic Rev Bone Miner Metabol. 5(4):249-261, 2008.

74. Sibonga JD, Evans HJ, Sung HG, Spector ER, Lang TF, Oganov VS, Bakulin AV, Shackelford LC, LeBlanc AD. Recovery of spaceflight-induced bone loss: bone mineral density after long-duration missions as fitted with an exponential function. Bone 41:973-978, 2007.

75. Silvestrini G, Ballanti P, Leopizzi M, Sebastiani M, Berni S, Di Vito M, Bonucci E. Effects of intermittent parathyroid hormone (PTH) administration on SOST mRNA and protein in rat bone. J Mol Histol 38:261-269, 2007.

76. Smith SM, Heer MA, Shackelford LC, Sibonga JD, Ploutz-Snyder L, Zwart SR. Benefits for bone from resistance exercise and nutrition in long-duration spaceflight: Evidence from biochemistry and densitometry. J Bone Miner Res 27:1896-1906, 2012.

77. Smith BJ, Lucas EA, Turner RT, Evans GL, Lerner MR, Brackett DJ, Stoecker BJ, Arjmandi BH. Vitamin E provides protection for bone in mature hindlimb unloaded male rats. Calcif Tissue Int 76:272-279, 2005.

78. Smith MC Jr, Rambaut PC, Vogel JM, Whittle MW. (1977) Bone mineral measurement-experiment M078. In: Johnston RS, Dietlein LF (eds.) Biomedical results from Skylab (NASA SP-377). National Aeronautics and Space Administration, Washington, DC, pp 183-190.

79. Smith SM, Wastney ME, O'Brein KO, Morukov BV, Larina IM, Abrams SA, Davis-Street JE, Oganov V, Shackelford LC. Bone markers, calcium metabolism,

and calcium kinetics during extended-duration space flight on the Mir space station. JBMR 20(2):208-218, 2005.

80. Smith SM, Zwart SR, Heer M, Lee SMC, Meuche S, Macias BR, Shackelford LC, Schneider S, Hargens AR. WISE-2005: Supine treadmill exercise within lower body negative pressure and flywheel resistive exercise as a countermeasure to bed rest-induced bone loss in women during 60-day simulated microgravity. Bone 42(3):572-581, 2008.

81. Smith SM, Zwart SR, Kloeris V, Heer M. (2009) Nutritional biochemistry of space flight. Nova Science Publishers, New York.

82. Swift JM, Gasier HG, Swift SN, Wiggs MP, Hogan HA, Fluckey JD, Bloomfield SA. Increased training loads do not magnify cancellous bone gains with rodent jump resistance exercise. J Appl Physiol 109:1600-1607, 2010.

83. Swift JM, Nilsson MI, Hogan HA, Sumner LR, Bloomfield SA. Simulated resistance training during hindlimb unloading abolishes disuse bone loss and maintains muscle strength. J Bone Miner Res 25:564-574, 2010.

84. Swift JM, Swift SN, Nilsson MI, Hogan HA, Bouse SD, Bloomfield SA. Cancellous bone formation response to simulated resistance training during disuse is blunted by concurrent alendronate treatment. J Bone Min Res 26(9):2140-2150, 2011.

85. Tian XY, Jee WSS, Li X, Paszty C, Ke HZ. Sclerostin antibody increases bone mass by stimulating bone formation and inhibiting bone resorption in a hindlimb-immobilization rat model. Bone 48(2):197-201, 2011.

86. Tosteson ANA and CS Hammond. Quality of life assessment in osteoporosis: Health status and preference based measures. Pharmacoeconomics, 20(5):289-303, 2002.

87. Trappe S, Costill D, Gallagher P, Creer A, Peters JR, Evans H, Riley DA, Fitts RH. Exercise in space: human skeletal muscle after 6 months aboard the International Space Station. J Appl Physiol 106(4):1159-1168, 2009.

88. Tseng W, Lu J, Bishop GA, Watson AD, Sage AP, Demer L, Tintut Y. Regulation of interleukin-6 expression in osteoblasts by oxidized phospholipids. Journal of Lipid Research 51:1010-1016, 2010.

89. van Beek ER, Cohen LH, Leroy IM, Ebetino FH, Lowik CW, Papapoulos SE. Differentiating the mechanisms of antiresorptive action of nitrogen containing bisphosphonates. Bone 33(5):805-811, 2003.

90. van't Hof RJ and Ralston SH. Nitric oxide and bone. Immunology 103: 255-261, 2001.

91. Vico L, Bourrin S, Very JM, Radziszowska M, Collet P, Alexandre C. Bone changes in 6-mo-old rats after head-down suspension and a reambulation period. J Appl Physiol 79:1426-1433, 1995.

92. Vico L, Collet P, Guignandon A, Lafage-Proust MH, Thomas T, Rehaillia M, Alexandre C. Effects of long-term microgravity exposure on cancellous and cortical weight-bearing bones of cosmonauts. Lancet 355:1607-1611, 2000.

93. Vico L, Novikov VE, Very JM, Alexandre C. Bone histomorphometric comparison of rat tibial metaphysis after 7-day tail suspension vs. 7-day spaceflight. Aviat Space Environ Med 62:26-31, 1991.

94. Wagner EB, Granzella NP, Saito H, Newman DJ, Young LR, Bouxsein ML. Partial weight suspension: a novel murine model for investigating adaptation to reduced musculoskeletal loading. J Appl Physiol 109:350-357, 2010.

95. Wang F, J Ko, L Weng, D Yeh, H Ke, S Wu. Inhibition of glycogen synthase kinase-3β attenuates glucocorticoid-induced bone loss. Life Sciences, 85:685-692, 2009.

96. Willey JS, Lloyd SA, Nelson GA, Bateman TA. Ionizing radiation and bone loss: space exploration and clinical therapy. Clinical Reviews in Bone and Mineral Metabolism 9(1):54-62, 2011.

97. Willey JS, Lloyd SA, Robbins ME, Bourland JD, Smith-Sielicki H, Bowman LC, Norrdin RW, Bateman TA. Early increase in osteoclast number in mice after whole-body irradiation with 2 Gy X-rays. Radiat Res 170:388–392, 2008.

98. Williams BO, Insogna KL. Where Wnts Went: The exploding field of Lrp5 and Lrp6 signaling in bone. J Bone Miner Res 24:171–178, 2009.

99. Xiong, J and O'Brien CA. Osteocyte RANKL: new insights into the control of bone remodeling. J Bone Miner Res 27(3): 499-505, 2012.

100. Yumoto K, Globus RK, Mojarrab R, Arakaki J, Wang A, Searby ND, Almeida EAC, Limoli CL. Short-term effects of whole-body exposure to 56Fe ions in combination with musculoskeletal disuse on bone cells. Radiation Research 173(4):494-504, 2010.

101. Zaman G, Saxon LK, Sunters A, Hilton H, Underhill P, Williams D, Price JS, Lanyon LE. Loading-related regulation of gene expression in bone in the

contexts of estrogen deficiency, lack of estrogen receptor alpha and disuse. Bone 46:628-642, 2010.

102. Zhao W and Robbins ME. Inflammation and chronic oxidative stress in radiation-induced late normal tissue injury: therapeutic implications. Curr Med Chem 16:130-143, 2009.

APPENDIX A*

J Appl Physiol 112: 918–925, 2012.
First published December 15, 2011; doi:10.1152/japplphysiol.00978.2011.

HIGHLIGHTED TOPIC | *Physiology and Pathophysiology of Physical Inactivity*

Simulated resistance training, but not alendronate, increases cortical bone formation and suppresses sclerostin during disuse

B. R. Macias,[1] J. M. Swift,[1] M. I. Nilsson,[1] H. A. Hogan,[2,3] S. D. Bouse,[2] and S. A. Bloomfield[1,4]

Departments of [1]Health and Kinesiology, [2]Mechanical Engineering, [3]Biomedical Engineering, and [4]Intercollegiate Faculty of Nutrition, Texas A&M University, College Station, Texas

Submitted 5 August 2011; accepted in final form 13 December 2011

Macias BR, Swift JM, Nilsson MI, Hogan HA, Bouse SD, Bloomfield SA. Simulated resistance training, but not alendronate, increases cortical bone formation and suppresses sclerostin during disuse. *J Appl Physiol* 112: 918–925, 2012. First published December 15, 2011; doi:10.1152/japplphysiol.00978.2011.—Mechanical loading modulates the osteocyte-derived protein sclerostin, a potent inhibitor of bone formation. We hypothesized that simulated resistance training (SRT), combined with alendronate (ALEN) treatment, during hindlimb unloading (HU) would most effectively mitigate disuse-induced decrements in cortical bone geometry and formation rate (BFR). Sixty male, Sprague-Dawley rats (6-mo-old) were randomly assigned to either cage control (CC), HU, HU plus either ALEN (HU+ALEN), or SRT (HU+SRT), or combined ALEN and SRT (HU+SRT/ALEN) for 28 days. Computed tomography scans on *days −1* and *28* were taken at the middiaphyseal tibia. HU+SRT and HU+SRT/ALEN rats were subjected to muscle contractions once every 3 days during HU (4 sets of 5 repetitions; 1,000 ms isometric + 1,000 ms eccentric). The HU+ALEN and HU+SRT/ALEN rats received 10 μg/kg ALEN 3 times/wk. Compared with the CC animals, HU suppressed the normal slow growth-induced increases of cortical bone mineral content, cortical bone area, and polar cross-sectional moment of inertia; however, SRT during HU restored cortical bone growth. HU suppressed middiaphyseal tibia periosteal BFR by 56% vs. CC ($P < 0.05$). However, SRT during HU restored BFR at both periosteal (to 2.6-fold higher than CC) and endocortical (14-fold higher than CC) surfaces ($P < 0.01$). ALEN attenuated the SRT-induced BFR gains during HU. The proportion of sclerostin-positive osteocytes in cortical bone was significantly higher (+121% vs. CC) in the HU group; SRT during HU effectively suppressed the higher proportion of sclerostin-positive osteocytes. In conclusion, a minimum number of high-intensity muscle contractions, performed during disuse, restores cortical BFR and suppress unloading-induced increases in sclerostin-positive osteocytes.

resistance exercise; Wnt; hindlimb unloading; histomorphometry; load

THE ESTIMATED LIFETIME RISK of an osteoporotic fracture is ~50% in women and ~22% in men (14); annual direct-care costs attributable to osteoporotic fractures in the United States are estimated to be as high as $18 billion (38). Regular weight-bearing exercise can help preserve or add small amounts of bone mass in adult women and men (9). The development of bisphosphonate therapies has helped to reduce fracture risk. However, no medical therapy is yet available to prevent osteoporosis, characterized by aggressive bone resorption and unchanged or decreased bone formation. It is well established that the mechanical loading that occurs with weight-bearing exercise is a potent anabolic stimulus to bone (25). In fact, mechanical loading via the Wnt/β-catenin (canonical) signaling pathway in bone cells plays a pivotal role in translating the forces imposed on bone into upregulated bone cell activity, resulting in a net gain of bone mass (26). Therefore, the mechanical loading that occurs during weight-bearing activity is requisite to the maintenance of bone mass and quality.

Bone and muscle tissues do not have to resist the force of gravity when "ambulating" in space, and it is hypothesized that this lack of mechanical load results in lower body musculoskeletal deconditioning (21). Biomechanical loads of the lower body musculoskeletal tissues during Mir Missions were calculated to be 30–40% less than those present on Earth when using treadmill exercise with bungee cords (40). Somewhat higher loads were achieved with treadmills on Shuttle flights (36). In-shoe measures of ground reaction force during treadmill, ergometer, and resistance exercise of International Space Station (ISS) crewmembers were less than those forces for a similar activity on Earth (5, 12). Furthermore, recent studies performed aboard the ISS demonstrate the need for development of improved exercise countermeasures that involve higher loading profiles to weight-bearing bones and muscles (8, 16, 37).

The lack of sufficient mechanical stimuli to weight-bearing regions of the skeleton during spaceflight has been documented during recent studies of ISS crewmembers. Volumetric quantitative computed tomography (QCT) measures of cortical bone mineral content (BMC) at the hip in 14 crewmembers before and after ISS missions (4–6 mo) show rates of loss to be −1.6%/mo at both the femoral neck and trochanter (16). In another study, 16 crewmembers on 4.5- to 6-mo ISS missions lost, on average, 11.9% in femoral neck cortical bone mass (17). Moreover, bone biomarkers, calcium metabolism, and calcium kinetics data collected during long-duration ISS and Mir missions suggest that the resulting bone loss is primarily due to increased bone resorption and decreased intestinal calcium absorption (30). These studies, taken together, highlight the robust thinning of the femoral neck cortex from the inner margin and presumed robust resorptive activity of osteoclasts during extended durations of microgravity exposure.

The rodent hindlimb unloading (HU) model is a well-established ground-based model for investigating disuse effects on bone (20). Previously, our laboratory has demonstrated that high-intensity muscle contractions at 100% peak isometric

Address for reprint requests and other correspondence: Susan A. Bloomfield, Dept. of Health and Kinesiology, MS 4243, Texas A&M Univ., College Station, TX 77843-4243 (e-mail: sbloom@tamu.edu).

*American Physiological Society permits whole published articles to be reproduced without charge in dissertations, which may be posted to theses repositories.

torque (P_o), produced during simulated resistance training (SRT) undertaken during a period of HU produced significant gains in middiaphyseal tibia cortical bone mineral density (BMD). These gains were associated with a fivefold greater periosteal bone formation rate (BFR) compared with control animals (32). Numerous studies have investigated the efficacy of a pharmacological treatment [alendronate (ALEN)] in inhibiting disuse-induced bone loss or in models of estrogen deficiency (1, 2, 28, 29). Bisphosphonate therapies potently suppress accelerated osteoclast-mediated bone resorption. Currently, ALEN, an anti-resorptive bisphosphonate, is being administered to some astronauts aboard the ISS to investigate the efficacy of this bone loss countermeasure strategy (17).

Our laboratory previously demonstrated that bisphosphonate treatment, when combined with moderate-intensity muscle contractions (75% P_o) during disuse, significantly increases proximal tibia total BMC (33). However, this combined drug/exercise countermeasure attenuates the cancellous bone formation response compared with the exercise-only group (33). The cellular mechanism by which SRT restores bone gain during unloading or how bisphosphonate treatment impacts the anabolic response of cortical bone to SRT remains undefined. To our knowledge, these are the first studies to employ a resistive exercise modality during HU with bisphosphonate treatment. The aim of this present investigation was to test the anabolic effects of SRT in combination with the anti-resorptive effects of ALEN during 28 days of HU in adult rats on disuse-induced cortical bone decrements. We hypothesized that SRT, in combination with ALEN therapy during HU, would better mitigate deleterious changes in cortical bone mass, cortical bone geometry, cortical BFR, and that SRT but not ALEN would mitigate elevations of sclerostin-positive osteocytes.

MATERIALS AND METHODS

Animals and experimental design. Sixty male Sprague-Dawley rats were obtained from Harlan (Houston, TX) at 6 mo of age and allowed to acclimate for 14 days before initiation of the study. All animals were singly housed after arriving at our animal facility in a temperature-controlled (23 ± 2°C) room with a 12:12-h light-dark cycle in an American Association for Accreditation of Laboratory Animal Care-accredited animal care facility and were provided standard rodent chow (Harlan Teklad 8604) and water ad libitum. Animal care and all experimental procedures described in this investigation were approved by the Texas A&M University Laboratory Animal Care Committee. Previously, tissues from these same animals were utilized to assess the impact of ALEN and SRT on cancellous bone (34).

Five experimental groups were studied: *1*) cage control (CC, n = 12); *2*) HU (n = 12); *3*) HU animals administered 10 μg/kg ALEN via subcutaneous injection 3 times/wk (HU+ALEN, n = 12); *4*) HU subjected to SRT (HU+SRT, n = 12); and *5*) HU rats subjected to both ALEN and SRT (HU+SRT/ALEN, n = 12). Animals in all groups except CC underwent 28 days of HU. HU+SRT and HU+ALEN/SRT animals underwent nine sessions of simulated resistive exercise conducted once every 3 days during the 28-day protocol. The HU and HU+ALEN groups were also administered the same regimen (frequency, dose, duration) of isoflurane anesthesia (Minrad, Bethlehem, PA) as used for SRT groups. The CC animals were allowed normal ambulatory cage activity, but not exposed to anesthesia.

Calcein injections (25 mg/kg body mass) were given subcutaneously 9 and 2 days before euthanasia to label mineralizing bone for histomorphometric analysis. HU animals were anesthetized before removal from tail suspension at the end of the study to prevent any weight bearing by the hindlimbs. At the end of the experiment, on *day 28*, all animals were anesthetized with 50 mg/kg body wt of ketamine (Fort Dodge Animal Health, Fort Dodge, IA) and 0.5 mg/kg body wt of medetomidine (Pfizer, New York, NY) and euthanized by decapitation. Distal left femora were fixed in formalin, decalcified, and stored at 4°C for immunohistochemistry analyses; proximal left tibiae were fixed in formalin and then stored in 70% ethanol at 4°C for histomorphometry analyses.

HU. HU was achieved by tail suspension, as previously described (32). The height of the animal's hindquarters was adjusted to prevent any contact of the hindlimbs with the cage floor, resulting in approximately a 30° head-down tilt. The forelimbs of the animal maintained contact with the cage bottom, allowing the rat full access to the entire cage. All animals were monitored daily for health, including assessment of tail integrity, and body weights were measured weekly.

SRT paradigm. SRT was completed as previously described (32). Briefly, left plantar flexor muscles from animals in the HU+SRT group were trained once every 3 days during 28-day HU using a custom-made rodent isokinetic dynamometer. Animals were anesthetized with isoflurane gas (~2.5%; Minrad, Bethlehem, PA) mixed with oxygen before removal from tail suspension to prevent any weight bearing by the hindlimbs. Each rat was then placed in right lateral recumbency on a platform, the left foot was secured onto the foot pedal, and the left knee was clamped so that the lower leg was perpendicular to the foot and the femur and tibia were at right angles to each other. This was referred to as the resting, 0° position. For isometric contractions, the foot pedal was held fixed in this position. For all contractions, the footplate was rotated in synchrony with muscle stimulation by a Cambridge Technology lever system (model 6900) interfaced with a 80486 66-MHz personal computer using custom software written in TestPoint (version 4.0; Capital Equipment, Billerica, MA). Torque generated around the footplate pivot (at the rat's ankle joint) was measured by the lever system's servomotor. Plantar flexor muscle stimulation was performed with fine-wire electrodes consisting of insulated chromium nickel wire (Stablohm 800B, H-ML Size 003, California Fine Wire), inserted intramuscularly straddling the sciatic nerve in the proximal thigh region. The stimulation wires were then attached to the output poles of a Grass Instruments stimulus isolation unit (model SIU5; Astro-Med, W. Warwick, RI) interfaced with a stimulator (S88; Astro-Med), which delivered current to the sciatic nerve and induced muscle contraction.

Voltage optimization to achieve P_o and stimulation frequency optimization of the eccentric torque were performed at the beginning of each session, as described previously (32). The eccentric phase of the muscle contraction was titrated to equal ~75% of each animal's daily P_o. The HU+SRT and HU+SRT/ALEN animals completed a combined isometric + eccentric SRT exercise paradigm, consisting of four sets of five repetitions, once every 3 days during HU (n = 9 total exercise sessions). The training paradigm consisted of a 1,000-ms isometric contraction (75%), immediately followed by a 1,000-ms eccentric contraction (75% of the peak isometric contraction).

Bisphosphonate treatment. Animals in the HU+ALEN and HU+SRT/ALEN groups were administered 10 μg/kg ALEN (Merck and Rathway) via subcutaneous injection 3 times/wk for the duration of the 28-day study. The ALEN dose of 30 $\mu g \cdot kg^{-1} \cdot wk^{-1}$ was the lowest dose (of three tested) that effectively mitigated reductions in cancellous volumetric BMD at the proximal tibia during 28 days of HU (unpublished data) and is similar to the 30 μg/kg ALEN (15 μg/kg, 2 times/wk) shown to maintain femur and lumbar spine bone mass and strength after ovariectomy (OVX) in rats (10). This ALEN dose of 30 $\mu g \cdot kg^{-1} \cdot wk^{-1}$ is, however, much lower than the dose (100 $\mu g \cdot kg^{-1} \cdot day^{-1}$) used in previously published clinical studies and in OVX rats, demonstrating pronounced increases in bone mass and strength (27). Rats in the CC, HU, and HU+SRT groups were administered an equal volume of vehicle (phosphate-buffered saline) by subcutaneous injection 3 times/wk.

Peripheral QCT. On *days −1* and *28* of the study, peripheral QCT (pQCT) scans were performed in vivo at the tibia middiaphysis with a Stratec XCT Research-M device (Norland, Fort Atkinson, WI), using a voxel size of 100 μm and a scanning beam thickness of 500 μm. Two slices centered at 50% of the tibial total length (determined from a scout view on the CT scanner) were collected. Calibration of this machine was performed on each day of scanning with a hydroxyapatite standard cone phantom. A standardized analysis for diaphyseal bone (contour mode 1, peel mode 2, outer threshold of 0.650 g/cm^3, inner threshold of 0 g/cm^3) was applied to each section.

Values of cortical BMC, cortical bone area, and the polar cross-sectional moment of inertia (CSMI) were averaged across the two slices at the tibial middiaphysis to yield a mean value. Polar CSMI was based on geometry only and not weighted by density. Machine precision (based on manufacturer's data) is ±9 mg/cm^3 for cortical bone. Reproducibility in our laboratory was determined from five repeat scans using an in vivo multiple-slice scanning method; resulting coefficients of variation for cortical tibia BMD was ±0.59%.

Dynamic histomorphometry analysis. Un-demineralized distal left tibiae were subjected to serial dehydration and embedded in methylmethacrylate (Sigma-Aldrich M5, 590–9, St. Louis, MO). Serial cross sections (150–200 μm) of midshaft cortical bone were cut starting 2.5 mm proximal to the tibiofibular junction with an Isomet diamond wafer low-speed saw (Buehler, Lake Bluff, IL). Sections were ground to reduce thickness (<80 μm) before mounting on glass slides. The histomorphometric analyses were performed by using the OsteoMeasure Analysis System, version 1.3 (OsteoMetrics, Atlanta, GA). Measures of labeled surfaces and interlabel widths were obtained at ×100 magnification of up to two slides per animal. Periosteal and endocortical mineral apposition rates (MAR, μm/day) were calculated by dividing the average interlabel width by the time between labels (7 days) and mineralizing surface (MS) for both periosteal and endocortical bone surfaces (BS) using the formula %MS/BS = {[(single-labeled surface/2) + double-labeled surface]/surface perimeter} × 100. BFR was calculated as (MAR × MS/BS).

Sclerostin immunohistochemistry. Distal left femora were fixed in 4% phosphate-buffered formalin for 48 h at 4°C, then decalcified in a sodium citrate-formic acid solution for 14 days, and stored in 70% EtOH. Following decalcification, the distal left femora were embedded in paraffin, and transverse sections at the midshaft were cut 10 μm thick and mounted on slides. Five slides, one slide from each group, were placed in a dry incubator at 60°C for 15 min to melt the paraffin. Slides were then washed in 70, 95, 100, and 100% ethanol solution for 3 min each. Slides were then washed in xylene twice for 5 min each. To quench endogenous hydrogen peroxides that may interfere with the horseradish peroxidase reaction, slides were soaked in a 0.3% hydrogen peroxide solution for 30 min. A hydrophobic perimeter was drawn around the tissue to maintain small-volume solutions above the tissue sample during incubation. Slides were washed twice in PBS for 5 min each, and then slides were washed in a PBS/0.5% Triton solution for 5 min. Slides were washed twice in PBS for 5 min each. Tissues were blocked with normal goat serum for 20 min, followed by a 5-min wash in PBS/2% normal goat serum solution. To reduce nonspecific binding, the tissue samples were treated with the avidin/biotin blocking kit per manufacturer's instructions (SP-2001, Vector Laboratories, Burlingame, CA), followed by three 5-min washes with PBS. Tissues were then placed on a wet-incubation tray, and each sample was loaded with the sclerostin primary antibody (1:250 dilution, R&D Systems, Minneapolis, MN) and incubated at 4°C overnight. Following overnight incubation, tissues were washed twice with a PBS/2% BSA/0.2% Tween solution, then washed twice with a PBS/2% BSA solution. The tissue samples were loaded with the biotinylated secondary antibody and incubated for 30 min (Vectastain Elite ABC Kit, Vector Laboratories, Burlingame, CA). Tissue was developed with a peroxidase substrate solution (NovaRED, Vector Laboratories, Burlingame, CA) for 10 min to stain sclerostin-positive osteocytes. Slides were washed quickly in PBS to terminate the reaction, taped dry, counterstained with hematoxylin, taped dry, coverslipped, and allowed to dry in the dark for 2 days. The region of interest for quantification of total (number of osteocytes) and sclerostin-positive osteocytes (SOST+ Ot) included the entire midshaft femur cross section using the OsteoMeasure Analysis System, version 1.3 (OsteoMetrics, Atlanta, GA). The percentage of sclerostin-positive osteocytes was calculated as (SOST+ Ot/total Ot) × 100.

Statistical analyses. All data are expressed as means ± SE and evaluated using the statistical package SPSS (version 15; Chicago, IL). Histomorphometry and sclerostin assays were first analyzed using a two-factor ANOVA (exercise and ALEN) to compare group differences between HU groups (HU, HU+ALEN, HU+SRT, and HU+SRT/ALEN). A Tukey's post hoc test was used for pairwise comparisons. Subsequently, a one-factor ANOVA was used to compare HU groups' values vs. that of the comparator CC group (Tukey's post hoc test for pairwise comparisons). A one-factor ANOVA was employed to determine significant longitudinal pQCT variable changes within each treatment group (in vivo pQCT data only). For all data, statistical significance was accepted at $P < 0.05$.

RESULTS

SRT during disuse restores normal age-related cortical bone accrual. HU for 28 days suppressed the normal growth gains in cortical BMC by 72%, compared with CC. The lack of BMC accrual in the HU+ALEN rodents (−0.44% change over 28 days) was similar to the HU-alone group (0.48%). However, when SRT was prescribed during 28 days of HU, normal growth gains in cortical BMC were restored (Table 1). ALEN administration did not appear to negatively affect the restoration of BMC by the mechanical load imposed by SRT (HU+SRT/ALEN group). The magnitude of changes in cortical area at the tibial middiaphysis was similar to those of changes in BMC. The SRT exercise provided a potent mechanical stimulus to restore the normal growth expansion of the cortical shell in both the HU+SRT (7.88%) and HU+SRT/ALEN (5.70%) groups, comparable to the gain in cortical area of the CC (5.61%) group. As expected, there was essentially no change in cortical bone area in the HU group. ALEN administration during HU did not rescue gains in cortical bone area and actually resulted in a slight reduction (−2.23%, $P = 0.079$). The increase in cortical bone area was accompanied by increased polar CSMI in the CC (14%), HU+SRT (13%), and HU+SRT/ALEN (10%) groups. Polar CSMI was significantly reduced in the HU+ALEN group by −5%. A similar decrease (−3%) was noted in the HU group; however, this change was not statistically significant. An increase in cortical volumetric BMD (0.3 to 1.8%) was observed among the groups; however, this change was not statistically significant.

ALEN blunts the cortical bone formation response to SRT during disuse. Markers of osteoblast activity on the periosteal surface of the tibia middiaphysis were substantially lower in the HU group vs. those in the CC group. Those animals given ALEN during HU show the lowest BFR, compared with all other groups. The application of SRT during HU produced significantly higher BFR on the periosteal surface at the tibia diaphysis (Fig. 1). The HU+SRT group demonstrated an eightfold higher BFR compared with HU. Moreover, when SRT was prescribed alone or in combination with ALEN treatment during HU, periosteal MS/BS was significantly higher than CC (+30 and 18%), HU (+130 and 109%), and HU+ALEN (+10-fold greater) groups. Periosteal MAR was lower in the HU+SRT/ALEN compared with HU+SRT; how-

Table 1. *SRT during disuse normalized cortical BMC, cortical area, and polar CSMI*

	CC	HU	HU+ALEN	HU+SRT	HU+SRT/ALEN
Cortical BMC, mg					
Day 0	8.08 ± 0.15	8.30 ± 0.22	8.10 ± 0.13	7.81 ± 0.16	8.14 ± 0.13
Day 28	8.55 ± 0.14*	8.43 ± 0.20[a]	8.07 ± 0.14[a]	8.53 ± 0.16*[b]	8.58 ± 0.19*[b]
%Change	5.90	0.48	−0.44	9.46	7.31
Cortical area, mm^2					
Day 0	6.14 ± 0.11	6.32 ± 0.17	6.20 ± 0.11	5.96 ± 0.12	6.21 ± 0.10
Day 28	6.48 ± 0.11*	6.30 ± 0.15[a]	6.05 ± 0.10[a]	6.42 ± 0.12*[b]	6.44 ± 0.14*[b]
%Change	5.61	−1.14	−2.23	7.88	5.70
CSMI, mm^4					
Day 0	12.48 ± 0.57	13.58 ± 0.93	12.54 ± 0.58	12.29 ± 0.48	13.04 ± 0.58
Day 28	14.22 ± 0.57*	13.38 ± 0.79[a]	11.77 ± 0.39*[a]	13.81 ± 0.52*[b]	13.74 ± 0.65*[b]
%Change	14.48	−3.12	−4.94	13.05	10.34

Values are group means ± SE. Hindlimb unloading (HU) suppressed changes in bone mineral content (BMC), cortical area, and polar cross-sectional moment of inertia (CSMI). Unexpectedly however, simulated resistance training (SRT) was a potent stimulus during HU, effectively restoring cortical bone geometric properties. CC, cage control; ALEN, alendronate. *$P < 0.05$ vs. prevalue. [a,b] HU groups not sharing the same letter for respective measures are significantly different from each other ($P < 0.05$).

ever, MAR of the HU+SRT/ALEN group remained nearly twofold higher than that of CC and HU.

Mechanical loading paradigms typically do not show robust bone formation effects at the endocortical surface. However, when SRT was prescribed alone or in combination with ALEN treatment during HU, endocortical MS/BS was significantly higher than CC (+270 and 420%), HU (+280 and 440%), and HU+ALEN (+28- and 40-fold greater) groups (Fig. 1). SRT

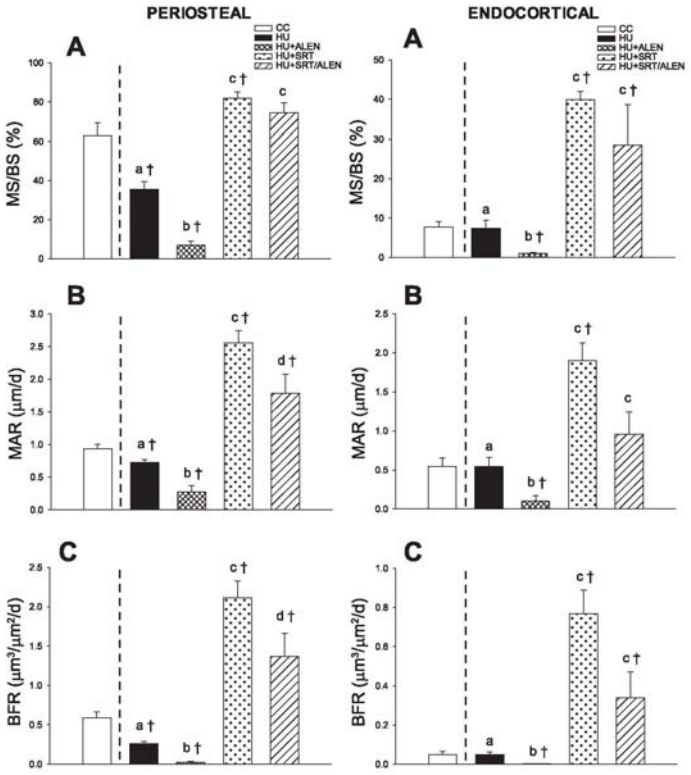

Fig. 1. Effects of hindlimb unloading (HU), with or without alendronate (ALEN) treatment and/or simulated resistance training (SRT), on periosteal and endocortical surface dynamic histomorphometric analyses measured at the tibia diaphysis. *A*: mineralizing surface [%MS/bone surface (BS)]. *B*: mineral apposition rate (MAR). *C*: bone formation rate (BFR). Vertical dashed line indicates separation of cage control (CC) from the experimental groups for preliminary ANOVA. Values are means ± SE. [a,b,c,d] HU groups not sharing the same letter for respective surface measures are significantly different from each other ($P < 0.05$). †Significantly different vs. CC ($P < 0.05$).

alone or in combination with ALEN administration during HU show significantly higher MAR and BFR at the endocortical surface. As expected, the BFR in the HU+ALEN was maximally suppressed and significantly lower than all other groups. The endocortical-BFR was significantly higher in the HU+SRT/ALEN group compared with CC (+7-fold), HU (+7-fold), and HU+ALEN (+167-fold); however, it was significantly less than the HU+SRT group (−56%). ALEN did dampen the robust endocortical bone formation (MS/BS, MAR, and BFR) to SRT during HU; however, HU+SRT/ALEN was not significantly less than the HU+SRT group. The impaired bone formation by ALEN administration can be seen visually by narrower widths of calcein labeling on the periosteal and endocortical surfaces when comparing the HU+SRT/ALEN with HU+SRT groups (Fig. 2).

The proportion of sclerostin-positive cortical osteocytes is suppressed by muscle contractions, but not ALEN treatment. Complete unloading of the hindlimb in the HU animals resulted in a significantly higher number of sclerostin-positive osteocytes vs. that observed in weight-bearing CC animals. ALEN treatment of HU animals had no effect on the proportion of sclerostin-positive osteocytes. By contrast, both groups subjected to SRT during unloading exhibited much lower prevalence of sclerostin-positive osteocytes, close to CC rat values (Fig. 3).

DISCUSSION

Our major finding in these studies was that ALEN treatment blunted the BFR response to SRT during rodent HU. Our data did not support our hypothesis that the combination of ALEN and resistance exercise therapies would better ameliorate deleterious changes in cortical bone than with ALEN or SRT administration alone.

Previously, we demonstrated that a similar simulated resistive exercise training paradigm with isometric and eccentric components (both at 100% peak isometric strength) effectively mitigates losses in muscle strength and provides a potent stimulus to bone during prolonged disuse (32). In the present study, a similar resistance exercise paradigm was utilized; however, the force of contractions, isometric and eccentric components, was titrated down to 75% of peak isometric strength. Even with this 25% reduction in muscle contraction intensity, this exercise modality elicited a robust bone formation response and restoration of normal bone accrual during a period of disuse. The gains in midshaft cortical BMC and in cortical area with the reduced intensity protocol were only slightly smaller than those observed with the previous higher intensity regimen; the gain in polar CSMI, a key predictor of bending strength, was identical in both protocols. Furthermore, the prescription of SRT at 100% P_0 or 75% P_0 during HU elicits a similar periosteal and endocortical bone forming response (as measured by MS/BS, MAR, and BFR) of cortical bone. Interestingly, visual inspection of the data appear to show more single and double labeling at the posterior-lateral and anterior-medial surfaces than other cortical bone surfaces of the tibia. Taken together, these data suggest that a 25% reduction in SRT intensity may not elicit a proportional reduction in the positive responses observed in bone geometry and bone formation in the context of disuse. Using a training intensity commonly used by humans performing resistance training programs, the present training regimen effectively prevented the suppression of cortical bone gain observed with unloading.

ALEN treatment given during HU produced significant further reductions in actively mineralizing surfaces (%MS/BS) and MAR beyond that observed with unloading alone, suggesting that ALEN treatment reduces both the number of remodeling sites and vigor of the individual osteoblast units (2). When given to animals also receiving infrequent bouts of SRT during HU, ALEN attenuated the cortical bone formation response primarily via a blunting of MAR without any significant impact on %MS/BS. Interestingly, when another common bisphosphonate, risedronate, is administered along with mechanical loading of mouse tibiae, no negative effects are observed in cortical geometric bone gains (31), consistent with the present data that ALEN and mechanical loading can exert independent effects. It is highly likely that the decreased bone formation observed at the periosteal surfaces with ALEN treatment at 28 days of HU would eventually impact on cross-sectional geometry, and/or local BMC were the period of disuse prolonged, resulting in changes in bone density and mechanical properties that could not be detected with the present study's limited time frame.

In general, cancellous bone is more responsive to disuse than is cortical bone, exhibiting more rapid declines in bone formation activity and in bone volume (4). Even so, we observed that cortical bone formation was significantly impaired on the periosteal surface during 28 days of HU, contributing to an

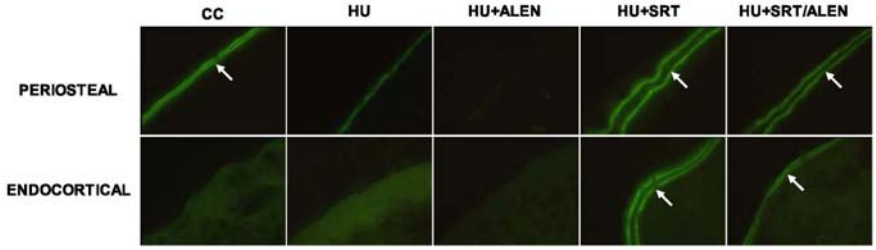

Fig. 2. Visual depiction (×100 magnification) of calcein labeling of the periosteal and endocortical surfaces of cortical bone at the tibia diaphysis. Note the extensive fluorochrome labeling in CC, HU with SRT (HU+SRT), and HU+SRT and ALEN (HU+SRT/ALEN) and large interlabel width (HU+SRT and HU+SRT/ALEN).

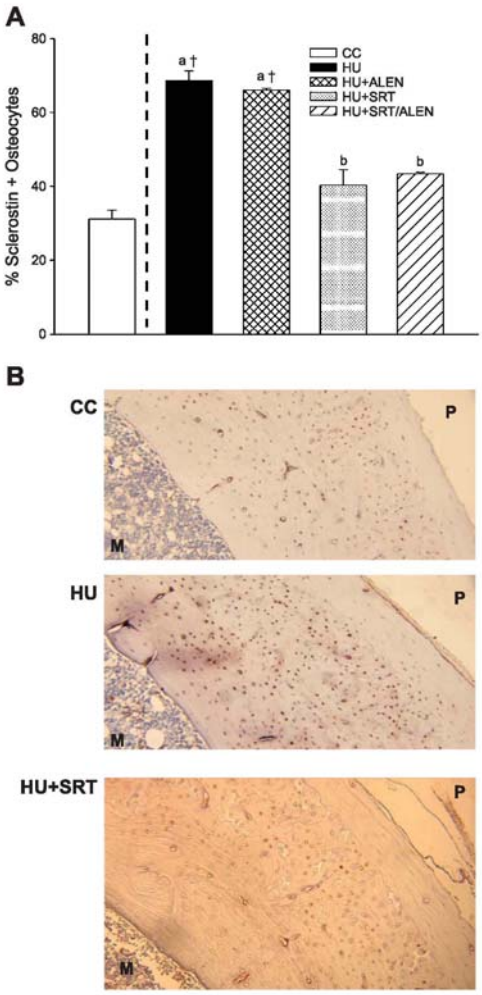

Fig. 3. Effects of HU with or without ALEN treatment and/or SRT on cortical bone osteocyte expression of sclerostin measured at the tibia diaphysis (×100 magnification). *A*: HU shows significantly greater number of sclerostin-positive osteocytes, where SRT (HU+SRT) tends to suppress sclerostin-positive (SOST+) osteocytes, with no untoward effects of ALEN administration. Data are expressed as a percentage of sclerostin-positive osteocytes [(SOST+ osteocytes/total osteocytes) × 100]. ^{a,b} HU groups not sharing the same letter for respective surface measures are significantly different from each other ($P < 0.05$). †Significantly different vs. CC ($P < 0.05$). *B*: note higher intensity staining in the HU group of the tibial cross section. M, marrow space; P, periosteal surface.

inhibition of the slow midshaft cortical bone growth observed in these male rats. This adaptation of cortical bone is consistent with previous studies of space-flown and HU rats that document a reduction in radial bone growth and bone strength (20, 21). In the present study, cortical BFR in unloaded animals was further suppressed by ALEN administration, which contrasts with our laboratory's previous observations of no additional effect of ALEN administration on disuse-induced reductions on cancellous BFR in the proximal tibia (33). The major impact of disuse on osteoblast activity in the cancellous compartment may have occurred early in the 28-day unloading period, whereas the slower response of cortical bone to disuse enabled the present study to detect ALEN effects on bone formation within the same period. However, when ALEN was given to HU animals experiencing intermittent mechanical loading (HU+SRT/ALEN), the resulting robust increases in bone formation were impaired at both cortical and cancellous (33) bone sites, as measured over the last 9 days of the experiment.

Bisphosphonates may directly affect osteoblast precursors and osteoblast activity. For example, Gasser et al. (11) demonstrates that ALEN administration before PTH administration reduces MAR, possibly by blunting the bone-lining cell transition to osteoblast. In addition, risedronate treatment causes osteoblasts to adopt a flatter cell morphology, a reminiscent cell shape of bone-lining cells, suggesting that risedronate retards normal osteoblast activity (22). Therefore, the present study demonstration of ALEN blunting of BFR on the periosteal surface is consistent with previous reports that ALEN may have direct effect on osteoblast precursor cells and activity.

There are data to suggest that exercise, in combination with anti-resorptive compounds, provides additive, and perhaps synergistic, benefits to bone mass and strength. More data are available testing bisphosphonates' impact on bone loss subsequent to estrogen deficiency and less documenting effects of exercise during disuse. For example, etidronate treatment and treadmill exercise show significantly higher BMD at the midshaft femur in an OVX rat bone loss model (34). Similarly, OVX rats treated with ALEN and treadmill exercise therapy show higher midshaft femur BMC and cortical thickness (10). Therefore, at some bone sites, combined bisphosphonate and exercise therapy show added and perhaps synergistic effects at cortical bone sites. However, zoledronic acid and treadmill exercise therapy of OVX rats show no additive effect on cortical BMC or BMD (18). In addition, when OVX rats are exposed to both external mechanical loading of the ulna and ALEN treatment, the bone formation response to mechanical loading is not impaired (7). Conversely, ALEN given to rapidly growing young rats during HU inhibits cortical BFR and MAR at the tibia diaphysis by ~15% (3). A more mature (300 g) rat treated with ALEN during HU, but without exercise, shows higher cortical BMC (tibia and femur) compared with vehicle-treated animals (2). Collectively, these data suggest that certain bisphosphonate treatments, when given to an ambulatory full-weight-bearing rat, may prevent OVX-induced bone loss. However, in the context of reduced weight bearing, bisphosphonates may attenuate the bone formation response to mechanical loading.

The Wnt pathway coordinates communication between mechanosensing osteocytes (via secreted sclerostin) and bone-forming osteoblasts by the binding of sclerostin to lipoprotein

receptor-related protein (Lrp) 4/5/6 (6, 9, 39). Loss-of-function mutation of the Lrp5 gene results in decreases in bone mass and osteoblast proliferation (13). Sclerostin disrupts the interaction of Wnt proteins with Lrp4/5/6 receptors, effectively reducing Wnt signal transduction and resulting osteogenesis (25). Interestingly, mechanical loading in vivo downregulates sclerostin-positive osteocytes, the gene SOST, and upregulates osteogenic gene expression (26). Moreover, when sclerostin-null mice are subjected to simulated microgravity, the Wnt pathway is unaffected, and bone loss does not occur (19). Therefore, the robust increase of sclerostin-positive osteocytes during disuse observed in the present study is consistent with previous work demonstrating higher Sost transcript levels at *day 3* of HU and reduced numbers of sclerostin-positive osteocytes after 2 days of ulnar loading (without muscle contraction) (26).

In the present investigation, ALEN treatment did not significantly affect the number of sclerostin-positive osteocytes. Although ALEN is effective in preventing osteocyte apoptosis (23, 24, 33), it does not appear to alter the mechanosensing function of osteocytes to load or the proportion of sclerostin-positive osteocytes. This finding suggests that the modulation of osteoclast activity and apoptosis by ALEN may be independent of sclerostin control.

In conclusion, the present study demonstrates that moderate-intensity, low-volume loading of bone by active muscle contraction during a period of imposed disuse reduces sclerostin-positive osteocytes, coincident with increased bone formation activity to levels higher than those observed in weight-bearing control animals. These data extend previous work utilizing the SRT paradigm (low-volume/high-intensity exercise via physiological muscle contraction), which mitigates cancellous bone loss and prevents suppression of middiaphyseal periosteal apposition during unloading (1). Future studies should investigate the intracellular signaling pathway responsible for the dampening of the bone formation response to SRT by ALEN given during HU. In addition, the inclusion of a weight-bearing recovery component to the present study may help elucidate if bisphosphonate treatment impairs long-term bone formation capability.

ACKNOWLEDGMENTS

The authors gratefully acknowledge Janet Stallone for assistance with animal care, and Drs. Gordon Warren (Georgia State University) and Ken Baldwin (University of California, Irvine) for assistance with the simulated resistive exercise programming and procedures. Alendronate was generously provided by Merck Pharmaceuticals.

Present address of J. M. Swift: Radiation Combined Injury Program, Armed Forces Radiobiology Research Institute, Uniformed Services University of the Health Sciences, Bethesda, MD 20889-5603.

GRANTS

These studies were funded through the National Aeronautics and Space Administration Cooperative Agreement NCC 9-58 with the National Space Biomedical Research Institute (S. A. Bloomfield). B. R. Macias and J. M. Swift were supported by National Space Biomedical Research Institute Graduate Training Fellowship NSBRI-RFP-05-02. B. R. Macias is a National Science Foundation Graduate Research Fellow.

DISCLAIMER

The views, opinions, and findings contained herein are those of the author J. M. Swift and do not necessarily reflect official policy or positions of the Department of the Navy, Department of Defense, nor the United States Government.

DISCLOSURES

No conflicts of interest, financial or otherwise, are declared by the author(s).

AUTHOR CONTRIBUTIONS

B.R.M., J.M.S., M.I.N., H.A.H., and S.A.B. conception and design of research; B.R.M., J.M.S., M.I.N., H.A.H., S.D.B., and S.A.B. performed experiments; B.R.M., J.M.S., M.I.N., H.A.H., S.D.B., and S.A.B. analyzed data; B.R.M., J.M.S., M.I.N., H.A.H., S.D.B., and S.A.B. interpreted results of experiments; B.R.M., J.M.S., M.I.N., H.A.H., and S.A.B. prepared figures; B.R.M., J.M.S., M.I.N., H.A.H., and S.A.B. drafted manuscript; B.R.M., J.M.S., M.I.N., H.A.H., S.D.B., and S.A.B. edited and revised manuscript; B.R.M., J.M.S., M.I.N., H.A.H., S.D.B., and S.A.B. approved final version of manuscript.

REFERENCES

1. **Apseloff G, Girten B, Walker M, Shepard DR, Krecic M, Stern LS, Gerber N.** Aminohydroxybutane bisphosphonate and clenbuterol prevent bone changes and retard muscle atrophy respectively in tail-suspended rats. *J Pharmacol Exp Ther* 264: 1071–1078, 1993.
2. **Apseloff G, Girten B, Weisbrode SE, Walker M, Stern LS, Krecic M, Gerber N.** Effects of aminohydroxybutane bisphosphonate on bone growth when administered after hind-limb bone loss in tail-suspended rats. *J Pharmacol Exp Ther* 267: 515–521, 1993.
3. **Bikle DD, Morey-Holton ER, Doty SB, Currier PA, Tanner SJ, Halloran BP.** Alendronate increases skeletal mass of growing rats during unloading by inhibiting resorption of calcified cartilage. *J Bone Miner Res* 9: 1777–1787, 1994.
4. **Bloomfield SA, Allen MR, Hogan HA, Delp MD.** Site- and compartment-specific changes in bone with hindlimb unloading in mature adult rats. *Bone* 31: 149–157, 2002.
5. **Cavanagh PR, Genc KO, Gopalakrishnan R, Kuklis MM, Maender CC, Rice AJ.** Foot forces during typical days on the international space station. *J Biomech* 43: 2182–2188, 2010.
6. **Choi HY, Dieckmann M, Herz J, Niemeier A.** Lrp4, a novel receptor for dickkopf 1 and sclerostin, is expressed by osteoblasts and regulates bone growth and turnover in vivo. *PLos One* 4: e7930, 2009.
7. **Feher A, Koivunemia A, Koivunemia M, Fuchs RK, Burr DB, Phipps RJ, Reinwald S, Allen MR.** Bisphosphonates do not inhibit periosteal bone formation in estrogen deficient animals and allow enhanced bone modeling in response to mechanical loading. *Bone* 46: 203–207, 2010.
8. **Fitts RH, Trappe SW, Costill DL, Gallagher PM, Creer A, Colloton PA, Peters JR, Romatowski JG, Bain JL, Riley DA.** Prolonged space flight-induced alterations in the structure and function of human skeletal muscle fibres. *J Physiol* 588: 3567–3592, 2010.
9. **Forwood MR, Burr DB.** Physical activity and bone mass: exercise in futility? *Bone Miner* 21: 89–112, 1993.
10. **Fuchs RK, Shea M, Durski SL, Winters-Stone KM, Widrick J, Snow CM.** Individual and combined effects of exercise and alendronate on bone mass and strength in ovariectomized rats. *Bone* 41: 290–296, 2007.
11. **Gasser JA, Kneissel M, Thomsen JS, Mosekilde LI.** PTH and interactions with bisphosphonates. *J Musculoskelet Neuronal Interact* 1: 53–56, 2000.
12. **Genc KO, Gopalakrishnan R, Kuklisc MM, Kuklis MM, Maender CC, Rice AJ, Bowersox KD, Cavanagh PR.** Foot forces during exercise on the International Space Station. *J Biomech* 43: 3020–3027, 2010.
13. **Gong Y, Slee RB, Fukai N, Rawadi G, Roman-Roman S, Reginato AM, Wang H, Cundy T, Glorieux FH, Lev D, Zacharin M, Oexle K, Marcelino J, Suwairi W, Heeger S, Sabatakos G, Apte S, Adkins WN, Allgrove J, Arslan-Kirchner M, Batch JA, Beighton P, Black GCM, Boles RG, Boon LM, Borrone C, Brunner HG, Carle GF, Dallapiccola B, Paepe AD, Floege B, Halfhide ML, Hall B, Hennekam RC, Hirose T, Jans A, Jüppner H, Kim CA, Keppler-Noreuil K, Kohlschuetter A, LaCombe D, Lambert M, Lemyre E, Letteboer T, Peltonen L, Ramesar RS, Romanengo M, Somer H, Steichen-Gersdorf E, Steinmann B, Sullivan B, Superti-Furga A, Swoboda W, van den Boogaard M, Van Hul W, Vikkula M, Votruba M, Zabel B, Garcia T, Baron R, Olsen BR, Warman ML, The Osteoporosis-Pseudoglioma Syndrome Collaborative Group.** LDL receptor-related protein 5 (LRP5) affects bone accrual and eye development. *Cell* 107: 513–523, 2001.
14. **Johnell O, Kanis J.** Epidemiology of osteoporotic fractures. *Osteoporos Int* 16: S3–S7, 2005.

15. **Lang T, LeBlanc A, Evans H, Lu Y, Genant H, Yu A.** Cortical and trabecular bone mineral loss from the spine and hip in long-duration spaceflight. *J Bone Miner Res* 19: 1006–1012, 2004.
16. **Lang T, Leblanc A, Evans H, Lu Y.** Adaptation of the proximal femur to skeletal reloading after long-duration spaceflight. *J Bone Miner Res* 21: 1224–1230, 2006.
17. **LeBlanc A, Schneider V, Shackelford L, West S, Oganov V, Bakulin A, Voronin L.** Bone mineral and lean tissue loss after long duration space flight. *J Musculoskelet Neuronal Interact* 1: 157–160, 2000.
18. **Lespessailles E, Jaffre C, Beaupied H, Nanyan P, Dolleans E, Benhamou CL, Courteix D.** Does exercise modify the effects of zoledronic acid on bone mass, microarchitecture, biomechanics, and turnover in ovariectomized rats? *Calcif Tissue Int* 85: 146–157, 2009.
19. **Lin C, Jiang X, Dai Z, Guo X, Weng T, Wang J, Li Y, Feng G, Gao X, He L.** Sclerostin mediates bone response to mechanical unloading through antagonizing wnt/b-catenin signaling. *J Bone Miner Res* 24: 1651–1661, 2009.
20. **Morey-Holton E, Globus RK, Kaplansky A, Durnova G.** The hindlimb unloading rat model: literature overview, technique update and comparison with space flight data. *Adv Space Biol Med* 10: 7–40, 2005.
21. **Morey-Holton ER, Whalen RT, Arnaud SB, Van Der Meulen MC.** The skeleton and its adaptation to gravity. In: *Handbook of Physiology. Environmental Physiology.* Bethesda, MD: Am. Physiol. Soc., 1996, sect. 4, vol. I, chapt. 31, p. 691–719.
22. **Nakamura M, Udagawa N, Matsuura S, Mogi M, Nakamura H, Horiuchi H, Saito N, Hiraoka BY, Kobayashi Y, Takaoka K, Ozawa H, Miyazawa H, Takahashi N.** Osteoprotegerin regulates bone formation through a coupling mechanism with bone resorption. *Endocrinology* 144: 5441–5449, 2003.
23. **Plotkin LI, Aguirre JI, Kousteni S, Manolagas SC, Bellido T.** Bisphosphonates and estrogens inhibit osteocyte apoptosis via distinct molecular mechanisms downstream of extracellular signal-regulated kinase activation. *J Biol Chem* 280: 7317–7325, 2005.
24. **Plotkin LI, Weinstein RS, Parfitt AM, Roberson PK, Manolagas SC, Bellido T.** Prevention of osteocyte and osteoblast apoptosis by bisphosphonates and calcitonin. *J Clin Invest* 104: 1363–1374, 1999.
25. **Robling AG, Castillo AB, Turner CH.** Biomechanical and molecular regulation of bone remodeling. *Annu Rev Biomed Eng* 8: 455–498, 2006.
26. **Robling AG, Niziolek PJ, Baldrige LA, Condon KW, Allen MR, Alam I, Mantila SM, Gluhak-Heinrich J, Bellido TM, Harris SE, Turner CH.** Mechanical stimulation of bone in vivo reduces osteocyte expression of Sost/Sclerostin. *J Biol Chem* 283: 5866–5875, 2008.
27. **Rodan GA, Seedor Balena R.** Preclinical pharmacology of alendronate. *Osteoporos Int* 3: 7–12, 1993.
28. **Sato M, Grasser W, Endo N, Akins R, Simmons H, Thompson DD, Golub E, Rodan GA.** Bisphosphonate action. Alendronate localization in rat bone and effects on osteoclast ultrastructure. *J Clin Invest* 88: 2095–2105, 1991.
29. **Schenk R, Eggli P, Fleisch H, Rosini S.** Quantitative morphometric evaluation of the inhibitory activity of new aminobisphosphonates on bone resorption in the rat. *Calcif Tissue Int* 38: 342–349, 1986.
30. **Smith SM, Wastney ME, O'Brien KO, Morukov BV, Larina IM, Abrams SA, Davis-Street JE, Oganov V, Shackelford LC.** Bone markers, calcium metabolism, and calcium kinetics during extended-duration space flight on the mir space station. *J Bone Miner Res* 20: 208–218, 2005.
31. **Sugiyama T, Meakin LB, Galea GL, Jackson BF, Lanyon LE, Ebetino FH, Russell RGG, Price JS.** Risedronate does not reduce mechanical loading-related increases in cortical and trabecular boen mass in mice. *Bone* 49: 133–139, 2011.
32. **Swift JM, Nilsson MI, Hogan HA, Sumner LR, Bloomfield SA.** Simulated resistance training during hindlimb unloading abolishes disuse bone loss and maintains muscle strength. *J Bone Miner Res* 25: 564–574, 2010.
33. **Swift JM, Swift SN, Nilsson MI, Hogan HA, Bouse SD, Bloomfield SA.** Cancellous bone formation response to simulated resistance training during disuse is blunted by concurrent alendronate treatment. *J Bone Miner Res* 26: 2140–2150, 2011.
34. **Tamaki H, Akamine T, Goshi N, Kurata H, Sakou T.** Effects of exercise training and etidronate treatment on bone mineral density and trabecular bone in ovariectomized rats. *Bone* 23: 147–153, 1998.
35. **Thompson DD, Seedor G, Weinreb M, Rosini S, Rodan GA.** Aminohydroxybutane bisphosphonate inhibits bone loss due to immobilization in rats. *J Bone Miner Res* 5: 279–285, 1990.
36. **Thornton W.** Work, exercise and space flight. III. Exercise devices and protocols. In: *Proceedings of the 1986 Workshop on Exercise Prescription for Long-Duration Space Flight*, edited by Harris BA Jr and Stewarts DF. Washington, DC: NASA, 1989, p. 31–42.
37. **Trappe S, Costill D, Gallagher P, Creer A, Peters JR, Evans H, Riley DA, Fitts RH.** Exercise in space: human skeletal muscle after 6 months aboard the International Space Station. *J Appl Physiol* 106: 1159–1168, 2009.
38. **US Department of Health and Human Services.** *Bone Health and Osteoporosis: A Report of the Surgeon General.* Rockville, MD: US Department of Health and Human Services, Office of the Surgeon General, 2004.
39. **Williams BO, Insogna KL.** Where Wnts Went: the exploding field of Lrp5 and Lrp6 signaling in bone. *J Bone Miner Res* 24: 171–178, 2009.
40. **Whalen R.** Musculoskeletal adaptations to mechanical forces on Earth and in space. *Physiologist* 36: S127–S130, 1993.